Efficient Magnetic Resonance Wireless Power Transfer Systems

By

Thabat Fakhri Younis Thabet

A thesis submitted for the degree of ***Doctor of Philosophy***

School of Computer Science and Electronic Engineering

University of Essex

September 2018

Abstract

This thesis aims to improve the performance of magnetic resonance wireless power transfer systems. Different factors have different effects on the performance and the efficiency of the maximum transfer of power in the system. These factors are: the resonance frequency; the quality factor of the resonators; the value and shape of the coils; the mutual inductance, including the distance between the coils; and the load. These systems have four potential types of connection in the transmitter and receiver. These types are Serial to Serial (SS), Serial to Parallel (SP), Parallel to Serial (PS) and Parallel to Parallel (PP). Each type has different applications because it has a different performance from the others.

Magnetic resonance wireless power systems in some applications consist of one transmitter and one receiver, while in other applications there is a demand to transfer the power to more than one receiver simultaneously. Hence the importance of studying multiple receiver systems arises. The serial to serial type connection was studied along with the effects of all the other factors on the efficiency, including the existence of multiple receivers.

The symmetric capacitance tuning method was presented as a solution to the frequency splitting problem that usually appears in SS wireless power transfer systems with a small gap between the two resonators. Compared to other existing methods, this method provides advantages of high efficiency and keeps the frequency within the chosen Industrial Scientific Medical (ISM) band.

The impact of the connection type on the efficiency of wireless power transfer systems and the effect of the load impedance on each type was studied.

Finally, an algorithm for intelligent management and control of received wireless power was offered to run a load that requires more than the received power.

To my family with love

Acknowledgements

First and foremost I want to thank Allah, who has given me the strength and patience to carry out this work. I would like to address my sincerest thanks to my supervisor Dr. John Woods, who supported and guided me through my PhD journey by his technical advice, helpful guidance, and humanity.

I also would like to thank the Ministry of Higher Education and Scientific Research and Technical College of Mosul in Iraq for offering me a scholarship to obtain the PhD degree, and giving me the opportunity to undertake this experience.

Special thanks are presented to the staff of the School of Computer Science and Electronic Engineering; especially the Supervisory Panel members: Professor Anthony Vickers, and Dr Nick Zakhleniuk, and the staff of Lab. 8: Mr Tony De Roy, Mr Robin Dowling, and Mr Ian Dukes.

Many thanks are due to all my friends and colleagues at the University of Essex; specially Mrs Sameera Abdul-Kader, Mrs Maysa Almulla Khalaf, Miss Nora Alkhamees, and Mr Arturo Wulfrano.

Thanks to my colleagues Mr Mohamad Baidoun, Mr Hadi Mourtada, and Mr Yalcin Aygul as we cooperated in some stages.

A special thanks to Mr Jeremy Ratcliffe for proofreading my thesis and for the valuable comments and suggestions.

I would like to express my gratitude to my family, and friends in Iraq in Mosul who have wished me success while they were living in really difficult situations. Last but not least, I would like to thank my dearest husband Adnan who supported and encouraged me in all stages; him and my lovely children.

Contents

List of Figures

List of Tables

Abbreviations

AIM	Adaptive Impedance Matching
AM	Amplitude Modulation
CAR	Coil Area Ratio
CMT	Coupled-Mode Theory
CT	Circuit Theory
HF	High Frequencies
IR	Infrared Communication
ISM	Industrial Scientific Medical
Li-Fi	Visible Light Communication
MIT	Massachusetts Institute of Technology
MRC	Magnetic Resonant Coupling
PAC	Programmable Array of Capacitors
PP	Parallel to Parallel
PS	Parallel to Serial
RF	Radio Frequency
RFID	Radio Frequency Identification
RLT	Reflected Load Theory
SCT	Symmetric Capacitive Tuning
SP	Serial to Parallel
SS	Serial to Serial

Symbols

A	receiver radius
A	transmitter radius
A_1, A_2, A_3, A_4	variables
C	speed of light
$C, C_1, C_2, C_3 \ldots C_n$	capacitance
D	distance between axes of coils
di/dt	variation rate of current
$d\phi/dt$	variation rate of magnetic flux
dl_1, dl_2	incremental sections
D	distance between coils
E	second kind of the complete elliptic integral
Exp	experimental results
F	frequency
f_0	resonant frequency
f_1, f_2	splitting frequencies
G	distance between planes of coils
i, i_1, i_2	current
I_1, I_2, I_3, I_4	loop's currents.
I_s	the microcontroller current during sleep mode
I_r	the average current when the microcontroller is on
j	$\sqrt{-1}$
j_1, j_2	variables
K	coupling coefficient
K	first kind of the complete elliptic integral
$L, L_1, L_2, \ldots L_n$	inductance
M, M_{total}	mutual inductance
$M_{j1\,j2}, M_{12}, M_{13}, \ldots$	mutual inductance between the transmitter and the receiver
N_1, N_2	number of turns
N	the number of readings during charging time
N_d	the number of readings during discharging
P	pitch between any two turns

P_a	accumulated power
P_r	power consumption of the microcontroller for each voltage reading
P_s	power consumption of the microcontroller during sleep time
P_{out}, P_{out1}, P_{out2}, P_{out3}	output power
P_{in}	input power
$P_{in(max)}$	maximum input power
R_{ch}	the equivalent serial resistance
R_d	the equivalent parallel resistance
R_{in}	real part of input impedance
R_L, R_2, R_3	load resistor
R_S	internal resistor of the source
t_1, t_2, t_3, t_4	time at each reading
t_r	charging time of regular reading method
t_p	charging time of proposed method
t_{sleep}	the required time to reach the target voltage
t_{on}	the required time to reach the target voltage
T_d	discharging time
T_r	the wake up time for each reading
T_s	sleep time
Th	theoretical results
V	induced voltage
V_c	capacitor voltage
V_{dc}	dc source
V_{in}	maximum voltage
V_{start}	initial voltage of discharging
V_{CC}	dc voltage of the microcontroller
$V_{target1}$, $V_{target2}$	target voltage
V_S	voltage source
V_0, V_1, V_2, V_3	voltage reading
X_{in}	imaginary part of input impedance
X_{C1}, X_{C2}	capacitive reactance

X_{L1}, X_{L2}	inductive reactance
X_M	reactance of the mutual inductance
Z_{in}	input impedance
Z_{11}, Z_{12}, Z_{13},.....	elements of impedance matrix
α	variable
β	variable
η	efficiency
η_0	figure of merit
λ	wavelength
φ	angle of the integration
ϕ	magnetic flux
ϕ_{12}, ϕ_{21}	magnetic flux between two coils
κ	variable
μ_o	permeability of free space
τ_{ch}	time constant for charging
τ_d	time constant for discharging
ν	variable
ω	angular frequency

Chapter 1

Overview

1.1 Introduction

Magnetic resonant coupling wireless power transfer systems use electric and magnetic coupling to send energy through a near-field [1]. The propagation in the near field is non-radiative, thus it is convenient, safe, and simple [2]. Wireless charging, which is one of the important applications using this technology, is more convenient and has a number of advantages over wired connections [3]. In wireless charging there is no physical connection between the load and the source, encouraging its use as a no spark application. Because of its reliance on magnetic resonance, this technology is also harmless from a biological point of view i.e. it is environmentally friendly [4]. The seminal work of this technique was conducted by Nikola in the late 19th century; he was one of the wireless power transmission pioneers [1],[5].

Recently the method was revisited by scientists at Massachusetts Institute of Technology (MIT) in 2007 [6], [7]. MIT announced a system that could transfer power wirelessly by magnetic resonance over two metres [8]. Following this, research in this

area has received increased attention from many large multinational companies such as Apple, Duracell and Qualcomm [9], and magnetic resonant wireless power has become the subject for many researchers.

1.2 Motivation

The magnetic resonant coupling wireless power transfer technique is safe and convenient; and it is a promising technology that inspires researchers to study and improve its performance. The following questions motivated our investigative work:

- Why do most papers work on serial to serial magnetic resonant wireless power transfer systems despite the frequency splitting problem?
- Is there a more efficient solution for the splitting problem than the known methods; impedance matching and frequency tracking?
- In some applications there is a demand to transfer power simultaneously to more than one receiver, such as in a multiple wireless charging system. Hence the importance of studying multiple receivers systems arises. So, the question here is: what is the effect of using more than one receiver in the system? Does the frequency splitting problem appear in this case?
- Is it possible to use other potential types of connection; serial to parallel, parallel to serial, and parallel to parallel, in magnetic resonant wireless power transfer systems? What are the differences in their performance?
- Can tiny amounts of power really do useful work? Can a device do useful work without access to a supply such as a battery?

The first stage was researching the previous studies about wireless power transfer, specifically the magnetic resonant coupling technology, in order to investigate the recent developments in the field.

We found that analysing the system is the answer to all the previous questions and the basis for all the following stages of research. Therefore, we presented an approach to analyse the system that can be applicable to other cases such as using more than one receiver. From this analysis, the performance of the system was investigated and how several factors affect this. After this comprehensive study, which is supported by experimental results, the frequency splitting problem was identified in order to address it in a more effective way.

The presented method: symmetric capacitance tuning is an effective technique to move the splitting curve to match one of the two new peaks with the original resonant frequency. It excels in efficiency and keeps the frequency inside the Industrial Scientific Medical (ISM) band compared to impedance matching and frequency tracking methods.

Following that, the idea of the analysis approach was re-used to study the other types of connection, considering the differences in each circuit. This study provides a comparison of the four types.

Next, power management was applied to answer the last question and to prove that tiny amounts of power can really do useful work in a magnetic resonance wireless power transfer system. This was achieved through intelligent control of running the load by using a microcontroller in the receiver side; and we have presented an algorithm to achieve that.

1.3 Research Objectives

This thesis focuses on the performance of magnetic resonance wireless power transfer systems. As mentioned before, the reason for choosing these types of systems is that there are several factors that affect the performance of various systems. Some of them still face challenges in the efficiency of the maximum transfer of power. Hence, the objective of this thesis is to improve the performance of such systems and present some solutions for the identified problems. To achieve this the following steps were carried out:

1. The magnetic resonance wireless power models of different circumstances were mathematically derived and simulated in software. These models include:
   - One, two and three receiver systems.
   - Four types of connection SS, SP, PS, and PP.
   - Use of solenoid and pancake coils.
2. The experiments were conducted for all previous models in order to verify the simulation results.
3. A microcontroller was used to implement some parts. These parts were:
   - Implementation of the wireless link of microcontrollers' communication in the proposal of symmetric capacitance tuning method.
   - Implementation of the power management to control the consumption of the received wireless power.
4. Sometimes, a circuit design program was used to test the performance of some circuits.

In conclusion all these steps aim to improve the performance of several models of magnetic resonance wireless power systems.

1.4 Contributions to the research field

Our major contributions to the field are:

- Multiple Receivers

We present a complete study on magnetic resonance wireless power transfer systems including the effect of various parameters on the performance of the system. These parameters are:

  - Resonant frequency
  - Distance between coils
  - Size of coils including cross sectional area and number of turns
  - Coil area ratio of receiver to transmitter
  - Existence of multiple receivers

- High efficiency with small coil area ratio

High efficiency can be achieved even with a small ratio between the cross sectional areas of the receiver coil relative to the transmitter coil which indicates the percentage of flux lines that are cut by the receiver.

- Frequency splitting solution

The symmetric capacitance tuning method is presented to solve the frequency splitting issue in magnetic resonance wireless power transfer systems as a more efficient method than the other existing methods of impedance matching and frequency tracking. Using this method enables the system to transfer the maximum power at different distances without moving out of the ISM band.

- Different connection types

A study of the four potential types of connection is presented in the analysis of magnetic resonance wireless power systems. These types are Serial to Serial (SS), Serial to Parallel (SP), Parallel to Serial (PS) and Parallel to Parallel (PP). In addition, the effect of the load on the efficiency of each type is considered in the study.

- Management and control of received wireless power

An algorithm is presented to manage the consumption of the received wireless power. The implementation of this algorithm enables tiny amounts of power to do useful work by including a microcontroller in the receiving resonator. This provides intelligent control of the time of switching the load on and off. It is an efficient mode to run the load when there is no mandatory need to do that constantly.

1.5 Publications

- T. Thabet, and J. Woods, “An Approach to Calculate the Efficiency for an N-Receiver Wireless Power Transfer System,” in International Journal of Advanced Computer Science and Applications IJACSA, vol. 6, no. 9, pp. 91-98, 2015.
- T. Thabet, and J. Woods, “Impact of connection type on the efficiency of wireless power transfer systems,” in Proc. IEEE International Conference on Circuits, System and Simulation, pp. 146-150, 2017.
- T. Thabet, and J. Woods, "Intelligent Management and Control of Received Wireless Power,” in Proc. IEEE International Conference on Circuits, System and Simulation, pp. 76-81, 2017.

- T. Thabet, and J. Woods, “Using Input Impedance to Calculate the Efficiency Numerically of Series-Parallel Magnetic Resonant Wireless Power Transfer Systems,” in Advances in Science, Technology and Engineering Systems Journal, Special Issue on Multidisciplinary Sciences and Engineering, vol.3, no. 3, pp. 38-42, 2018.

1.6 Thesis Structure

The rest of the thesis is structured as follows.

Chapter 2: consists of two main parts, the research background, and a literature review about magnetic resonant coupling wireless power transfer. The former part discusses the features and the advantages of the proposed method over the other power transfer technologies. Then, the concepts are gradually introduced in order to explain the principle of magnetic resonant coupling wireless power transfer, including near field, far field, Industrial Scientific Medical (ISM) bands, electromagnetic induction, and resonance. The latter part is a literature review that surveys the related works for each area of our work separately.

Chapter 3: includes an extensive study, including analysis, simulation results supported by experiments, and discussion of magnetic resonant coupling wireless power transfer systems. It examines the effect of different factors on the performance of the system. These factors are the frequency of resonance, the quality factor of the resonators, the value and the shape of the coils, the distance and the mutual inductance between the coils, and the load. In addition one, two and three receiver systems are considered in this study. The problem of frequency splitting is also identified in this chapter.

Chapter 4: presents a method to solve the frequency splitting problem. This is the symmetric capacitance tuning method which leads to moving the splitting curve to match one of the two new peaks with the original resonant frequency. The chapter also includes an evaluation for this method by comparing it with other known methods such as impedance matching and frequency tracking.

A design to implement this method practically is suggested in this chapter.

Chapter 5: contains an analysis of the impact of the type of connection on magnetic resonant wireless power systems. The study includes analysis, simulation results supported by experiments, and discussion of the four potential connection types. These are SS, SP, PS, and PP. Circular pancake coils are used in this part.

Chapter 6: presents an algorithm to manage the received power in the magnetic resonance wireless system. This technique is required in the case of the receiver receiving less power than the load's requirement. The chapter contains an explanation of how the microcontroller controls turning the load on and off, an evaluation of the proposed algorithm, and the details of the system implementation in the real environment.

Chapter 7: summarises our findings and presents a discussion based on the results described in the previous chapters. It also contains suggestions for future work.

Chapter 2

Literature Review on Magnetic Resonance Wireless Power Transfer

2.1 Research Background

Wireless power transfer in general is distinguished from normal electricity in that the power is delivered without any connection between the source and the load. This can be achieved by different methods such as microwaves, laser, mutual induction, and magnetic resonant coupling. The latter is a promising technique and has several advantages such as being safe, economical and convenient for small and moderate distance applications [4]. This technology is the subject of this research.

2.1.1 Features and comparison

Using magnetic resonance to transfer power wirelessly has advantages over other methods:

- Compared with traditional electricity (wired electricity), magnetic resonant coupling wireless power transfer is more convenient as there is no need for connectors and therefore no spark hazards [2], [10], [11].
- Comparing magnetic resonant coupling with mutual induction wireless power transfer (normal transformer without a core) is sensible as both methods are within near field technologies. The former method transfers the power through a very small distance such as some wireless chargers that are currently available in markets for phones and electric toothbrushes. It seems that using magnetic resonance can achieve higher efficiency with longer distances in spite of the weak coupling coefficients [12], [13], [14], [15].
- Due to the principle of work (using a magnetic field to deliver power) and the selected frequency range (only a few MHz), this method is safer than other technologies such as laser and microwaves [4], [16].
- Magnetic resonance allows for power transmission through different obstacles (such as people, walls, and some types of furniture), as long as the magnetic field does not interact with them [16].
- The amount of power transfer depends on the secondary coil intersection with primary coil flux lines and it is not a directional beam [17], as shown in Figure 2.1. By contrast, laser and microwaves both use oriented beams [16], [18].
- Since the used equipment is cheap and available, magnetic resonant coupling wireless power transfer systems are relatively economical [4].

However, each technology has various applications due to different performance from the others.

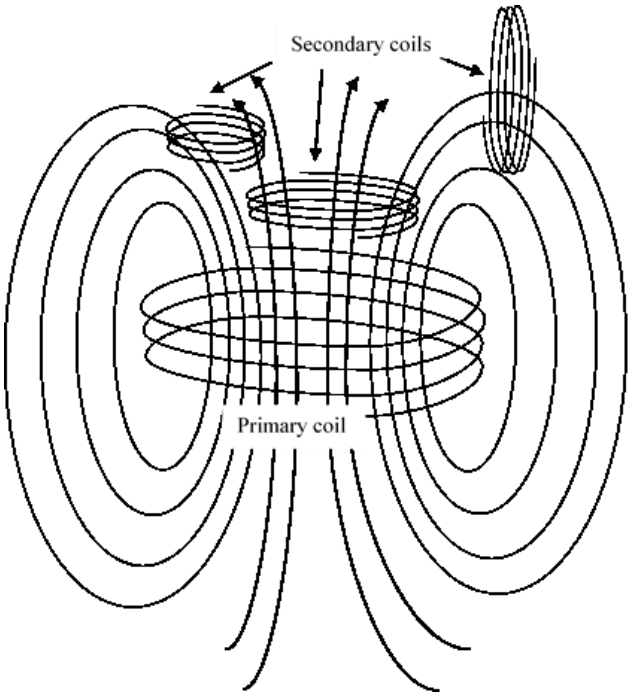

Figure 2.1 Intersection of magnetic flux lines

2.1.2 Near field and far field

Radio frequencies are used to transfer the power wirelessly in the magnetic resonant coupling method [19]. These frequencies can propagate as electromagnetic waves, which consist of electrical and magnetic fields. The synchronized oscillations of the two fields spread at the speed of light through space. Wave propagation produces two different regions around any transmitter, near field and far field, as well as a transition zone between them [20]. All these regions are shown in Figure 2.2, and they are related to the wavelength of the transmitted frequency. The relation between the frequency and the wavelength is [21]:

$$\lambda = \frac{c}{f} \tag{2.1}$$

where λ is the wavelength, c is the speed of light (3×10^8 m/s), and f is the frequency.

Near field expression refers to the region of the electromagnetic field around a transmitter and ends at a distance of one wavelength of the transmitted frequency, while far field is represented by an electromagnetic radiation region that starts at a distance of two wavelengths [22].

As shown in Figure 2.2, the first part of the near field that is a reactive and non-radiative field ends at a distance of one wavelength divided by 2π [23]. This area is the proper range to wirelessly transfer power in magnetic resonant coupling technology [24], [17].

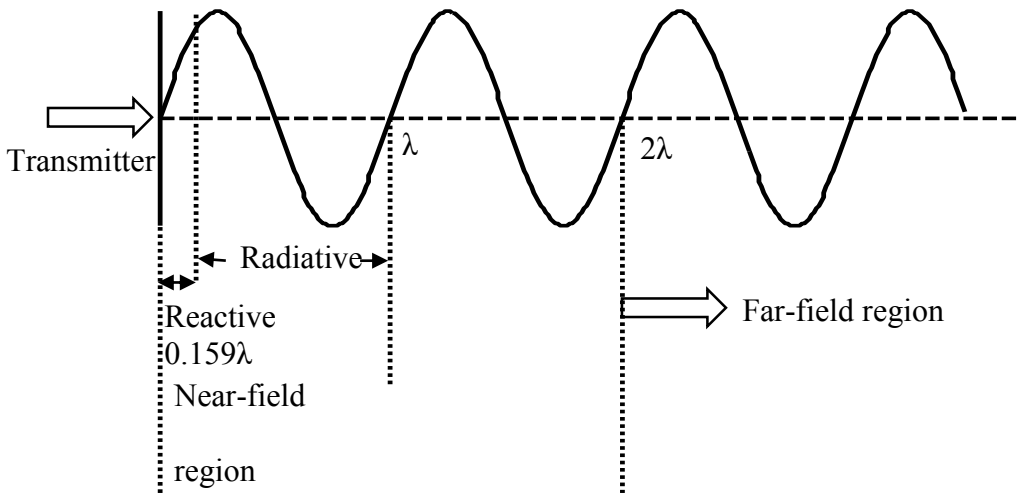

Figure 2.2 Field region for antennas

2.1.3 Frequency domain and ISM bands

The commonly used radio frequency range in magnetic resonant coupling technology is the high frequencies band HF that covers the range of 3-30 MHz [25]. This is because of the convenience of the reactive region ($\lambda/2\pi$) to the wireless distance requirements [20], [26]. The existing industrial scientific medical (ISM) radio bands through HF are shown in Table 2.1 with their details [27].

Table 2.1: ISM radio bands through the HF range

Centre frequency of ISM band	Frequency range	Wavelength (λ)	reactive area $\lambda/2\pi$
6.78 MHz	6.765-6.795 MHz	44.247 m	7.035 m
13.56 MHz	13.553-13.567 MHz	22.123 m	3.517 m
27.12 MHz	26.957-27.283 MHz	11.061 m	1.758 m

Work at the lowest frequency among these ISM bands is the best in terms of components values; in practical it is not easy to deal with small values of coils and capacitors that are required to the high frequencies. Work at higher frequencies provides an opportunity to send the power through a greater distance between any two specific coils; however, the small capacitor value is the practical limitation to rise the frequency. Hence, 13.56 MHz is the commonly used frequency in some wireless power transfer applications such as Radio Frequency Identification (RFID). Using this frequency enables the transfer of power wirelessly through its reactive distance 3.517m, which is the required range in these applications.

2.1.4 Electromagnetic induction

According to Ampère's law, there is a reciprocal relationship between a magnetic field and electrical current, where passing current through a wire or a coil produces a magnetic field around it [22]. Also, a moving magnetic field around a coil induces current through it and then induced voltage across it. Hence, coils can store energy in the form of a magnetic field. Faraday expressed this relation in his law as [21]:

$$V = -\frac{d\phi}{dt} \tag{2.2}$$

or, defining $L = d\phi/di$:

$$V = -L\frac{di}{dt} \tag{2.3}$$

where V is the induced voltage (volt), $d\boldsymbol{\phi}/dt$ is the variation rate of magnetic flux (weber per second), L is the inductance value (henry), and di/dt is the variation rate of current (ampere per second). The negative sign means that an induced current has an opposite magnetic field direction to the one that induced the current.

2.1.5 Self-inductance and mutual inductance

Inductance (L) is a property of a coil and, when the magnetic flux ($\boldsymbol{\phi}$) is proportional to the current (i), it can be written as the ratio [21]:

$$L = \frac{\phi}{i} \tag{2.4}$$

Self-inductance, or just inductance, refers to the electromagnetic inductance in a current carrying coil due to the current changing in the coil itself. The value of the inductance L depends on the geometrical arrangement of the coil.

Mutual inductance refers to the electromagnetic inductance in the coil due to the current changing in another coil that is close enough to it. For example, the circuit shown in Figure 2.3 has two coils L_1 and L_2. The figure also shows V_S, R_S, and R_L as the voltage source, the internal resistance of the source and the load resistor, respectively. The varying current i_1 produces a magnetic field when passing through the first coil L_1. This field intersects the second coil L_2 and creates current flow i_2. Hence, the induced current through L_2 will have its own magnetic field that interacts with the magnetic field of L_1. The mutual inductance between the two coils depends on the geometrical arrangement of them both as well as the distance between them. If the coils are far apart, the magnetic flux through L_2 due to the current i_1 will be small as well as the mutual inductance [21].

$$M = \frac{d\phi_{12}}{di_2} = \frac{d\phi_{21}}{di_1} \tag{2.5}$$

where ϕ_{12} is the flux through L_1 due to i_2 and vice versa. If all the flux produced by one coil passes through the other, then:

$$M = \sqrt{L_1 L_2} \tag{2.6}$$

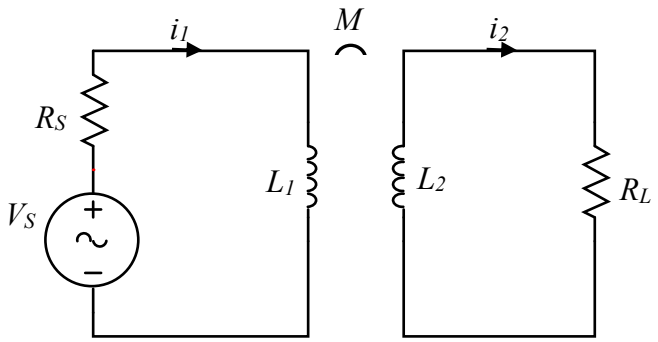

Figure 2.3 Inductance and mutual inductance

2.1.6 Coupling coefficient

The coupling coefficient k is the factor that represents the interaction level between any two coils. It is simply found from the following equation [12]:

$$k = \frac{M}{\sqrt{L_1 L_2}} \tag{2.7}$$

A coupling coefficient equal to 1 indicates that the two coils totally interact, and a coefficient of 0 means there is no interaction between them. It is easier to deliver power between the coils with a high coupling coefficient, while a small amount or no power may be transferred in the case of a low coupling coefficient unless the two coils resonate at the same frequency [28], [29]. It is necessary to know what resonance means.

2.1.7 Resonance and quality factor

Resonance is a general concept in physics which simply means vibration at a specific frequency and it is a property of resistor-inductor-capacitor RLC circuits. These kinds

of circuits consist of a resistor (R), an inductor (L), and a capacitor (C), connected in series or in parallel, as shown in Figure 2.4a and 2.4b, respectively. The figure also shows the phase diagram for both of them.

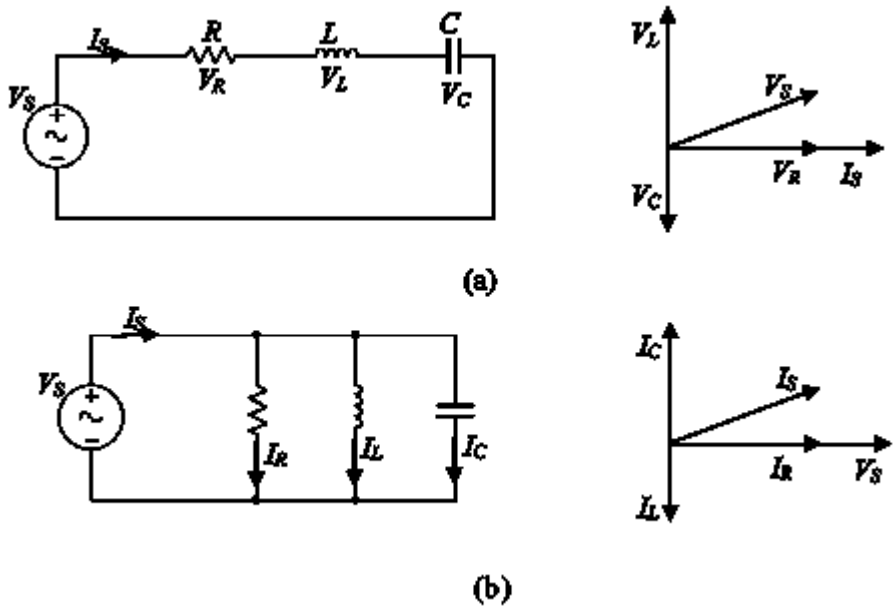

Figure 2.4 RLC circuit and phase diagram (a) Series (b) Parallel

The voltage source of the series RLC circuit is the directional summation of the voltage of each element, as:

$$\overrightarrow{V_S} = \overrightarrow{V_R} + \overrightarrow{V_L} + \overrightarrow{V_C} \tag{2.8a}$$

$$\overrightarrow{V_S} = \overrightarrow{I_S}\left(R + j\left(X_L - X_C\right)\right) \tag{2.8b}$$

where V_S, V_R, V_L and V_C are the voltage of the source, resistor, inductor and capacitor, respectively; I_S is the current of the circuit; X_L and X_C are the inductive and capacitive reactance, respectively.

The total current of the parallel RLC circuit is the summation of the current of each element, as:

$$\overrightarrow{I_S} = \overrightarrow{I_R} + \overrightarrow{I_L} + \overrightarrow{I_C} \tag{2.9a}$$

$$\overrightarrow{I_S} = \overrightarrow{V_S}\left(\frac{1}{R} + j\left(\frac{1}{X_C} - \frac{1}{X_L}\right)\right) \tag{2.9b}$$

where I_S, I_R, I_L and I_C are the current of the source, resistor, inductor and capacitor, respectively.

In both circuits, resonance occurs when the inductive reactance magnitude equals the magnitude of the capacitive reactance, causing energy to oscillate between the electric field of the capacitor and the magnetic field of the inductor. The resonant frequency f_r of any combination of inductance L and capacitance C is [30]:

$$X_L = X_C \tag{2.10}$$

$$2\pi f_r L = \frac{1}{2\pi f_r C} \tag{2.11}$$

$$f_r = \frac{1}{2\pi\sqrt{LC}} \tag{2.12}$$

The quality factor Q of the resonator is the ratio of the energy stored in the circuit to the energy dissipated per cycle and it can be expressed by the reactance and the resistance as following:

$$Q = \frac{X_L}{R} = \frac{X_C}{R} \tag{2.13a}$$

$$Q = \frac{1}{R}\sqrt{\frac{L}{C}} \tag{2.13b}$$

2.1.8 Magnetic resonant wireless power transfer systems

These kind of systems can easily consist of two resonators. As shown in Figure 2.5, there are two coils. One of them is a transmitter and the other is a receiver. Both of them have to resonate at the same frequency to obtain maximum transfer of wireless power between them [31], as proofed in section 3.4.1. That can be achieved by choosing the right capacitance for each coil to match the resonance frequency [12].

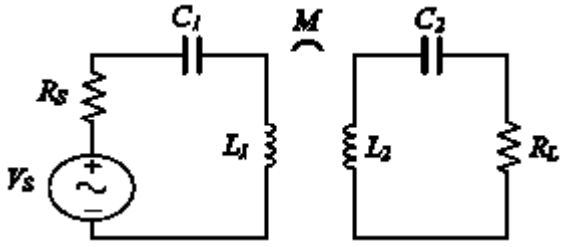

Figure 2.5 Magnetic resonant coupling wireless power transfer system

The power transfer efficiency of the system is affected by several factors [32], [33]. The first one is the frequency of the system, working at a higher frequency enables the system to send the power through a greater distance for the same coils [34]. The second one is the quality factor of the resonators [28]. At the same frequency, using two resonators with a higher quality factor leads to higher power transfer. The third factor is the value and the shape of the coils. The fourth one is the distance between the coils. (The last two factors impact the mutual inductance between the coils, and then the

power transfer of the system [33].) The fifth factor is the load which affects the input impedance of the system and thus the maximum transfer of power [35].

2.1.9 Impedance matching

The performance of a magnetic resonant wireless power transfer system differs due to the factors stated in the previous section. The system achieves the maximum power transfer efficiency when the impedance is matched between the source and the load. Various modes have been presented to match the impedance to improve the power transfer of the system as shown below.

To maintain maximum wireless power transfer efficiency, a group of researchers added an Adaptive Impedance Matching (AIM) to both sides (transmitter and receiver) [36]. It consists of a coil connected with variable capacitors as π-match network, as shown in Figure 2.6. They presented an algorithm to compute the matching network component values.

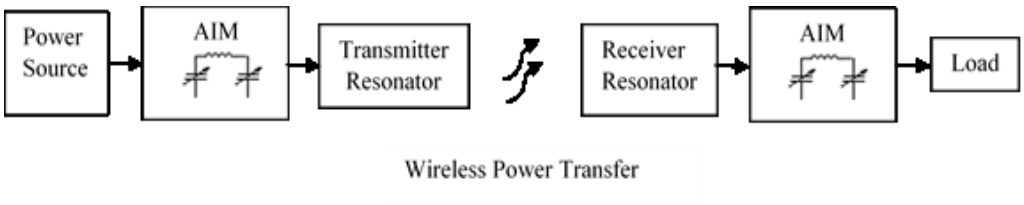

Figure 2.6 Block diagram of the impedance matching wireless power system

Lee et al. in [37], matched the impedance in a different way. They used an arbitrary number of coils with flexible position to match the impedance, instead of adding an impedance matching network, as shown in Figure 2.7. A similar idea was implemented by Kim et al. [38]. They analysed the power transfer efficiency of the wireless power

transfer system by setting up an intermediate perpendicular resonator to the transmitter and the receiver to improve the power transfer of the system and extend the distance between the transmitter and the receiver [38].

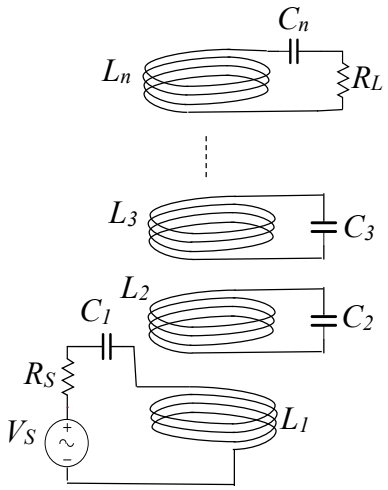

Figure 2.7 Wireless power transfer systems using multiple coils

Kim et al. in [39], combined the two modes. They added switchable impedance matching networks in the free positioning wireless power transfer system with multiple devices.

2.2 Literature Review

Wireless power transmission is a desired technique to dispose of cables and connectors; this idea was the aim of Tesla [1], [40], [41]. He explained the details of his invention, which is apparatus to transmit electrical energy, and gave some recommendations about its performance [42]. Some factors such as lack of funding prevented him from continuing the work to make the method more efficient and widely applicable [16].

In the 1960s, William Brown pioneered microwave power transmission as a far field wireless technology instead of the traditional systems of high voltage power lines. The distinct disadvantage of these lines in addition to the physical connection is the significant effect of their surrounding electromagnetic fields on the environment along their path [16]. To avoid the physical connection, the directive beam of a microwave signal could be a better alternative to transfer the power over a large distance [43].

In microwave technology, the power is transmitted as a wireless beam from one place to another [16]. The microwave beam with high intensity is harmful to humans because of the propensity for heating biological matter. Where most of the content of a body cell is H_2O and the H_2O molecule is resonant at microwave frequency [44]. The difference between the effects of the two technologies on health is due to the travelled distance of the signal. Compared with the harm caused by the long path of the high voltage power lines, the microwave signal has to travel only about 200 km through the atmosphere and the rest of the path to the reflector satellite in a specific orbit does not have any environmental interaction [43]. To some extent this can reduce the danger of the microwaves, but still, controlling the microwave beam power density in this 200 km is important to conform to safety limits [16].

The absence of physical connectors, and the directivity of the microwave beam, are both advantages in making microwave technology attractive in some applications. It is possible to use microwave radiation to transfer the power generated in space by solar panels carried by a satellite placed in a specific orbit to the earth [45], [46], [47]. However, it is clear that microwave technology applies for large distance applications [4], and there is no need to use it in moderate wireless power applications for two reasons [16]. Firstly: the efficiency; where it is inversely proportional to the frequency squared due to Friis transmission formula [16], [48]. Secondly: microwaves are

injurious to health [4] and have a more stringent exposure safety limit than RF because of the heating property [16]. The requirements of moderate applications could be the transferring of a few watts of power through a few metres, which can be achieved at a frequency lower than microwave frequencies to improve the safety and increase the efficiency of the system [16].

Later, in 2007, scientists at Massachusetts Institute of Technology (MIT) revisited the concept of wireless power transfer by announcing a testbed which wirelessly transferred tens of watts over a distance of greater than two metres [8]. This method is a near field technique which is more appropriate for consumer electronic devices because it based on magnetic induction to transfer the power wirelessly [16]. The transmission here is non-radiative because the distance between the two resonators is less than the wavelength of the selected frequency [49]. This technique is valid for a specific distance due to the practical limitations of the various parameters of the system. Recent research relating to this field has been increasingly conducted by many of the large companies such as Apple, Duracell and Qualcomm [40], [9].

Magnetic resonant coupling wireless power transfer has been the subject for many researchers. Some of them focus on the advantages of the method and compare it with other wireless power technologies [4], [12]. Others have reviewed the history of the wireless power transfer down to magnetic resonant method [40], [41], [50]. Some researchers show the stages of the development of wireless power transmission using different techniques and how these technologies change from far to near field [16].

2.2.1 Analysis of multiple receivers magnetic resonant wireless power transfer systems

Analysing a magnetic resonant wireless power transfer system is necessary to understand how it works and how its performance can be improved. Generally, there are two main methods to analyse the system. These methods are coupled-mode theory (CMT) and circuit theory (CT) [51]. In the former method (CMT), the system can be described by differential equations [9], [52], [53]. However, according to [54] this method is complicated, undesirable and inconvenient relating to design the circuits around the system. Therefore, researchers tend to use the equivalent circuit for a magnetic coupled system.

The second method (CT) is more familiar to circuit designers than the coupled-mode theory chosen by physicists. In this method, the magnetic coupling is represented as the mutual inductance between the two coils. The equivalent circuit of the wireless power transfer system can be formulated as a two ports network, which can be represented by either an impedance matrix or a scattering matrix [52]. The impedance matrix relates the input and output voltages to the input and output currents. Whereas the scattering matrix relates the outgoing waves to the incoming waves that are incident on the two-port. Under this general concept of (CT), many researchers have used different modes with different names to study the magnetic resonant wireless power transfer system, such as reflected load theory (RLT) [28], [9], [55], [56], and magnetic resonant coupling (MRC) [54], [57], [58].

The RLT method is commonly used to analyse transformers by electrical engineers, and it can be used to analyse magnetic resonant wireless power transfer systems. The method states that the current in the transmitter coil is dependent on the load in the

receiver coil, and the reflected load in the transmitter is not always the same as the actual load [9]. Applying the impedance matrix on a magnetic resonant wireless power transfer system, is achieved by representing each loop (transmitter and receiver) in the system as an equation [59], [60], [5].

The MRC method is used to study magnetic resonant wireless power transfer systems by applying a scattering matrix [35], [54], [57]. This method is used because the practical measuring of scattering parameters is more convenient than other parameters at high frequencies.

However, in spite of the amount of research that has been done to study the one receiver wireless power transfer system, there is still a lack of similar studies about multiple receivers systems. Although some researchers work on three coils, four coils or even more, these coils refer to one transmitter and one receiver and each one consists of two or more loops [9], [38], [59], [60], [61], [62], [63], [64]. Adding one or more relay resonators between the transmitter and the receiver leads to expansion of the range of power transmission and optimisation of the frequency response of the wireless system over larger distances [65]. In other words, this can extend the distance between the transmitter and the receiver [66].

The lack of studies about multiple receivers motivated us to present our approach to calculate the power transfer efficiency for multiple receivers in a magnetic resonant wireless system. In addition, most researchers work on coils with equal cross sectional areas whereas this is not always the case in real world systems. Studying different cross sectional areas is necessary in order to continue with multiple receiver systems. The full analysis of the system via our method, depending on circuit theory, is included in chapter three.

2.2.2 A solution to frequency splitting using double sided symmetric capacitors

A magnetic resonant wireless power transfer system delivers the maximum power at a specific distance between the two coils where the conditions of the impedance matching are met; that is because of the distance dependence of the mutual inductance. After this distance, the received power decreases. Unexpected decrease happens with a smaller distance between the coils. This drop is due to the overmatching between the two coils and the impedance matching conditions are not met anymore which leads to a frequency splitting into two new frequencies around the original one [57], [60], [5]. This is a real problem in the performance of a magnetic resonant wireless power transfer system.

A notable number of studies have been done to explain or solve the frequency splitting problem. In [67], the authors analyse the basic construction of a magnetic wireless system and explain the reasons for this phenomenon. Imura et al. in [57], presented the performance of the system at a high frequency with a large amount of power in addition to the large air gap, which are the requirements of electric vehicle charging. They show the frequency splitting at different distances.

To solve the frequency splitting problem and improve the power transfer efficiency at a specific distance, different ideas have been presented [58]. These are: impedance matching [37], [54], frequency tracking [68], [69], [70], and changing the parameters of the resonators [71] or the coupling between them [72], [73], [74]. The changing methods are not practical because most systems consist of a fixed pair of resonators. In the frequency tracking and frequency matching techniques, the power source tracks one of the two new frequencies that transfer maximum power. This looks acceptable

unless the tracked frequency moves out of the ISM bands, which is more likely to happen when the two peaks diverge [58].

The most common method is impedance matching. Beh et al. in [54], used a variable capacitor to match the impedance so as to tune the antenna receiver to the original resonance frequency at different air gaps by adding a matching circuit in the transmitter with a variable capacitor and varying it manually to tune the resonance frequency. After that Beh et al. in [58], tried in another study to solve the problem with a more realistic model. They measured and reduced the reflected wave ratio at the transmitting side by adding a set of capacitors and coils, and controlled them by multiple relays as an impedance matching circuit to adjust the resonance frequency [58]. Zhang et al. in [5], proposed adding an adjustable impedance matching network at the input side.

However, the previous methods are either impractical or potentially unacceptable. This motivated us to present our method which has advantages even over impedance matching. In our method, it is possible to keep the frequency inside the ISM band and achieve the maximum transfer of power similar to the original frequency without adding any impedance matching circuit. The full analysis of the proposed method is included in chapter four.

2.2.3 Studying the impact of connection type on power transfer efficiency

As mentioned previously, a magnetic resonant wireless power transfer system consists of two coils resonating at the same frequency by adding a capacitor to each one. The connection of this capacitor can be either in series or parallel according to the application of the system. Therefore, the system may have one of four potential

topologies; series - series (SS), series - parallel (SP), parallel - series (PS), or parallel - parallel (PP). Due to the differences between series resonance circuits and parallel resonance circuits, it is expected that the performance of each topology will differ from the others. However, most papers that study and analyse magnetic resonant wireless systems work on the series - series connection type [35], [54], [57], [58], [5], [75], [34].

The lack of analysis of systems with other types of connections (SP, PS, and PP), inspired us to apply our approach to calculate the power transfer efficiency of these topologies. The full analysis of them via our method is included in chapter five. The chapter also presents another mode to find out the maximum power transfer efficiency of the wireless system and its associated frequency which can be different from the resonant frequency in some cases. The method includes the numerical solution of the input impedance equation. The series - parallel type connection has been chosen to examine the method and calculate the required values.

2.2.4 Intelligent management and control of received wireless power

In this section it is important to know about the concept of energy harvesting. This is the process of deriving energy from one of different external sources such as solar, thermal, vibration, or wireless RF [76]. The main application for energy harvesting is charging remote batteries or powering battery free applications [77], [78].

Wireless charging can be achieved by broadcasting radio waves and even by a directed beam (point-to-point). The key technology in both cases is the rectifying antenna (rectenna). This is a passive element with rectifying diodes that works without an internal power source [79]. The rectenna converts the received RF waves to a dc

voltage which charges the target battery [80]. Some devices include capacitors instead of batteries to act in the same role (dc source for the application) [81].

The performance of energy harvesting systems is affected by the characteristics of its elements. Some researchers present different studies to improve the performance. The effect of the capacitor characteristics on the harvesting efficiency is examined in [81]. A special design of rectenna which consists of Shottky diodes and circular dipole antennas was investigated to increase the dc level and then the received power in [82]. Another group of researchers tried to improve the harvesting efficiency in a different way [83]. They present a multiband harvesting method, where numbers of narrowband rectifier chains followed the wideband antenna. Each one consists of three steps: band pass filter, tuning network and a rectifier. This technique can be effective in mobile applications.

Practically, there are some devices which have been producted by Power-Cast Group. These products are power harvester receivers [84]. These devices can harvest RF energy and convert it into dc power for either remotely charging batteries or remotely charging the internal capacitor of a battery free device. These two types of products are P1110B 915 MHz RF Power Harvester Receiver and P2110B 915 MHz RF Power Harvester Receiver, respectively. Another device related to the same group is TX91501 – 915 MHz powercaster transmitter [85] which can transmit the radio frequency.

However, the received power has to cover the requirement of the load application. Otherwise, the load stops working. This motivated us to present our algorithm to manage insufficiently received power via an intelligent control system. Chapter five presents the details about storing the energy and the used control algorithm.

Chapter 3

Analysis of Magnetic Resonance Wireless Power Transfer System

As mentioned before, circuit theory (CT) is more convenient for designers and engineers to analyse magnetic resonant wireless power transfer systems. In this method, the equivalent circuit of the wireless system is found. In the circuit, the mutual inductance represents the magnetic coupling between the transmitter and the receiver coils. Then the equivalent circuit is expressed in different equations to calculate the power transfer efficiency. Some researchers depend on a scattering matrix while others work on an impedance matrix [52]. As an example of using a scattering matrix, the researchers analysed an equivalent circuit wireless system and found its power transfer efficiency at different distances between the transmitter and the receiver, demonstrating optimum performance at a specific point [35]. It is clear that the performance of wireless power transfer changes due to several factors such as the distance between the transmitter and the receiver [32, 33, 35].

Magnetic resonance wireless systems in some applications consist of one transmitter and one receiver such as a single wireless charging system of electric vehicles. However, in other applications there is a demand to transfer power at the same time to

more than one receiver, such as the multiple wireless charging system of mobile phones or small rechargeable equipment. Hence the importance of studying systems with multiple receivers arises.

In this chapter, a complete study is presented to analyse magnetic resonant wireless power transfer systems. An essential part of this study is the calculation of the mutual inductance between coils in different spatial situations. The study consists of the effect of various factors on the performance of the system, such as resonant frequency, distance between coils, size of coils including the cross sectional area and number of turns. Coils with asymmetric cross sectional areas are considered in the work. In addition, one, two and more receivers are used in the study. The equivalent circuit of the magnetic coupling system is proposed to study the power transfer efficiency of wireless power transfer with one or multiple receivers. The optimum performance of the wireless power transfer system has been demonstrated for various cases.

The findings of our study can be used to form the basis of any multiple receiver system. The proposed method can also be applied analytically at different frequencies. To investigate the results practically, experiments have been conducted inside a Faraday cage at different frequencies of 2.1MHz and 2.5MHz. Choosing these frequencies is due to practical considerations such as ac signal sources and the dimensions of the coils.

3.1 Mutual Inductance Calculation

3.1.1 Coaxial coils

According to [35], the Neumann formula can be applied to find the mutual inductance (M_{21}) between two current filaments:

$$M_{21} = \frac{\mu_0}{4\pi} \oint\oint \frac{dl_1 . dl_2}{|r_1 - r_2|} \tag{3.1}$$

where μ_0 is permeability of free space and dl_1 and dl_2 are infinitesimal line segments of the loop 1 and loop 2 at positions r_1 and r_2 respectively, as shown in Figure 3.1.

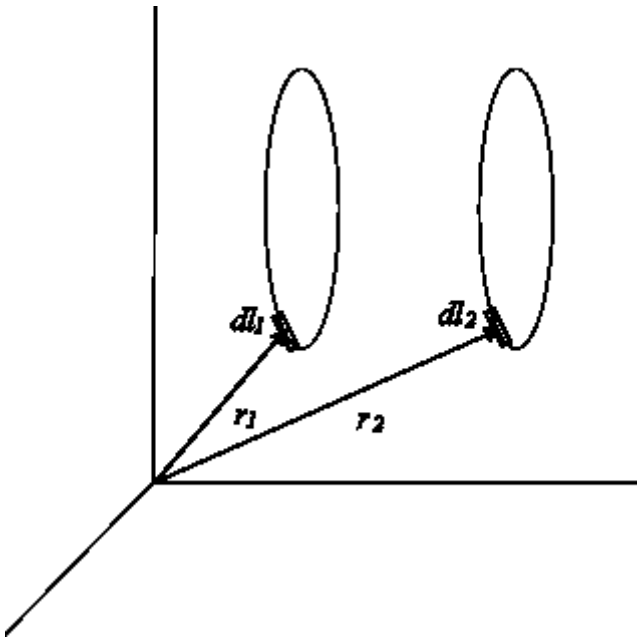

Figure 3.1 Mutual inductance between two loops by Neumann formula

For two coaxial turns with radiuses of A and a, and distance between centres of D, equation (3.1) can be written in terms of regular integral as:

$$M_{21} = \frac{\mu_o}{4\pi} \int_0^{2\pi}\int_0^{2\pi} \frac{Aa\cos(\varphi - \varphi')d\varphi d\varphi'}{\sqrt{A^2 + a^2 + D^2 - 2Aa\cos(\varphi - \varphi')}} \tag{3.2}$$

where φ and φ' are the azimuthal angle around the circular loops in cylindrical coordinates. The solution for this integral can be achieved by the next equation [86]:

$$M_{21} = \mu_o \sqrt{Aa}\left[\left(\frac{2}{\kappa} - \kappa\right)K(\kappa) - \frac{2}{\kappa}E(\kappa)\right] \tag{3.3}$$

$$\kappa = \frac{2\sqrt{Aa}}{\sqrt{(A+a)^2 + D^2}} \tag{3.4}$$

where K and E: the first and second kind of the complete elliptic integral and they are defined as:

$$K = \int_0^{\pi/2} \frac{d\varphi}{\sqrt{1-\kappa^2 \sin^2 \varphi}} \tag{3.5}$$

$$E = \int_0^{\pi/2} \sqrt{1-\kappa^2 \sin^2 \varphi} d\varphi \tag{3.6}$$

The mutual inductance between two coils is calculated by the summation of the mutual inductance between each two turns from the two coils. In case of a solenoid the gap between the two coils is not the same distance between all turns as shown in Figure 3.2.

As a modification to deal with the solenoid coil of more than one turn, the following expression was used instead of D in equation (3.4):

$$D(j_1, j_2) \rightarrow D + (j_1 - 1)p + (j_2 - 1)p \tag{3.7}$$

where p is the pitch between turns from centre to centre, $j_1 = 1 \rightarrow N_1$, $j_2 = 1 \rightarrow N_2$, N_1 and N_2 are the number of turns for each coil.

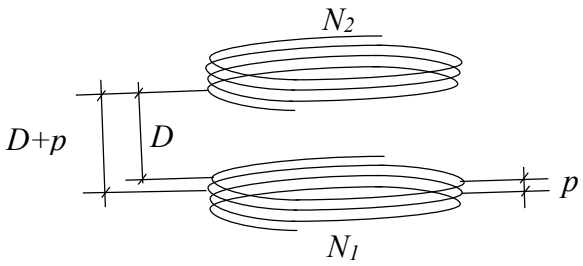

Figure 3.2 Two coaxial solenoid coils

Finally, the total mutual inductance between two coaxial coils with multiple turns can be found by [86]:

$$M_{total} = \sum_{j_1=1}^{N_1} \sum_{j_2=1}^{N_2} M_{j_1 j_2} \tag{3.8}$$

3.1.2 Parallel coils

Mutual inductance calculation between two parallel coils needs another formula instead of the equation (3.2). In [87], the researchers presented a formula to express the mutual inductance between two turns with lateral misalignment and two turns at the same level.

1) Lateral Misalignment

If the two turns are located at different levels as shown in Figure 3.3, the mutual inductance between them can be calculated by:

$$M = \frac{\mu_o}{\pi} \sqrt{Aa} \int_o^{\pi} \frac{\left(1 - \frac{d}{a}\cos\varphi\right)}{\sqrt{\nu^3}} \left(\left(\frac{2}{\kappa} - \kappa\right) K(\kappa) - \frac{2}{k} E(\kappa) \right) d\varphi \tag{3.9}$$

where

$$\kappa^2 = \frac{4\alpha\nu}{(1+\alpha\nu)^2 + \beta^2} \tag{3.10}$$

$$\nu = \sqrt{1 + \frac{d^2}{a^2} - \frac{2d}{a}\cos\varphi} \tag{3.11}$$

$$\alpha = \frac{a}{A} \tag{3.12}$$

$$\beta = \frac{g}{A} \tag{3.13}$$

where d is the distance between axes and g is the distance between planes of coils

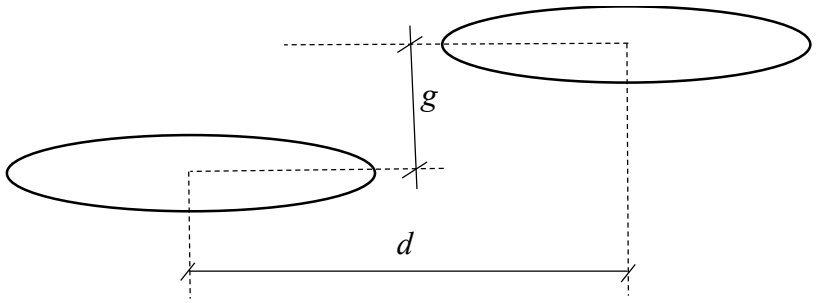

Figure 3.3 Lateral misalignment turns

2) Two turns at the same level

The same formula in equation (3.9) can be applied to calculate the mutual inductance between two turns at the same level; in this case (g) equals zero.

Again, the mutual inductance between each of the two turns of the two parallel coils can be summed by equation (3.8) to find the total mutual inductance.

3.2 Magnetic Resonance Wireless Power Transfer

As mentioned in chapter two, the principle of the mutual induction phenomena between two coils is the continuous passing of a varying current through one of the coils called the primary coil leading to the production of a magnetic field around it. The interaction of this magnetic field with the second coil, called the secondary coil, leads to an induced current in it as shown in Figure 3.4. The maximum interaction happens when the two coils work at the same frequency and the mutual induction here is called magnetic resonance [4], [6], [88].

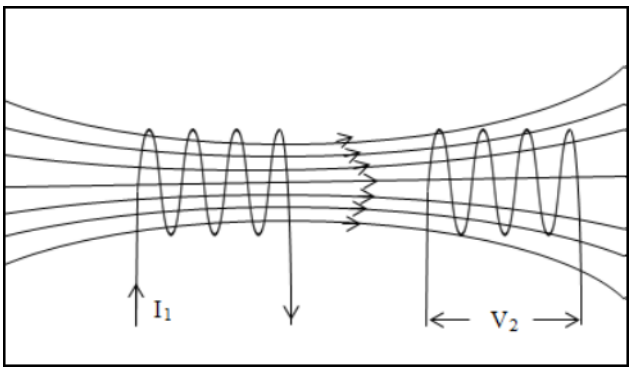

Figure 3.4 Mutual induction process

3.3 Resonance Coupled System Representation

3.3.1 One load system representation

A simple wireless power transmission system consists of a transmitter and a receiver as shown in Figure 3.5. The transmitter is represented by the source *Vs* and its internal

resistor R_S, the capacitor C_1 and the inductor L_1, while C_2 and L_2 are the capacitor and the inductor that achieve the resonance to transfer the power to the load resistor R_2. The oscilloscope is connected over R_2 in order to measure the output voltage.

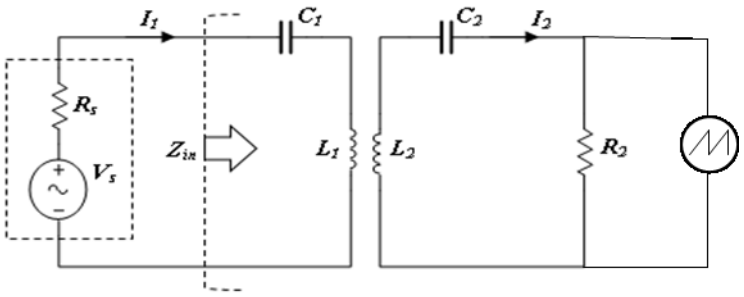

Figure 3.5 Equivalent circuit of a wireless power transfer system consists of one transmitter and one receiver

Due to the inductance value of each coil, capacitor values are chosen to achieve the resonance condition (when the inductive reactance X_L is equal to the capacitive reactance X_C) through the resonance frequency equation [89]:

$$f_o = \frac{1}{2\pi\sqrt{L_1 C_1}} = \frac{1}{2\pi\sqrt{L_2 C_2}} \tag{3.14}$$

3.3.2 Two load system representation

The same principle can be used to represent a system with two or more receivers. Figure 3.6 shows a schematic circuit of a resonant coupled system which consists of a transmitter and two receivers. It shows the basic variables which are used in the calculation of mutual inductance. The variables A and a are the radius of the transmitter and each receiver, respectively. The distances between the transmitter and each receiver and between the two receivers are represented by D and d, respectively. Finally, p is the pitch between any two turns in any of the coils. It is clear from this

circuit that the calculation method of mutual inductance between the transmitter and each receiver is different than the mutual inductance between the two receivers due to variation in location. Different methods are proposed to calculate the mutual inductance for each case [86, 87].

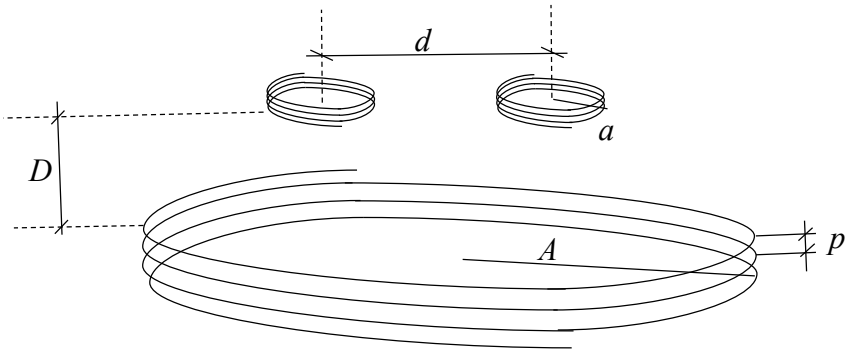

Figure 3.6 Schematic circuit of coils for a system consisting of one big transmitter coil and two small parallel receivers

The equivalent circuit of a wireless power transfer system with two receivers is shown in Figure 3.7. In the figure, the source V_S drives a transmitter coil and its internal resistance is R_S. L_1 and C_1 are the inductance and the capacitance of the transmitter. On the other side of the circuit, the first receiver is represented by L_2, C_2, and R_2 as an inductor, capacitor and load resistor, respectively. Similarly, L_3, C_3, and R_3 form the second receiver.

The second receiver should be under the resonance condition with the same resonance frequency.

$$f_0 = \frac{1}{2\pi\sqrt{L_3 C_3}} \tag{3.15}$$

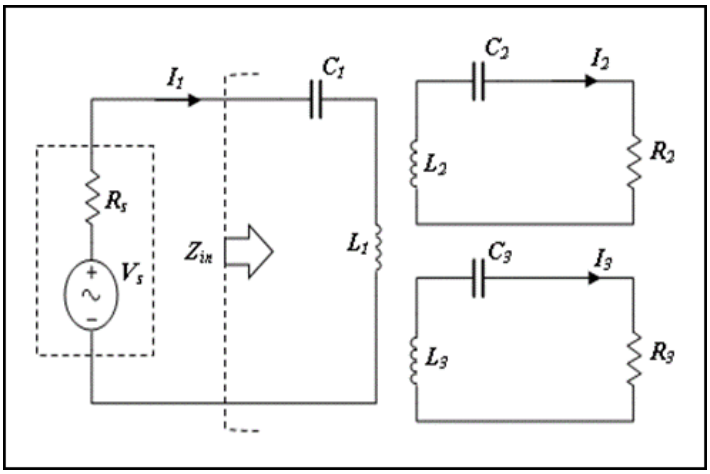

Figure 3.7 Equivalent circuit of a wireless power transfer system with one transmitter and two receivers

3.4 Basics of Theoretical Analysis

To start the analysis with one load system (Figure 3.5), Kirchhoff's law of voltage is applied to each loop (the transmitter and the receiver) in order to obtain the simultaneous equations.

$$V_S = Z_1 I_1 - j\omega M I_2 \tag{3.16a}$$

$$0 = -j\omega M I_1 + Z_2 I_2 \tag{3.16b}$$

where the complex impedances for each circuit are:

$$Z_1 = R_S + j\left(\omega L_1 - \frac{1}{\omega C_1}\right) \tag{3.17}$$

$$Z_2 = R_2 + j\left(\omega L_2 - \frac{1}{\omega C_2}\right) \tag{3.18}$$

M is the mutual inductance between the coils, ω is the angular frequency (=$2\pi f$), I_1 and I_2 are the loop's currents. Writing (3.16) in matrix form,

$$\begin{bmatrix} V_s \\ 0 \end{bmatrix} = \begin{bmatrix} Z_1 & -j\omega M \\ -j\omega M & Z_2 \end{bmatrix} \begin{bmatrix} I_1 \\ I_2 \end{bmatrix} \tag{3.19}$$

The solutions to (3.19) can be found via Cramer's rule and are

$$I_1 = \frac{Z_2 V_S}{Z_1 Z_2 + \omega^2 M^2} \tag{3.20}$$

$$I_2 = \frac{j\omega M V_S}{Z_1 Z_2 + \omega^2 M^2} \tag{3.21}$$

3.4.1 Maximum power transfer

From (3.20), the total impedance of the transmitter is defined as:

$$\frac{V_S}{I_1} = Z_1 + \frac{\omega^2 M^2}{Z_2} \tag{3.22}$$

and hence the input impedance seen by the source Z_{in}, as shown in Figure 3.5, is found from:

$$Z_{in} = \frac{V_S}{I_1} - R_S \tag{3.23}$$

Using (3.17) and (3.18) leads to:

$$Z_{in} = \frac{\omega^2 M^2 R_2}{R_2^2 + \left(\omega L_2 - 1/\left(\omega C_2\right)\right)^2} + j\left[\omega L_1 - \frac{1}{\omega C_1} - \frac{\omega^2 M^2 \left(\omega L_2 - 1/\left(\omega C_2\right)\right)}{R_2^2 + \left(\omega L_2 - 1/\left(\omega C_2\right)\right)^2}\right] \quad (3.24)$$

According to the power transfer theorem for complex impedances, the maximum power will be transferred when:

$$Z_S = Z_{in}^* \quad (3.25)$$

Where Z_S is the impedance of the source. In this case, we have $Z_S = R_S$, which is purely real, so the condition of (3.25) requires that the imaginary part of the input impedance given in (3.24) disappears. This is satisfied if $L_1 = L_2 = L$, $C_1 = C_2 = C$ and $\omega = \omega_0 = 1/\sqrt{LC}$, the resonance angular frequency of the circuits. This means resonance is a condition and leads to:

$$Z_{in} = \frac{\omega_0^2 M^2}{R_2} = R_S \quad (3.26)$$

The condition for maximum power transfer is then:

$$\frac{\omega_0^2 M^2}{R_2 R_S} = 1 \quad (3.27)$$

So, the optimal distance to transfer the maximum power between the coils is where this condition is achieved. Working at higher frequency for the same coils requires smaller mutual inductance to achieve the condition that means larger distance between these two coils.

We note that M will decrease with increasing distance between the transmitter and receiver coil. Proposing a dependency of the form:

$$M = M_0 e^{-D/D_0} \tag{3.28}$$

where M_0 is the maximum value of the mutual inductance at zero distance, and D_0 is the constant that specifies the rate of the decline of the mutual inductance. Consistent with the figure of mutual inductance against distance, we find from (3.27) and (3.28) that the optimal distance for maximum power transfer will be at

$$D_{\max} = \frac{D_0}{2}\left[\ln\left(\omega_0^2 M_0^2\right) - \ln\left(R_2 R_S\right)\right] \tag{3.29}$$

Neglecting any ω dependence on M_0, this result suggests that the optimal distance for power transfer will increase with frequency. In reality, M will be frequency dependent, since the extent of the reactive near-field of the transmitter will be proportional to the wavelength. This have the effective of reducing the optimal distance with frequency, meaning that overall, the optimal distance does not increase monotonically with distance.

3.4.2 Figure of merit

A figure of merit η_0 is defined in terms of the ratio of the output power to the input power under the condition of maximum power transfer. In other words η_0 describes the power transfer efficiency:

$$\eta_0 = \frac{P_{out}}{P_{in,\max}} \tag{3.30}$$

where:

$$P_{out} = \frac{1}{2}\left|I_2\right|^2 R_2 \tag{3.31}$$

From (3.30), η_0 is the normalization of the output power in terms of P_{in} constrained to the value for the maximum power transfer. That is, we place $Z_{in} = R_S$ and from $\left|I_1\right| = \left|V_S/\left(R_S + Z_{in}\right)\right|$ obtain:

$$P_{in,\max} = \frac{V_S^2}{8R_S} \tag{3.32}$$

The figure of merit is then:

$$\eta_0 = \frac{4\omega^2 M^2 R_2 R_S}{\left|Z_1 Z_2 + \omega^2 M^2\right|^2} \tag{3.33}$$

where, for matched inductances and capacitances in the circuits:

$$\left|Z_1 Z_2 + \omega^2 M^2\right|^2 = \left[R_S R_2 + \omega^2 M^2 - \left(\omega L - \frac{1}{\omega C}\right)^2\right]^2 + \left[\left(R_S + R_2\right)\left(\omega L - \frac{1}{\omega C}\right)\right]^2 \tag{3.34}$$

when $\omega = \omega_0$, (3.34) reduces to:

$$\left|Z_1 Z_2 + \omega^2 M^2\right|^2 = \left(R_S R_2 + \omega^2 M^2\right)^2 \tag{3.35}$$

and then:

$$\eta_0 = \frac{4\omega_0^2 M^2 R_S R_2}{\left(R_S R_2 + \omega_0^2 M^2\right)^2} \tag{3.36}$$

Imposing the condition for maximum power transfer of (3.27), leads to $\eta_0 = 1$.

3.5 Multiple Receivers Theoretical Analysis

Following the same theoretical analysis as for a single receiver system we extend the method for a number of receivers; this is the main contribution of this chapter.

3.5.1 Two receivers

For the circuit shown in Figure 3.7, Kirchhoff's law of voltage is applied to each loop (the transmitter and the two receivers) with regard to the mutual inductance between each pair of coils [5]. The mutual inductance between the transmitter and the first and second receiver are M_{12} and M_{13}, respectively. Both follow the same calculation method because of their location to the transmitter. As a special case, M_{12} is equal to M_{13} if the two receivers are identical, while M_{23}, the mutual inductance between the two receivers has to be calculated using another method due to their parallel nature.

$$V_S = Z_1 I_1 - j\omega M_{12} I_2 - j\omega M_{13} I_3 \tag{3.37a}$$

$$0 = -j\omega M_{21} I_1 + Z_2 I_2 + j\omega M_{23} I_3 \tag{3.37b}$$

$$0 = -j\omega M_{31} I_1 + j\omega M_{32} I_2 + Z_3 I_3 \tag{3.37c}$$

where I_1, I_2 and I_3 are the loop's currents; and the complex impedances of each circuit are:

$$Z_1 = R_S + j\left(\omega L_1 - \frac{1}{\omega C_1}\right) \tag{3.38}$$

$$Z_2 = R_2 + j\left(\omega L_2 - \frac{1}{\omega C_2}\right) \tag{3.39}$$

$$Z_3 = R_3 + j\left(\omega L_3 - \frac{1}{\omega C_3}\right) \tag{3.40}$$

Writing (3.37) in matrix form:

$$\begin{bmatrix} V_S \\ 0 \\ 0 \end{bmatrix} = \begin{bmatrix} Z_1 & -j\omega M_{12} & -j\omega M_{13} \\ -j\omega M_{21} & Z_2 & j\omega M_{23} \\ -j\omega M_{31} & j\omega M_{32} & Z_3 \end{bmatrix} \begin{bmatrix} I_1 \\ I_2 \\ I_3 \end{bmatrix} \tag{3.41}$$

The solutions to (3.41) can be found via Cramer's rule and are:

$$I_1 = Z_{1,1}^{-1} V_S \tag{3.42}$$

$$I_2 = Z_{2,1}^{-1} V_S \tag{3.43}$$

$$I_3 = Z_{3,1}^{-1} V_S \tag{3.44}$$

Here, the output power for each receiver can be calculated:

$$P_{out1} = \frac{1}{2}\left|I_2\right|^2 R_2 \tag{3.45}$$

$$P_{out2} = \frac{1}{2}\left|I_3\right|^2 R_3 \tag{3.46}$$

Under the condition of maximum transfer of power, the figure of merit for each receiver is then:

$$\eta_{01} = \frac{P_{out1}}{P_{in,\max}} = 4R_S R_2 \left|Z_{2,1}^{-1}\right|^2 \tag{3.47}$$

$$\eta_{02} = \frac{P_{out2}}{P_{in,\max}} = 4R_S R_3 \left|Z_{3,1}^{-1}\right|^2 \tag{3.48}$$

3.5.2 Three receivers

A similar representation for the two-receivers system can be applied to the three receivers system:

$$V_S = Z_1 I_1 - j\omega M_{12} I_2 - j\omega M_{13} I_3 - j\omega M_{14} I_4 \tag{3.49a}$$

$$0 = -j\omega M_{21} I_1 + Z_2 I_2 + j\omega M_{23} I_3 + j\omega M_{24} I_4 \tag{3.49b}$$

$$0 = -j\omega M_{31} I_1 + j\omega M_{32} I_2 + Z_3 I_3 + j\omega M_{34} I_4 \tag{3.49c}$$

$$0 = -j\omega M_{41} I_1 + j\omega M_{42} I_2 + j\omega M_{43} I_3 + Z_4 I_4 \tag{3.49d}$$

where I_1, I_2, I_3 and I_4 are the loop's currents; and the complex impedances of each circuit are:

$$Z_1 = R_S + j\left(\omega L_1 - \frac{1}{\omega C_1}\right) \tag{3.50}$$

$$Z_2 = R_2 + j\left(\omega L_2 - \frac{1}{\omega C_2}\right) \tag{3.51}$$

$$Z_3 = R_3 + j\left(\omega L_3 - \frac{1}{\omega C_3}\right) \tag{3.52}$$

$$Z_4 = R_4 + j\left(\omega L_4 - \frac{1}{\omega C_4}\right) \tag{3.53}$$

Writing (3.49) in matrix form:

$$\begin{bmatrix} V_S \\ 0 \\ 0 \\ 0 \end{bmatrix} = \begin{bmatrix} Z_1 & -j\omega M_{12} & -j\omega M_{13} & -j\omega M_{14} \\ -j\omega M_{21} & Z_2 & j\omega M_{23} & j\omega M_{24} \\ -j\omega M_{31} & j\omega M_{32} & Z_3 & j\omega M_{34} \\ -j\omega M_{41} & j\omega M_{42} & j\omega M_{43} & Z_4 \end{bmatrix} \begin{bmatrix} I_1 \\ I_2 \\ I_3 \\ I_4 \end{bmatrix} \tag{3.54}$$

The solutions to (3.54) can be found via Cramer's rule and are:

$$I_1 = Z_{1,1}^{-1} V_S \tag{3.55}$$

$$I_2 = Z_{2,1}^{-1} V_S \tag{3.56}$$

$$I_3 = Z_{3,1}^{-1} V_S \tag{3.57}$$

$$I_4 = Z_{4,1}^{-1} V_S \tag{3.58}$$

Here, the output power for each receiver can be calculated:

$$P_{out1} = \frac{1}{2}\left|I_2\right|^2 R_2 \tag{3.59}$$

$$P_{out2} = \frac{1}{2}\left|I_3\right|^2 R_3 \tag{3.60}$$

$$P_{out3} = \frac{1}{2}\left|I_4\right|^2 R_4 \tag{3.61}$$

Under the condition of maximum transfer of power, the figure of merit for each receiver is then:

$$\eta_{01} = \frac{P_{out1}}{P_{in,\max}} = 4R_S R_2 \left|Z_{2,1}^{-1}\right|^2 \tag{3.62}$$

$$\eta_{02} = \frac{P_{out2}}{P_{in,\max}} = 4R_S R_3 \left|Z_{3,1}^{-1}\right|^2 \tag{3.63}$$

$$\eta_{03} = \frac{P_{out3}}{P_{in,\max}} = 4R_S R_4 \left|Z_{4,1}^{-1}\right|^2 \tag{3.64}$$

3.5.3 N-receivers

The method can be applied in the general case for an N-receiver system and the general equation for any system is:

$$\begin{bmatrix} V_S \\ 0 \\ 0 \\ \vdots \\ 0 \end{bmatrix} = \begin{bmatrix} Z_1 & -j\omega M_{12} & -j\omega M_{13} & \cdots & -j\omega M_{1n} \\ -j\omega M_{21} & Z_2 & j\omega M_{23} & \cdots & j\omega M_{2n} \\ -j\omega M_{31} & j\omega M_{32} & Z_3 & \cdots & j\omega M_{3n} \\ \vdots & \vdots & \vdots & \cdots & \vdots \\ -j\omega M_{n1} & j\omega M_{n2} & j\omega M_{n3} & \cdots & Z_n \end{bmatrix} \tag{3.65}$$

3.6 Results and Discussion

The representation of a wireless power transfer system with one to N-receivers is programmed in Matlab to calculate the mutual inductance between coils and then the figure of merit. Practically, different sets of coils have been used to study the system and investigate the simulation results. Table 3.1 shows the parameters of each combination (coil and capacitor) to work at a particular frequency. The self-inductance of each prepared coil was measured by a digital multimeter.

Table 3.1: Parameters of combinations

Combination / **Parameters**	**1**	**2**	**3**	**4**
L (μH)	10.8	33	31.3	21.6
No. of turns	16	32	8	16
Pitch between the turns (mm)	3	3	3	3
Diameter of the coil (cm)	6	6	24.5	8.4
C (pF) at f_o = 2.1 MHz	550	174	188	270
C (pF) at f_o = 2.5 MHz	-	120	128	-

3.6.1 Single receiver system

3.6.1.1 The performance of the magnetic resonant wireless power transfer system and the influential factors

As mentioned previously in chapter two, the basis of near field wireless power transfer between any two coils is the process of magnetic induction. Passing an alternating

current through the first coil (transmitter), produces a magnetic field around it, and cutting the produced magnetic flux lines by the second coil (receiver) creates an electromotive force across it [4]. The ratio between the cross sectional areas of the receiver coil relative to the transmitter coil (Coil Area Ratio CAR) indicates the percentage of flux lines that are cut by the receiver.

Wireless power transfer using magnetic resonance requires cutting flux lines generated from the transmitter coil by the receiver coil. This section shows that an exact one to one coil area ratio or CAR (i.e. primary relative to secondary) is not a pre-condition to obtain high figure of merit.

Identical coils:

That is a one to one coil area ratio.

Experiment 1

As a starting point to demonstrate the previous analysis, a wireless power transfer system with two identical resonators was practically implemented by using a couple of combination 1 which is shown in Table 3.1. Each coil, with 3cm radius, 16 turns and 3mm pitch between the turns, and has an inductance equal to 10.8μH. One of them is the transmitter and the other is the receiver. Specific parameters, such as resonance frequency at 2.1 MHz, load resistor 50Ω, $C_1 = C_2 = 550$pF (which includes the natural capacitance of the coil) and the distance between the two coils of 3cm, were chosen. Next, finding the figure of merit over a range of frequencies was achieved as shown in Figure 3.8. The theoretical results (Th) are compared with the experimental results (Exp) in the figure. Practically, the voltage of the load resistor was measured by oscilloscope (as shown in Figure 3.5) over the range of frequencies to calculate the output power as:

$$P_{out} = \frac{|V_2|^2}{2R_2} \tag{3.66}$$

And then using (3.32) and (3.30) to find the experimental values of $P_{in,max}$ and η_0, respectively.

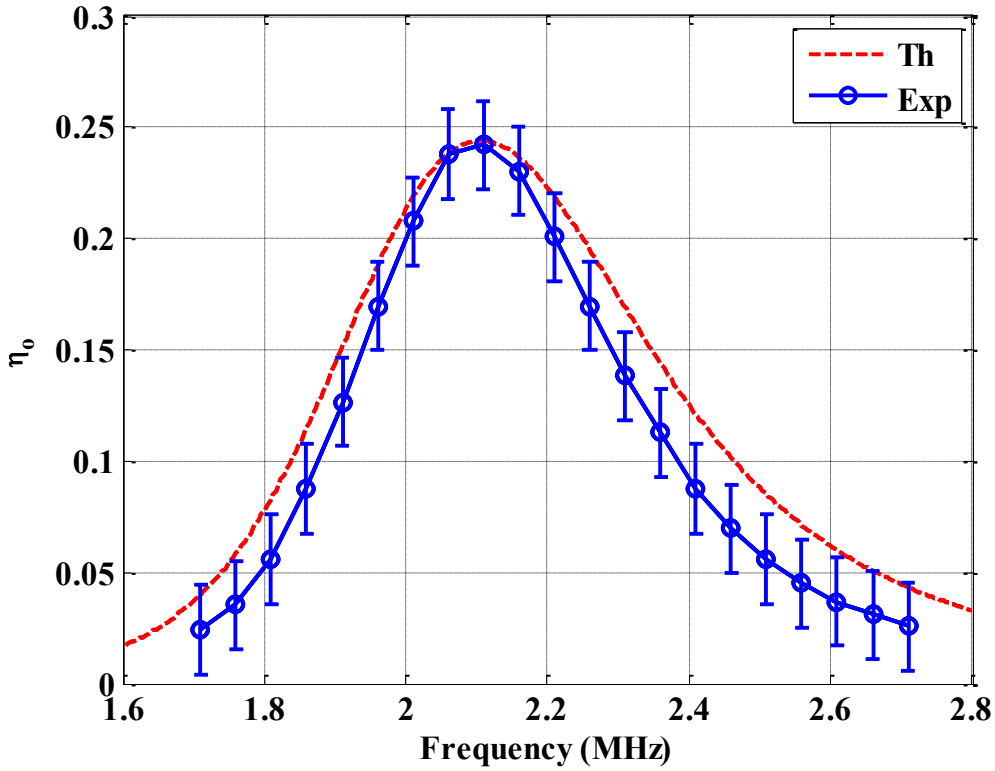

Figure 3.8 Figure of merit versus frequency for transmitter and receiver of combination 1 at 3cm distance, f_o = 2.1MHz, R_L = 50Ω

It is clear from Figure 3.8 that the highest figure of merit of 0.24 for wireless transfer happens at the resonance frequency. The figure shows the error bars for this case which represent the uncertainty (±0.02) for each calculated value due to the approximation in the least significant bit. The subsequent figures have similarly-sized uncertainties because they all have similar method of calculation. However, there is a good match

between the theoretical and practical results. However, the figure of merit here is relatively low; that is because of the small value of mutual inductance between the two coils, equal to 1.008μH.

A. Effect of mutual inductance

Experiment 2

The mutual inductance between any coupled coils is directly proportional to their number of turns. Substituting the two resonators of experiment 1 with a set of combination 2 in Table 3.1, increases the mutual inductance to 1.4μH. The coil in combination 2 has a higher number of turns than combination 1. Each coil has an inductance equal to 33μH, with 3cm radius, 32 turns and 3mm pitch between the turns. The environment of this experiment is shown in Figure 3.9. At the resonant frequency the system has a figure of merit of 0.42 at 3cm as shown in Figure 3.10.

Figure 3.9 Environment of experiment 2; combination 2 at 3cm distance, f_o = 2.1MHz, R_L = 50Ω

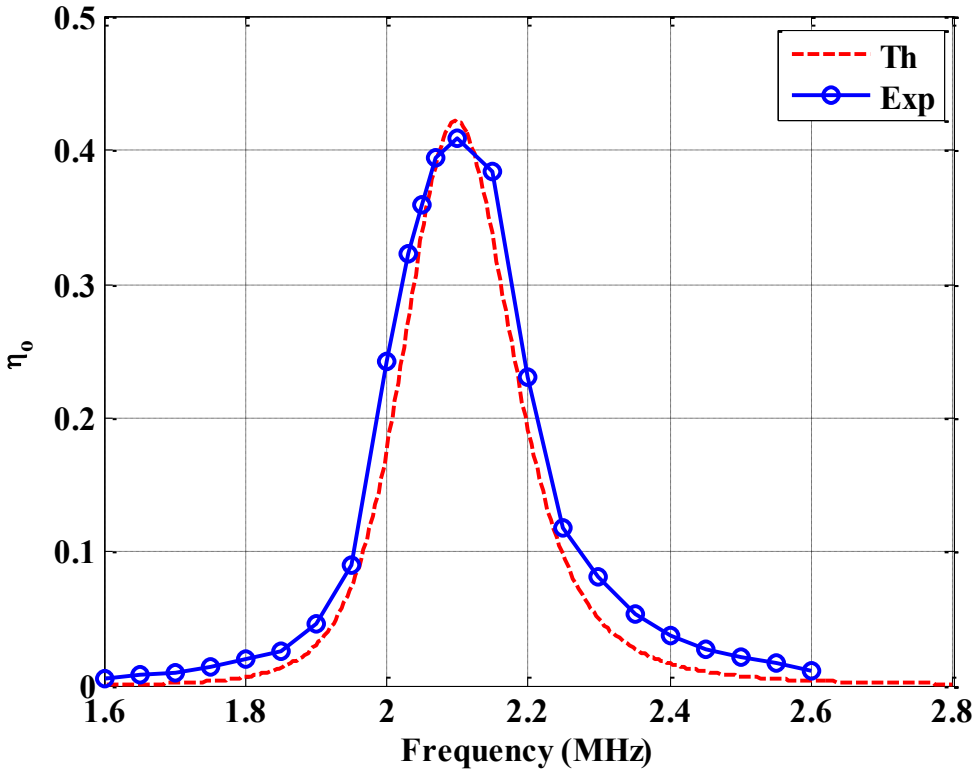

Figure 3.10 Figure of merit versus frequency for transmitter and receiver of combination 2 at 3cm distance, f_o = 2.1MHz, R_L = 50Ω

Experiment 3

The mutual inductance between any coupled coils is also directly proportional to their cross sectional area. In this experiment, the selected resonators are a couple of combination 3 in Table 3.1. Each coil has a 12.25cm radius, 8 turns and 3mm pitch between the turns, and 31.3 μH inductance. Working at the same frequency of 2.1MHz, 188pF capacitors are required for the transmitter and receiver.

The results are initially surprising; higher figure of merit occurs at a 16cm gap, in spite of near full flux being intersected for all cases. The reason is the difference in the mutual inductance which depends on the size of the two coils. In this experiment, the mutual inductance between the two coils is 2.05μH, which is larger compared with the

previous experiments. At the resonant frequency the system has a figure of merit of 0.7 at 16 cm, as shown in Figure 3.11.

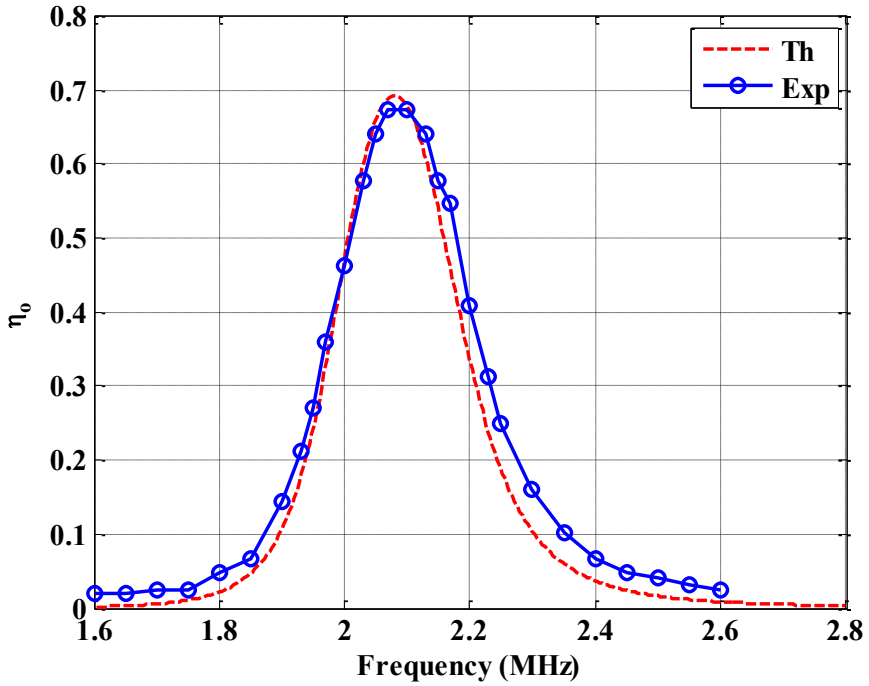

Figure 3.11 Figure of merit versus frequency for transmitter and receiver of combination 3 at 16 cm distance, f_o = 2.1MHz, R_L = 50Ω

B. Effect of distance

It was explained in section 2.1.5 that mutual inductance increases when the two coils approach. Figure 3.12 shows the effect of changing the distance between these two coils on the mutual inductance.

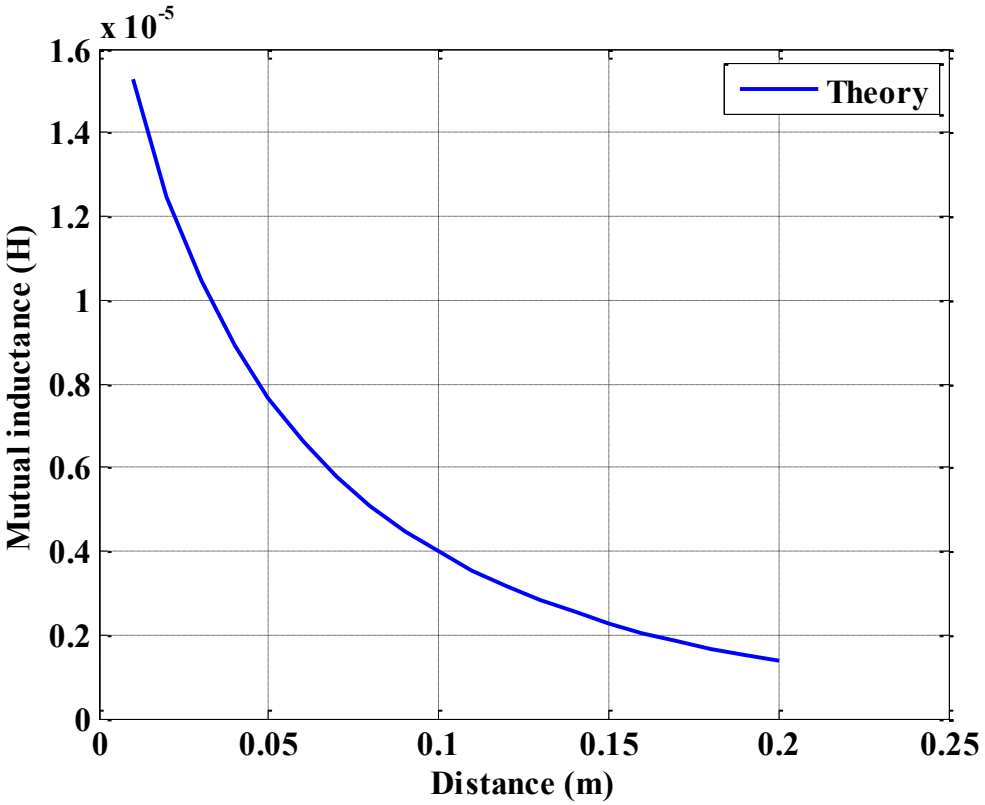

Figure 3.12 Mutual inductance versus distance for transmitter and receiver of combination 3

Experiment 4

Using the same coils (combination 3 in Table 3.1) at smaller distances, the figure of merit at the same resonant frequency gradually increases until it approaches the maximum value at a distance of 10.5cm. The figure of merit of the system as a function of frequency at this point is shown in Figure 3.13.

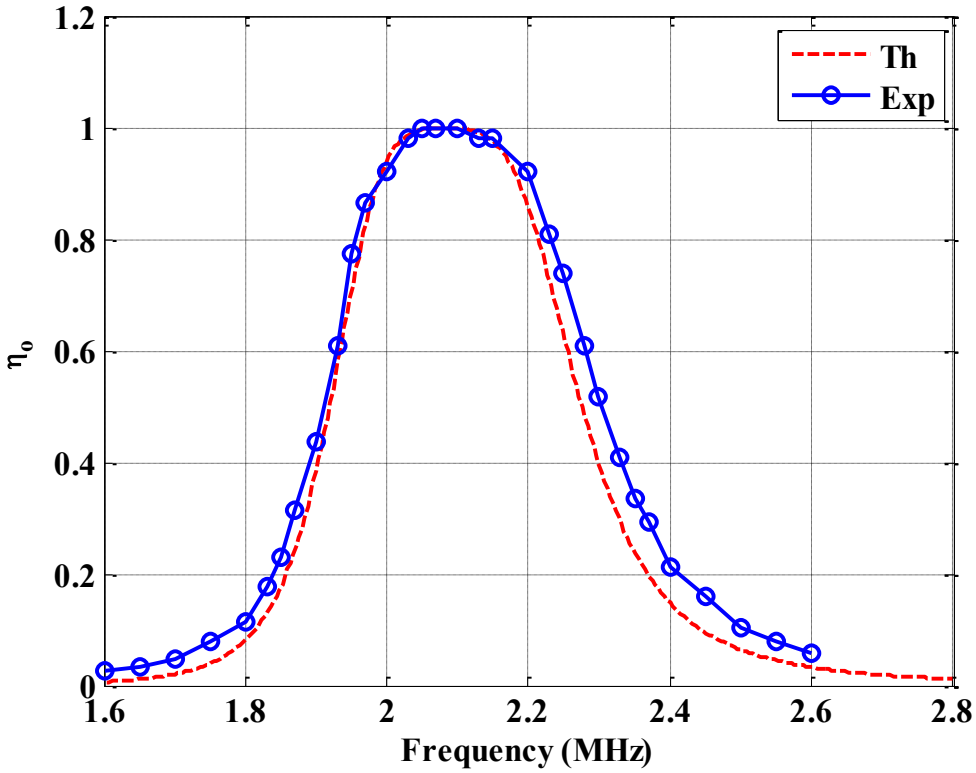

Figure 3.13 Figure of merit versus frequency for transmitter and receiver of combination 3 at 10.5cm distance, f_o = 2.1MHz, R_L = 50Ω

Experiment 5

A further decrease in the distance surprisingly leads to a decrease in the figure of merit of the system. As shown in Figure 3.14, there is a splitting in the figure of merit of the system at a distance of 3.5cm. This splitting starts to appear as the mutual inductance increases between the two coils (the transmitter and the receiver), increasing when the two coils are approaching. This effect shifts the maximum figure of merit to two distinct frequencies around the resonance frequency. The real environment of this experiment is shown in Figure 3.15.

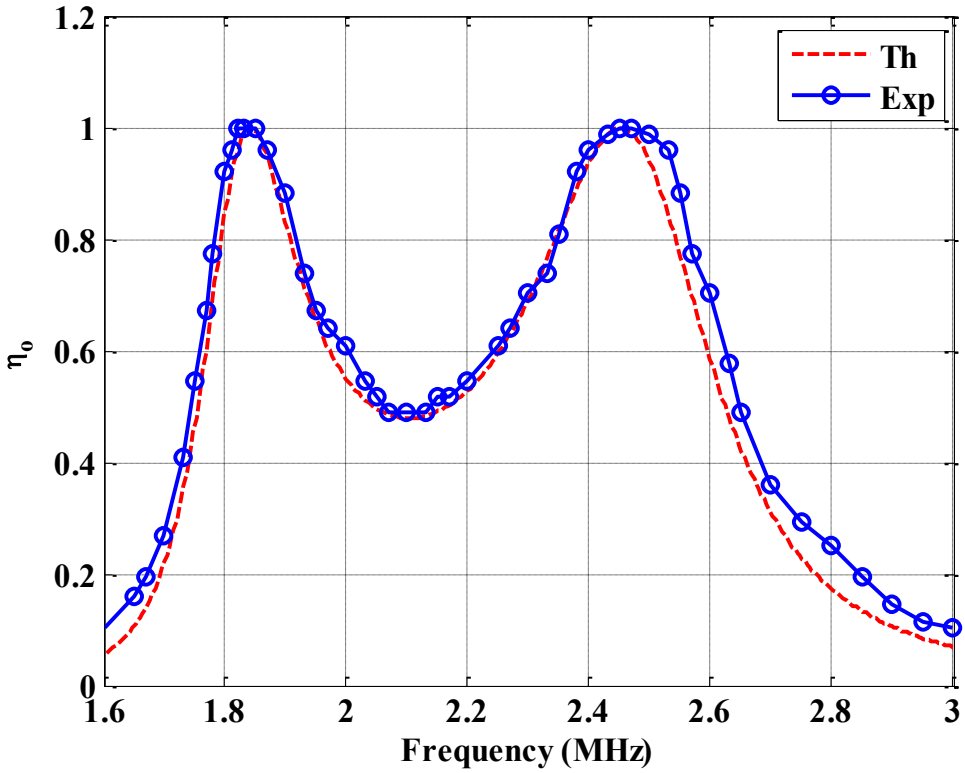

Figure 3.14 Figure of merit versus frequency for transmitter and receiver of combination 3 at 3.5cm distance, f_o = 2.1MHz, R_L = 50Ω

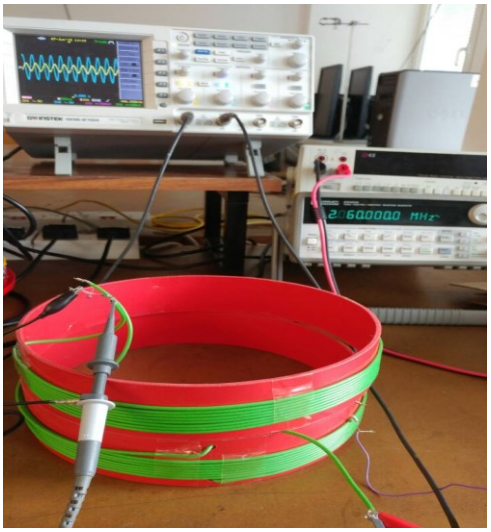

Figure 3.15 Environment of experiment 5; combination 3 at 3.5cm distance, f_o = 2.1MHz, R_L = 50Ω

Experiment 6

The last three experiments indicate that there is a perfect point to transfer the maximum power in the wireless system as shown in Figure 3.16 from the relationship between the figure of merit and the gap distance at the resonant frequency.

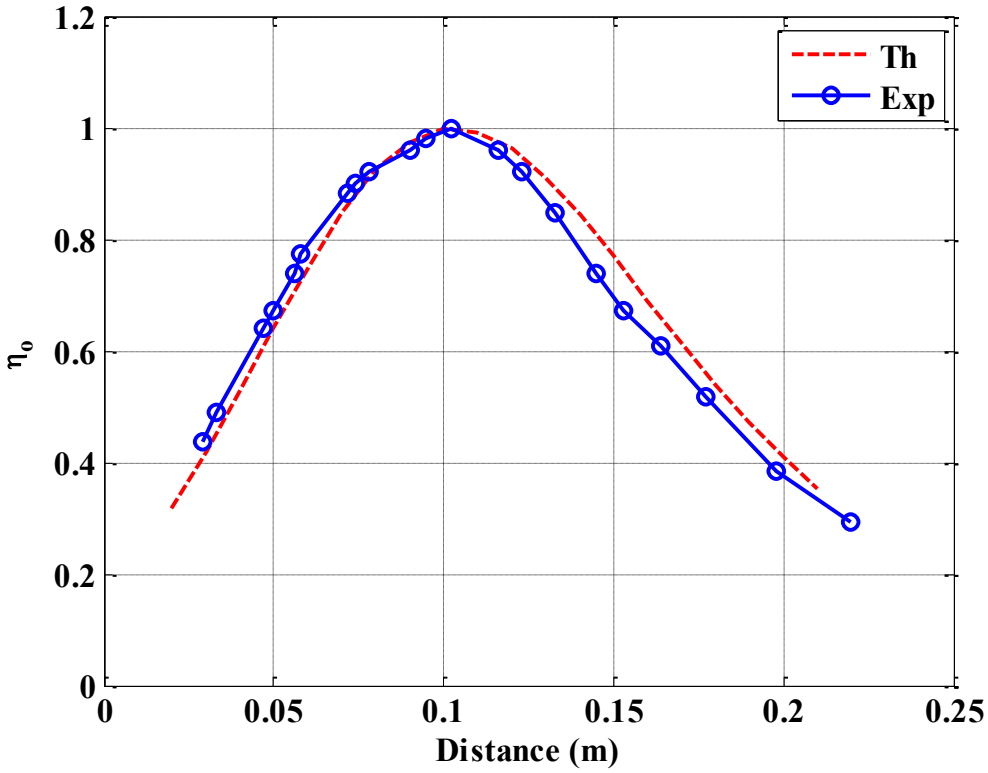

Figure 3.16 Figure of merit versus distance for transmitter and receiver of combination 3 at resonant frequency (f_o = 2.1MHz), R_L = 50Ω

The reason for this point is shown in Figure 3.17, where the input impedance of the system, which changes with the distance, equals 50Ω at this point. The 50Ω value is equal to the internal resistance of the source R_S which leads to the maximum transfer of power.

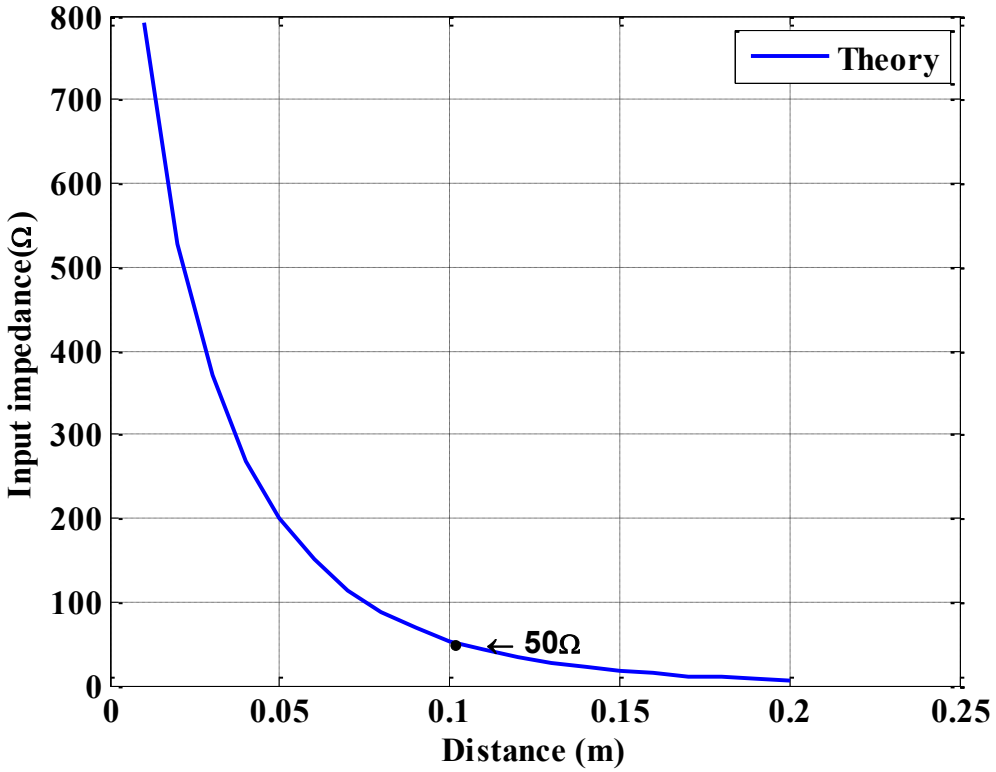

Figure 3.17 Input impedance versus distance for transmitter and receiver of combination 3 at resonant frequency (f_o = 2.1MHz), R_L = 50Ω

C. Effect of the load resistance

Experiment 7

Changing the value of the load resistor surely affects the input resistance of the system. Therefore, with a different load resistor, the maximum transfer of power happens at a different distance. Comparing with Figure 3.16, the system can transfer the maximum power for a larger distance (12.5cm) in the case of smaller load resistance (30Ω) and for a smaller distance (7.5cm) in the case of larger load resistance (100Ω) as shown in Figure 3.18a and 3.18b, respectively.

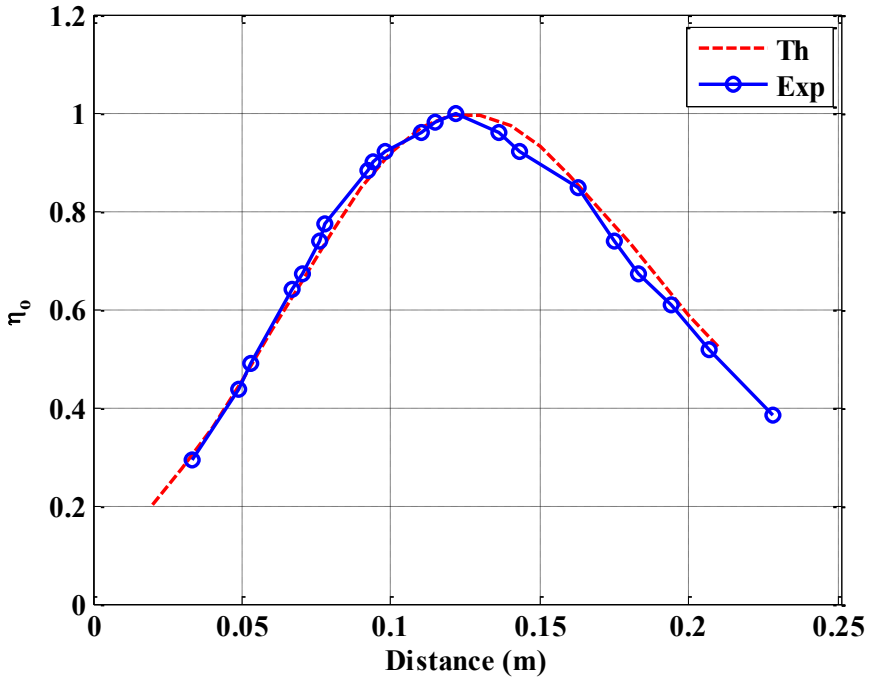

(a) $R_L = 30\Omega$

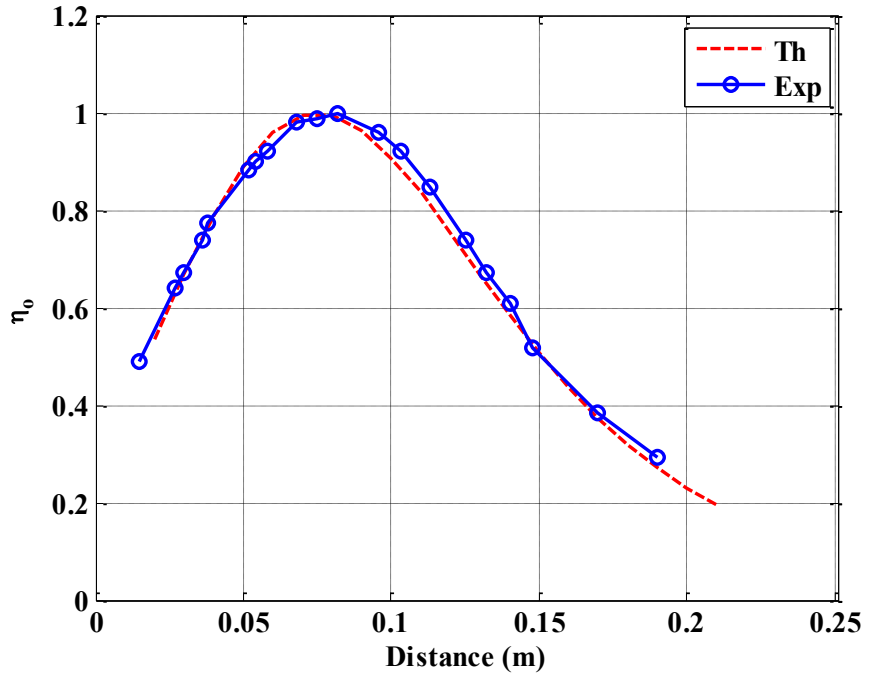

(b) $R_L = 100\Omega$

Figure 3.18 Figure of merit versus distance for transmitter and receiver of combination 3 at resonant frequency (f_o = 2.1MHz), with different load resistors

D. Effect of frequency

Experiment 8

Working at a different frequency will also affect the figure of merit of the wireless power transfer system. To show this effect, the capacitors of the transmitter and the receiver were adjusted from 188pF to 128pF in order to work at higher resonant frequency (2.52MHz). The figure of merit of the system versus frequency is shown in Figure 3.19 with 16cm distance between coils. Comparing with Figure 3.11, the higher frequency enables the system to transfer maximum power through a larger distance for the same coils, and this might be clearer through the next experiment.

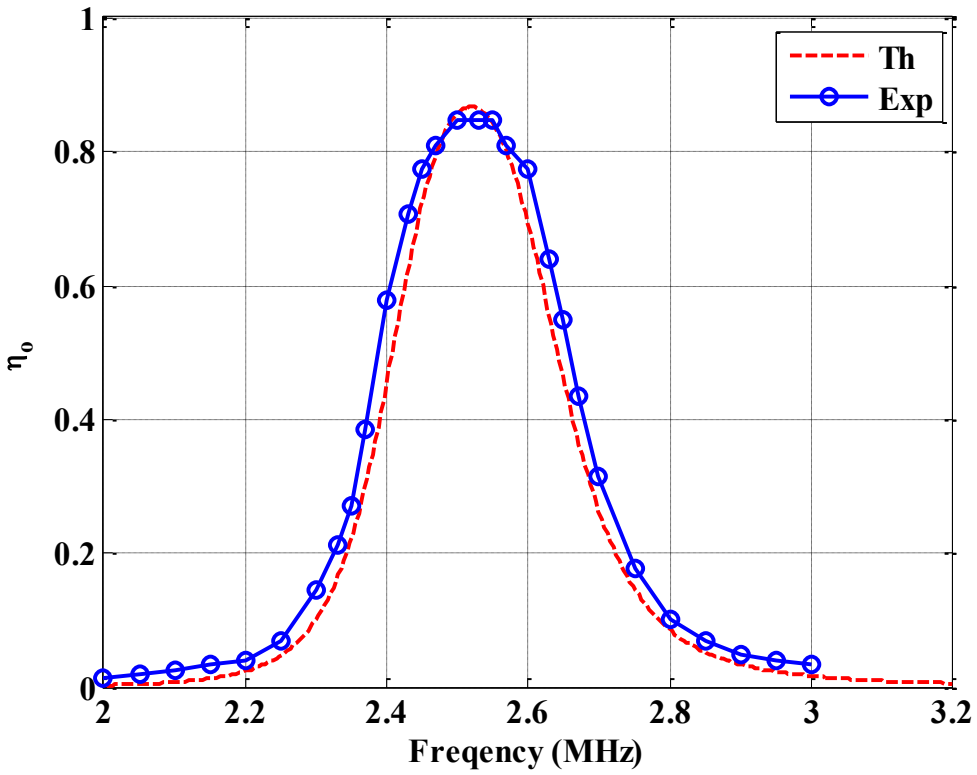

Figure 3.19 Figure of merit versus frequency for transmitter and receiver of combination 3 at 16cm distance, f_o = 2.5MHz, R_L = 50Ω

Experiment 9

Different measurements were taken with the same equipment from the last experiment. Comparing with Figure 3.16, it can be concluded that the distance of the perfect point increases at higher frequency, and it is 12cm at 2.5MHz as shown in Figure 3.20, but is ultimately limited by the frequency and mutual inductance in both coils.

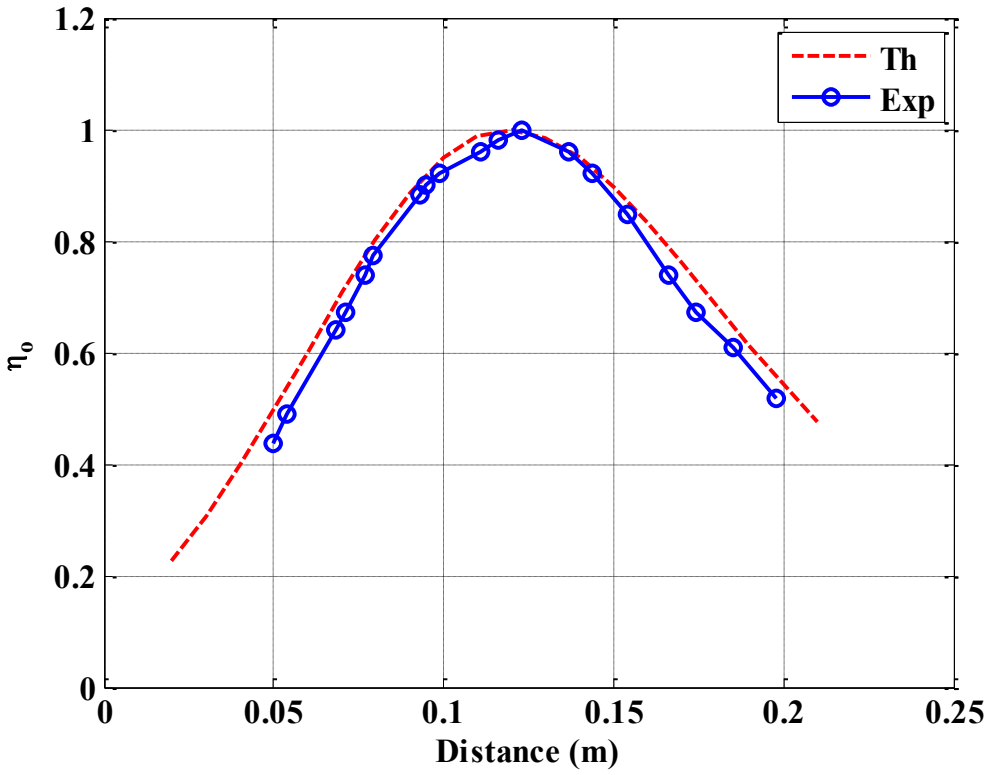

Figure 3.20 Figure of merit versus distance for transmitter and receiver of combination 3 at resonant frequency (f_o = 2.5MHz), R_L = 50Ω

E. Different size coils:

Experiment 10

Before studying multiple receivers, it is necessary to study the figure of merit of a small receiver with a large transmitter. In this part of the study, a small CAR is studied by using one resonator from combination 1 in Table 3.1 as a small coil receiver and

the other from combination 3 in the table as a large coil transmitter with a 3cm gap at a resonant frequency of 2.1MHz. As expected because of the small CAR (1:17) the system delivers less power than in the case of identical resonators of combination 3 (two big coils with 1:1 ratio, experiment 3 Figure 3.11). Yet the power transferred is greater than in the case of identical resonators of combination 1 (two small coils with 1:1 ratio, experiment 1 Figure 3.8) even though there is the small same ratio; this is because of the higher mutual inductance between the coils. The figure of merit versus frequency is shown in Figure 3.21.

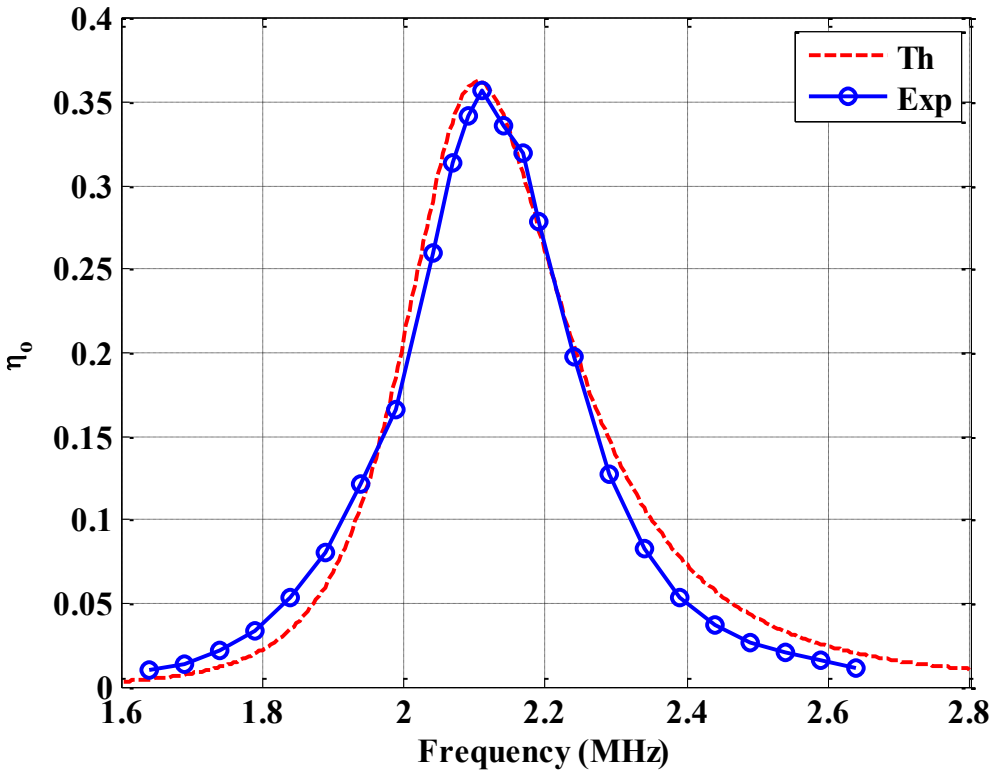

Figure 3.21 Figure of merit versus frequency for transmitter and receiver of combination 3 & 1, respectively, at 3cm distance, f_o = 2.1MHz, R_L = 50Ω

Experiment 11

Different measurements were taken with the same equipment of the last experiment to find the figure of merit as a function of distance as shown in Figure 3.22.

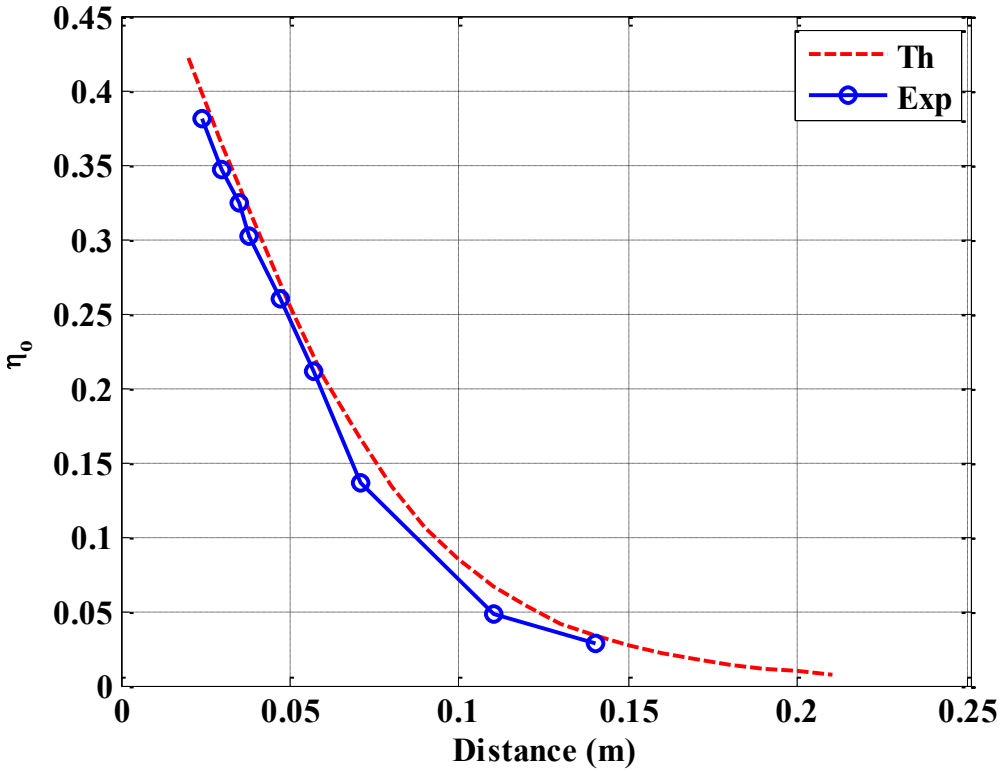

Figure 3.22 Figure of merit versus distance for transmitter and receiver of combination 3 & 1, respectively at resonant frequency (f_o = 2.1MHz), R_L = 50Ω

3.6.1.2 Higher figure of merit with a small coils area ratio

High figure of merit can be achieved for relatively small CARs by adjustment of the turns ratio. We go on to show that it is possible to achieve a higher figure of merit than the coil area ratio and the associated flux cut would indicate.

In a normal transformer, the primary coil produces the magnetic field and the secondary coil cuts all the flux line by virtue of an iron core. Therefore, transformers have nearly one figure of merit because of the high coupling. However, without the iron core, the coupling is quite small and it is difficult to achieve high figure of merit.

A promising technology to achieve wireless energy transfer at high figure of merit is magnetic resonance. That is carefully choosing a capacitor for each coil/inductor (transmitter and receiver) so they resonate at the same frequency f_r.

Transfer of power between two coils with a large cross sectional area can achieve higher figure of merit than the same transmitter and a smaller receiver. This is obvious because of the coils area ratio (CAR) and the percentage of flux lines being cut by the receiver. However, it is possible to obtain high figure of merit even with small *CARs*.

This section focuses on how to increase the figure of merit of the resonant power transfer with a relatively small CAR. It can be achieved by substituting the receiver resonator described in the last section with either a coil with larger cross sectional area or a coil with a higher number of turns.

F. Larger cross sectional area

Experiment 12

Using a coil which has double the cross sectional area and a suitable capacitor (combination 4 Table 3.1) as a receiver to resonate at the same frequency, leads to higher figure of merit than shown in Figure 3.21. Figure 3.23 shows figure of merit versus frequency, when the CAR is (2:17).

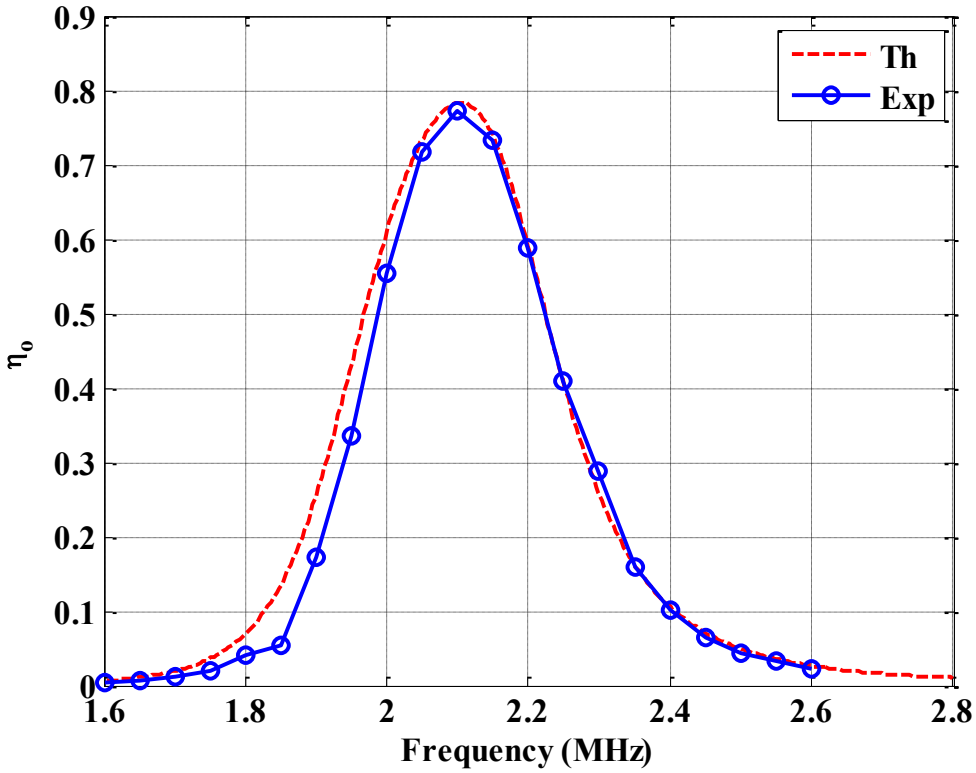

Figure 3.23 Figure of merit versus frequency for transmitter and receiver of combination 3 & 4, respectively, at 3cm distance, f_o = 2.1MHz, R_L = 50Ω

Experiment 13

Different measurements were taken with the same equipment of the last experiment to find the figure of merit as a function of distance as shown in Figure 3.24. Comparing with Figure 3.22, the effect of increasing the cross sectional area of the receiver is clear in the obtained high figure of merit.

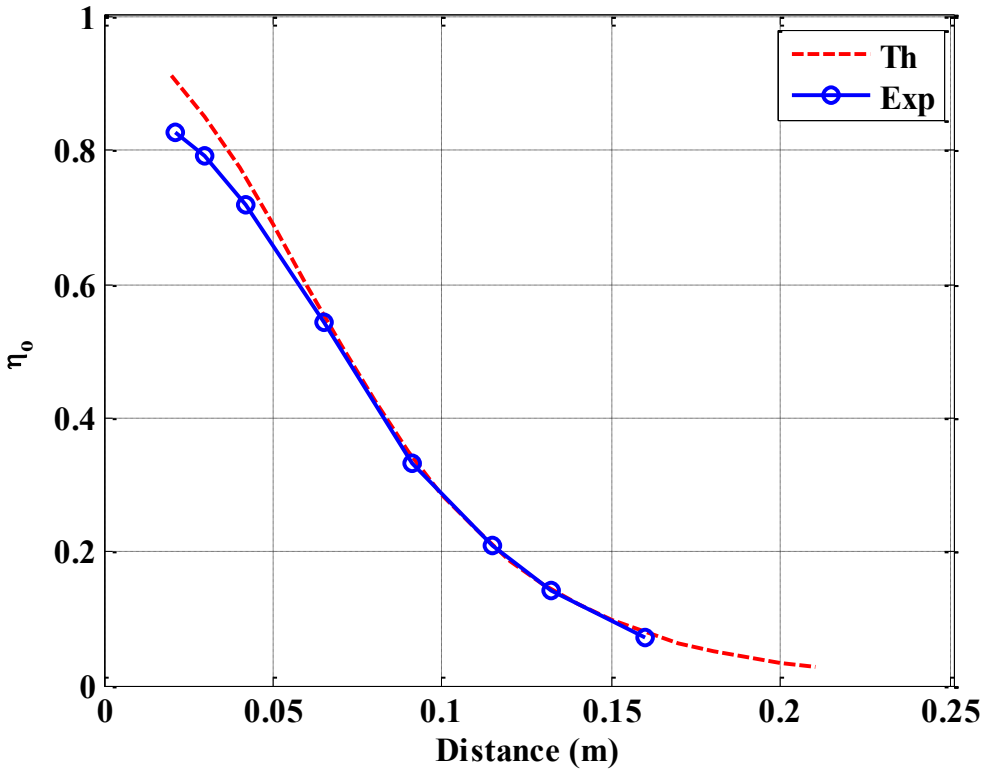

Figure 3.24 Figure of merit versus distance for transmitter and receiver of combination 3 & 4, respectively, at resonant frequency (f_o = 2.1MHz), R_L = 50Ω

G. Higher number of turns

Experiment 14

Using a coil which has twice the number of turns and a suitable capacitor (combination 2 Table 3.1) as a receiver to resonate at the same frequency, leads to higher figure of merit than Figure 3.21 shows. Figure 3.25 shows figure of merit versus frequency and the environment of this experiment is shown in Figure 3.26.

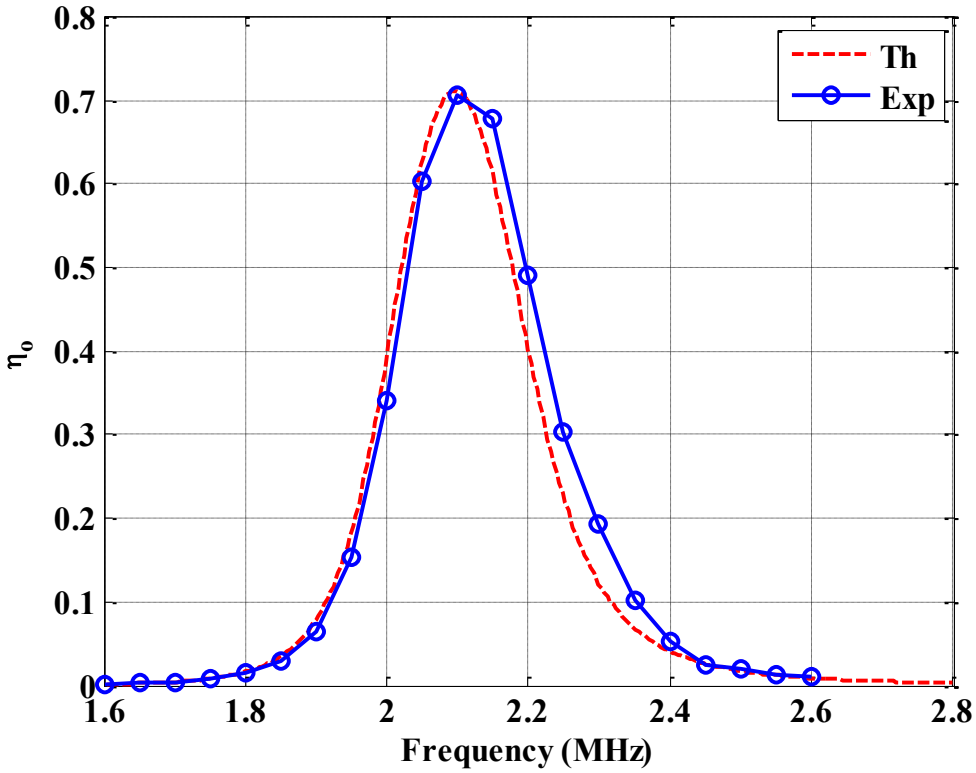

Figure 3.25 Figure of merit versus frequency for transmitter and receiver of combination 3 & 2, respectively, at 3cm distance, f_o = 2.1MHz, R_L = 50Ω

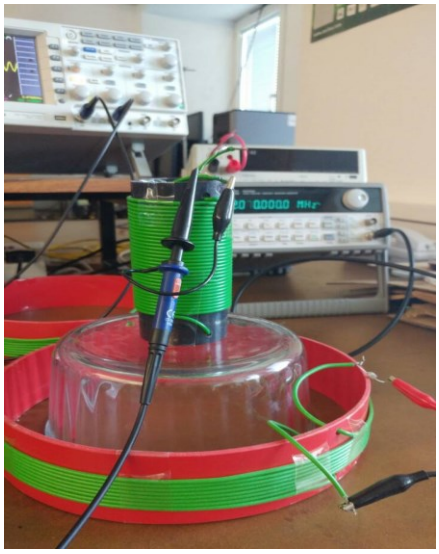

Figure 3.26 Environment of experiment 14 for transmitter and receiver of combination 3 & 2, respectively, at 3cm distance, f_o = 2.1MHz, R_L = 50Ω

Experiment 15

Different measurements were taken with the same equipment of the last experiment to find the figure of merit as a function of distance as shown in Figure 3.27. Comparing with Figure 3.22, the effect of increasing the number of turns of the receiver is clear in the obtained higher figure of merit.

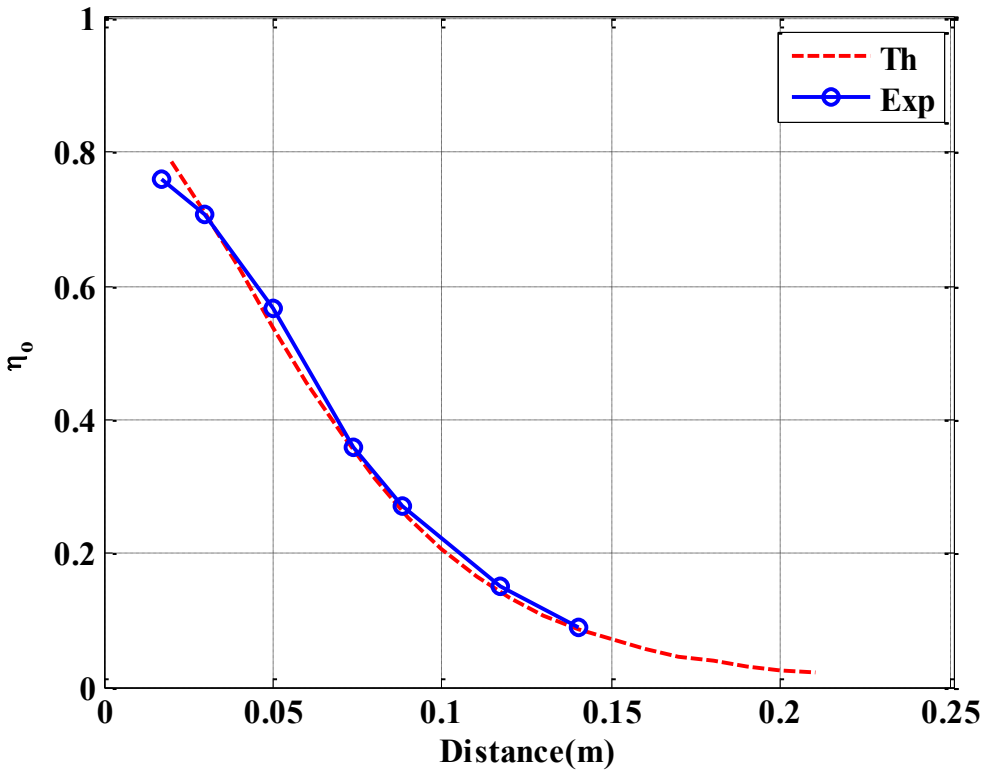

Figure 3.27 Figure of merit versus distance for transmitter and receiver of combinations 3 & 2, respectively, at resonant frequency (f_o = 2.1MHz), R_L = 50Ω

It can be concluded from these experiments that higher figure of merit can be achieved by increasing the number of turns in the receiver as well as by increasing the cross sectional area (doubling in this experiment). Therefore, we have shown that it is possible to achieve a higher energy transfer than the CAR and the associated flux cut would imply.

3.6.2 Two receiver system

Experiment 16

By using two identical receivers of 3cm radius (Table 3.1 Combination 1) and a transmitter of 12.25cm (Table 3.1 Combination 3), the figure of merit of a two coil system can be studied. The figure of merit of a receiver can be affected by the presence of another receiver in the same field. Figure 3.28 shows the figure of merit of each one of two closed receivers in the same transmitter field and Figure 3.29 shows the environment of this experiment. The distance between the transmitter and the two receivers is 3cm, and between their centres is 7cm. It appears, as expected, from the figure that the figure of merit here is less than it is in the case of just one receiver as shown in Figure 3.21 (experiment 10).

Logically, the received power is divided between the two receivers. Thus, it is expected to obtain half of the one receiver figure of merit (0.35) shown in Figure 3.21; however, each receiver has a figure of merit of 0.3 which is higher than 0.175 (half of 0.35). This is because the mutual inductance between the two receivers, strengthens the received power in each of them.

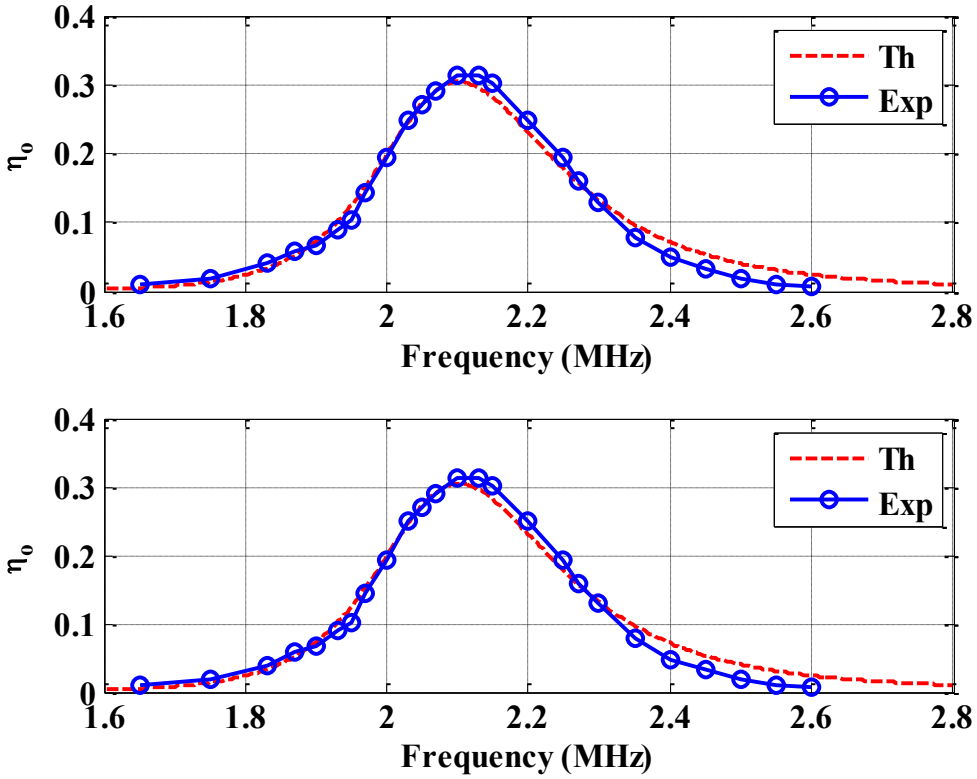

Figure 3.28 Figure of merit versus frequency for a two receivers system for transmitter and receivers of combination 3 & 1, respectively, at 3cm distance, f_o = 2.1MHz, R_L = 50Ω

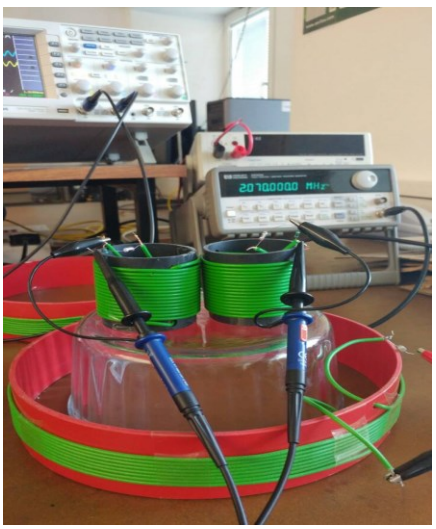

Figure 3.29 Environment of experiment 16 for a two receivers system; transmitter and receivers of combination 3 & 1, respectively, at 3cm distance, f_o = 2.1MHz, R_L = 50Ω

3.6.3 Three receiver system

Experiment 17

It is possible to apply our modelling and simulation approach for the case of more than two receivers, i.e. three to N. In the case of three receivers the figure of merit of each one of the three, if all three are together inside the field of the same transmitter, is shown in Figure 3.30. In this configuration the three identical receivers form a triangular shape at the same level (3cm gap to the transmitter). Each coil, with 3cm radius, 16 turns and 3mm pitch between the turns, has an inductance equal to 10.8μH (combination 1 Table 3.1). This means that the mutual inductance between any two of them is equal, which is 0.21μH. Moreover, the mutual inductance between the transmitter and any one of the receivers is also equal, which is 1.3μH. Moving a receiver to another location in the same field requires a new calculation for the mutual inductance between the coils.

As shown in Figure 3.30, in the case of three receivers, each one has a figure of merit of (0.25) which is higher than one third of one receiver figure of merit (0.35 in Figure 3.21). Again, this is because the mutual inductance between each two receivers strengthens the received power in all of them.

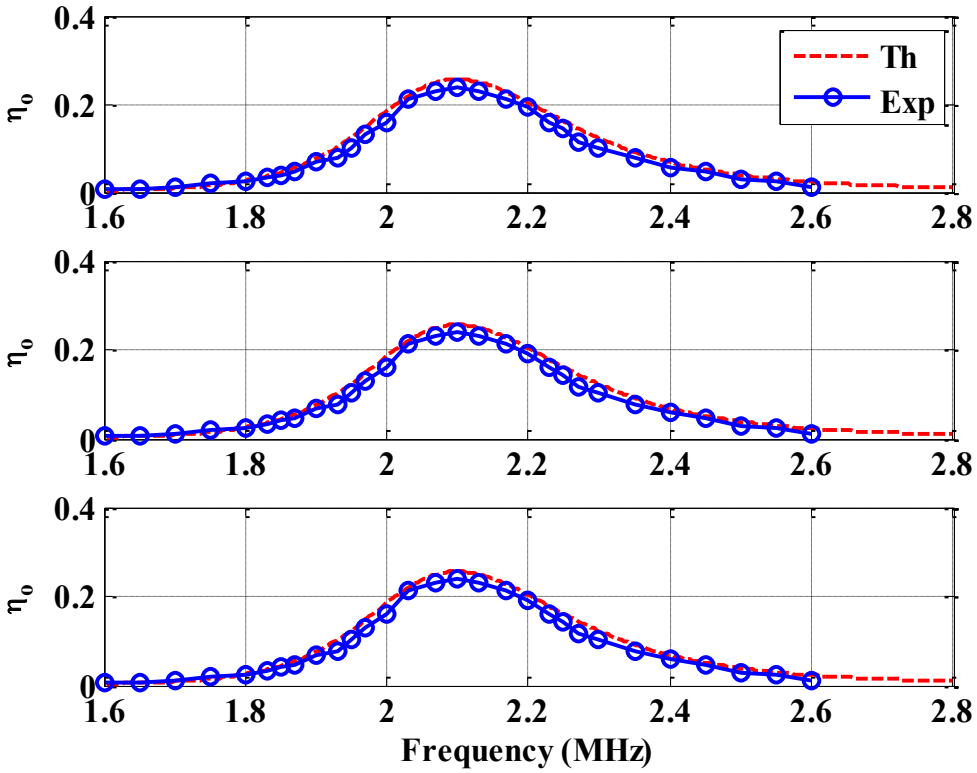

Figure 3.30 Figure of merit versus frequency for a three receivers system for transmitter and receivers of combination 3 & 1, respectively, at 3cm distance, f_o = 2.1MHz, R_L = 50 Ω

3.6.4 Frequency splitting with multiple receivers

Experiment 18

Frequency splitting is a phenomenon that appears at the overmatching between coils, as previously shown in experiment 5 (Figure 3.14), between the two large coils. In this part of the study, we tested this phenomenon with the multiple receivers. The overmatching was achieved by replacing the three receivers in the last experiment by a group of coils of combination 2 in Table 3.1 that each have 32 turns. The frequency splitting is very clear at the higher frequency of 2.52MHz with a 2cm gap between the transmitter and the receivers as shown in Figure 3.31. It shows the figure of merit of each receiver as a function of frequency.

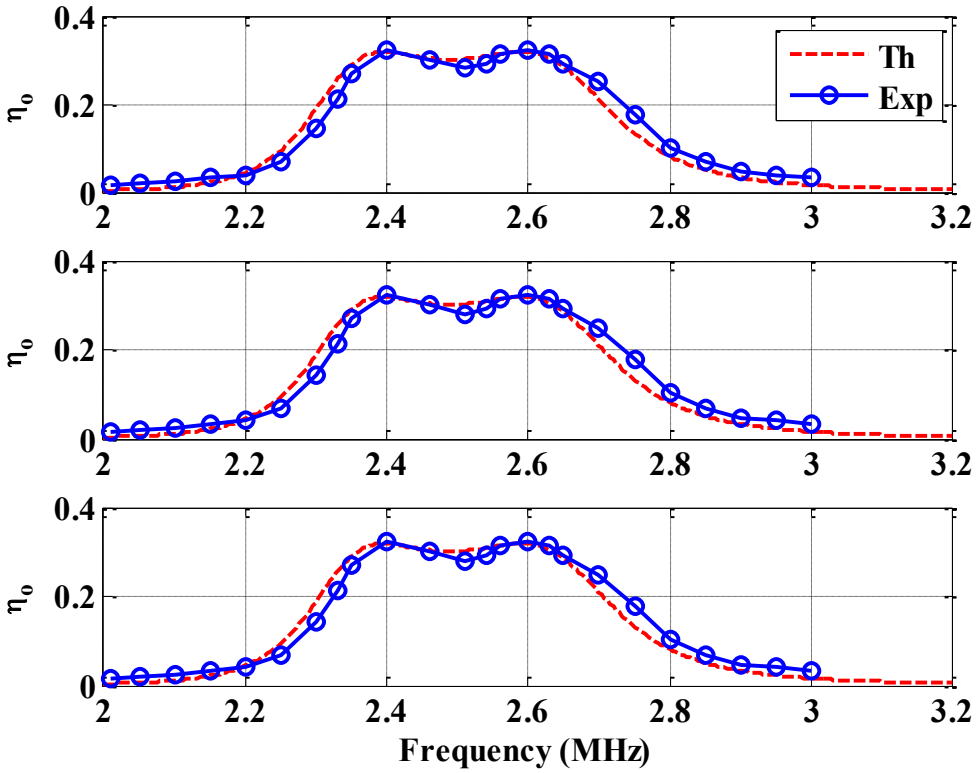

Figure 3.31 Figure of merit versus frequency for a three receivers system for transmitter and receivers of combination 3 & 2, respectively, at 2cm distance, f_o = 2.5MHz, R_L = 50 Ω

It can be concluded that the maximum figure of merit of the power transfer is 0.5 for each one of two receivers and 0.33 for each one of three receivers.

3.7 Conclusion

The figure of merit of a wireless power transfer system is dependent on factors such as: the resonance frequency; the size of the coils; the mutual inductance between them; the distance between coils and the presence of more than one receiver in the transmitter area. The following observations can be made:

- The mutual inductance between any two coils depends on their shape, their location and the distance between them. This study presented a method for the calculation of mutual inductance between any solenoid coils with different locations and gaps.
- There is a specific distance, where the input impedance of the system equals the internal resistor of the source, at which point the system has the maximum figure of merit and can transfer maximum power to the load.
- Frequency splitting occurs when the coils are overmatched.
- Higher frequencies lead to an increase in the distance at which the system has the maximum figure of merit subject to frequency and mutual inductance limitations.
- A larger transmitter size produces more flux around it, and also leads to an increase in the distance at which the system has the maximum figure of merit.
- The figure of merit of magnetic resonant wireless power transfer is controlled by the mutual inductance between the coils. Several factors affect the mutual inductance, such as the size of the coils, including the cross sectional area, and the number of turns. It is possible to increase the figure of merit by increasing one or both of them.
- Higher figure of merit can be achieved with small section coils or with small CARs by increasing the number of turns in order to increase the mutual induction between them. The limitation is the diminishing size of the capacitor to resonate at the desired frequency. We have shown that it is possible to achieve a higher energy transfer than the CAR and the associated flux cut would imply.

- The presence of more than one receiver gives decreased figure of merit for each individual one (compared to one coil), but the figure of merit of the complete multiple receiver system is greater than the figure of merit of the individual coil.
- There are a number of practical limitations observed at higher frequencies regarding measurements.

Applying the proposed method is an efficient and concise way to calculate the figure of merit for a wireless power transfer system with one to N receivers.

Chapter 4

Symmetric Capacitance Tuning

4.1 Related Work

Magnetic coupled wireless power transfer systems are a safe mode of power delivery [2, 4] as well as being more convenient than wired systems [3]. The demand for wireless charging of vehicles and mobile devices has led to much academic effort to improve the overall performance of these systems [35].

As mentioned before, the system in this technique consists of two coils (transmitter and receiver or primary and secondary) [23]; both resonate at the same frequency by adding a capacitor to each one [12] as shown in Figure 4.1. The figure shows the equivalent circuit of the system where V_S is the voltage source with an internal resistance R_S; R_L is the load resistor; (L_1 & C_1) and (L_2 & C_2) are resonator1 and resonator2, respectively. The figure of merit of the magnetic power transfer system is influenced by several factors [34]: the resonant frequency, the inductor and capacitor values, and the mutual inductance between the two coils (M in Figure 4.1).

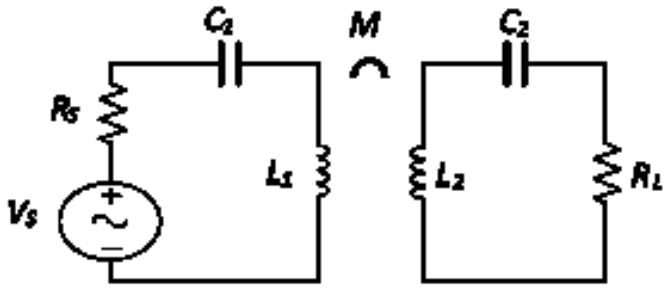

Figure 4.1 Equivalent circuit of magnetic coupling wireless power transfer system

The effect of the mutual inductance is producing electromotive force in a coil because of the change in the current in a coupled coil [90]. The mutual inductance is affected by the distance and the size of the two inductors. The mutual inductance is calculated by the Neumann formula that is explained in section 3.1.

Although the system seems simple, its performance is more complicated than might first appear. For each combination of coils and capacitors, there is a maximum transfer of power at a specific gap between the coils where the input impedance of the system matches the internal resistor of the source [36]. At smaller gaps between the coils, there will be a splitting in the frequency response of the system (see later in the theoretical analysis (section 4.2)), and the maximum transfer of power happens at two different frequencies around the original resonant frequency (f_o) [58].

$$f_o = \frac{1}{2\pi\sqrt{L_1 C_1}} = \frac{1}{2\pi\sqrt{L_2 C_2}} \tag{4.1}$$

In other words, if the resonators are coupled, the resonant frequencies split from the original one [5, 57, 60]. The explanation of this phenomenon is that the system reaches the resonant frequency in two cases [67]:

1) At a frequency less than f_o, the two loops have a capacitive effect. Therefore, the reflected effect of the secondary is inductive in the primary. The resonance happens when they cancel each other out.
2) At a frequency larger than f_o, the two loops have an inductive effect. Therefore, the reflected effect of the secondary is capacitive in the primary. Similarly, the resonance happens when they cancel each other out.

As the gap between a pair of coupled resonators varies, the frequency of resonance changes. Therefore a re-statement of the problem is to maintain resonant frequency as the gap alters. Many researchers have worked on this to improve the power transfer efficiency of the system at different gaps. This can be done by several different methods [58]: impedance matching [37, 54], frequency tracking [69, 70], and changing the parameters of the resonators or the coupling between them [39, 72]. The last two methods are not practical because most systems consist of a fixed pair of resonators. Frequency tracking or frequency matching has the potential disadvantage of moving out of the ISM (industrial, scientific, and medical) band [58]. The impedance matching method seems to be the best choice to improve the power transfer efficiency, where researchers add an impedance matching circuit in the transmitter side. However, using this method does not always offer full power transfer.

This chapter presents a new method to obtain maximum figure of merit or power transfer efficiency in all cases without moving out of the ISM band. The proposed method is conducted by tuning the capacitors on both sides (transmitter and receiver) at the same time and maintaining the same values. By this method, one of the new resonant frequencies can be moved to match

the original resonant frequency of the circuit and not violate the ISM band restrictions.

4.2 Theoretical Analysis

The circuit of Figure 4.1 can be expressed as:

$$\begin{bmatrix} V_S \\ 0 \end{bmatrix} = \begin{bmatrix} Z_1 & -j\omega M \\ -j\omega M & Z_2 \end{bmatrix} \begin{bmatrix} I_1 \\ I_2 \end{bmatrix} \tag{4.2}$$

where the complex impedances for each circuit are:

$$Z_1 = R_S + j\left(\omega L_1 - \frac{1}{\omega C_1}\right) \tag{4.3}$$

$$Z_2 = R_L + j\left(\omega L_2 - \frac{1}{\omega C_2}\right) \tag{4.4}$$

This can be used to derive the final equation to calculate the figure of merit η_0 as following:

$$\eta_0 = \frac{P_{out}}{P_{in,\max}} \tag{4.5}$$

where:

$$P_{out} = \frac{1}{2}|I_2|^2 R_L \tag{4.6}$$

Solving (4.2) leads to:

$$I_1 = \frac{Z_2 V_S}{Z_1 Z_2 + \omega^2 M^2} \tag{4.7}$$

$$I_2 = \frac{j\omega M V_S}{Z_1 Z_2 + \omega^2 M^2} \tag{4.8}$$

$$P_{in,\max} = \frac{V_S^2}{8R_S} \tag{4.9}$$

By substituting (4.6), (4.8) and (4.9) in (4.5), the figure of merit is then:

$$\eta_0 = \frac{4\omega^2 M^2 R_L R_S}{\left|Z_1 Z_2 + \omega^2 M^2\right|^2} \tag{4.10}$$

The input impedance Z_{in} of the system can be calculated as:

$$Z_{in} = \frac{V_S}{I_1} - R_S \tag{4.11}$$

Using (4.7) and (4.11) leads to:

$$Z_{in} = \frac{\omega^2 M^2 R_L}{R_L^2 + \left(\omega L_2 - 1/(\omega C_2)\right)^2} + j\left[\omega L_1 - \frac{1}{\omega C_1} - \frac{\omega^2 M^2 \left(\omega L_2 - 1/(\omega C_2)\right)}{R_2^2 + \left(\omega L_2 - 1/(\omega C_2)\right)^2}\right] \tag{4.12}$$

These equations have been used to study the performance of the wireless power transfer system in different cases and define the problem of frequency splitting and solve it.

In this work the set of two solenoid coils (12.25cm radius), with 8 turns and an inductance equal to 31.3μH, was used in all experiments along with capacitors of 188pF tuned to work at 2.1MHz. Both the load resistance and internal resistance of the source are set at 50Ω. Starting with the basics, the figure of merit of the system was calculated as a function of distance to show the maximum transfer of power at a specific distance which equals 10.5cm in this combination as shown in Figure 4.2.

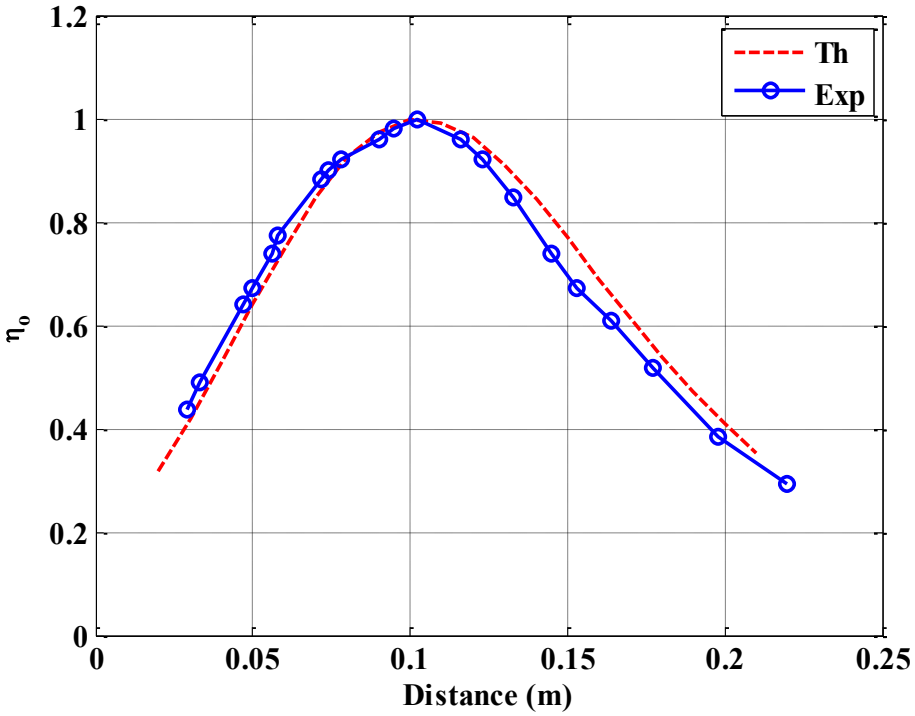

Figure 4.2 Figure of merit versus distance at resonance frequency 2.1MHz, R_L = 50Ω

Looking at this slightly differently, the figure of merit was calculated as a function of frequency at different gaps to show the splitting in the resonant frequency. As seen in Figure 4.3, when the gap = 10.5cm, the maximum figure of merit of power transfer is at the original frequency of 2.1MHz; as shown in Figure 4.4 at gap = 7.5cm, the maximum transfer of power will be at 1.98MHz and 2.24MHz, while Figure 4.5 shows that at gap = 5cm the system transfers the maximum power at the two new resonant frequencies 1.89MHz and 2.35MHz.

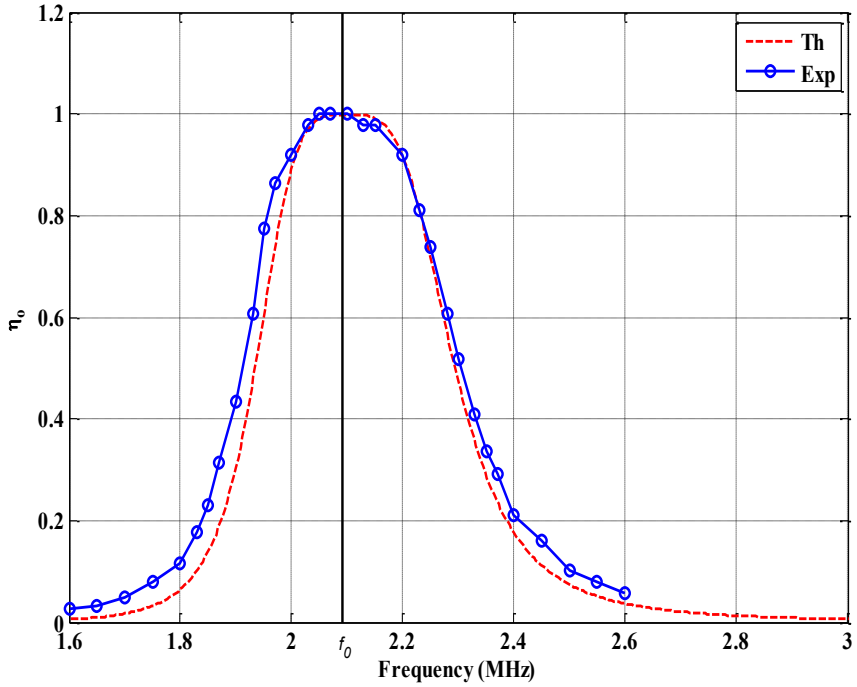

Figure 4.3 Figure of merit versus frequency at gap 10.5cm

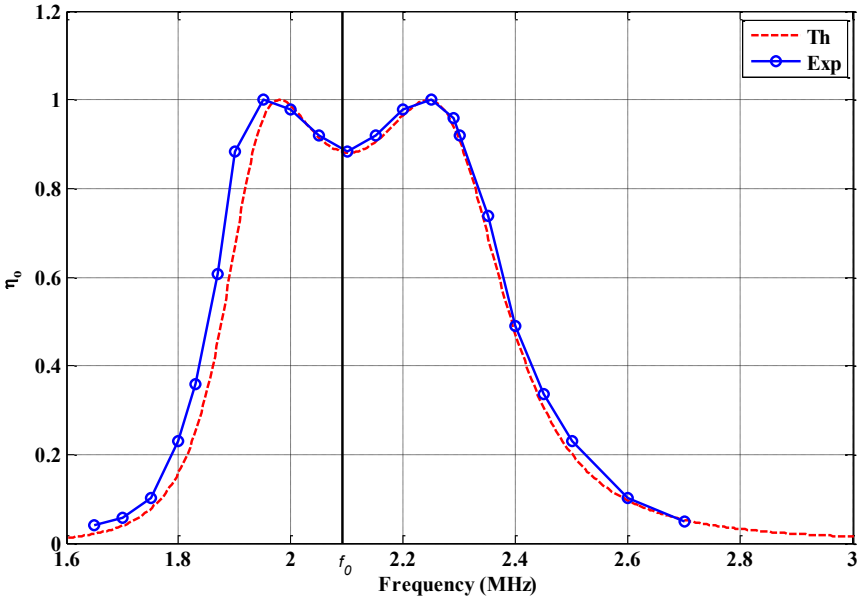

Figure 4.4 Figure of merit versus frequency at gap 7.5cm

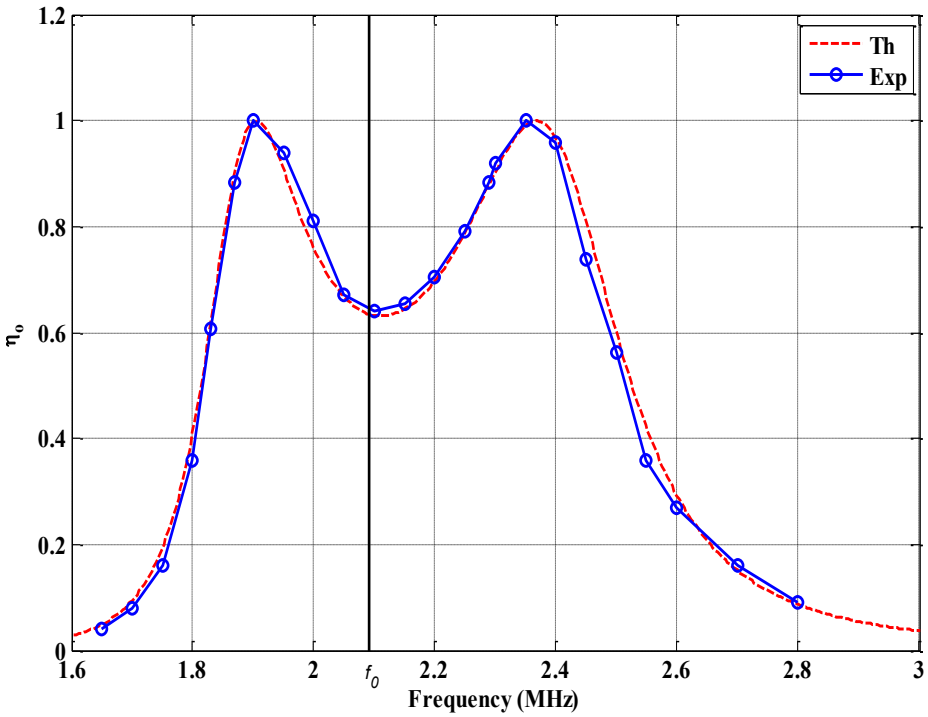

Figure 4.5 Figure of merit versus frequency at gap 5cm

These two new resonant frequencies can be estimated by:

$$f_{1,2} = \frac{1}{2\pi\sqrt{(L_1 \pm M)C_1}} \tag{4.13}$$

where f_1 and f_2 are the new low and high frequencies respectively.

To solve the problem of frequency splitting, capacitive tuning has been used. Firstly, by tuning one side, either transmitter or receiver; then tuning both sides together to try to find the best solution.

4.3 Improvement Idea of Figure of Merit

4.3.1 Tuning one side capacitor

Testing only one side by tuning either C_1 or C_2 shows that a figure of merit equal to or less than the original at the resonant frequency is achieved, as shown in Figure 4.6 and Figure 4.7. The former figure shows C_1 tuning and keeps the original value of C_2; where C_2 = 188pF, C_1 = 155pF (less than the original capacitor value), 188pF (the original value which equals C_2) and 238pF (higher than the original capacitor value); the best case is when $C_1 = C_2$. The latter figure demonstrates the same result by tuning C_2. The latter figure shows C_2 tuning and keeps the original value of C_1; where C_1= 188pF, C_2 = 155pF (less than the original capacitor value), 188pF (the original value which equals C_1) and 238pF (higher than the original capacitor value); the best case is when $C_1 = C_2$.

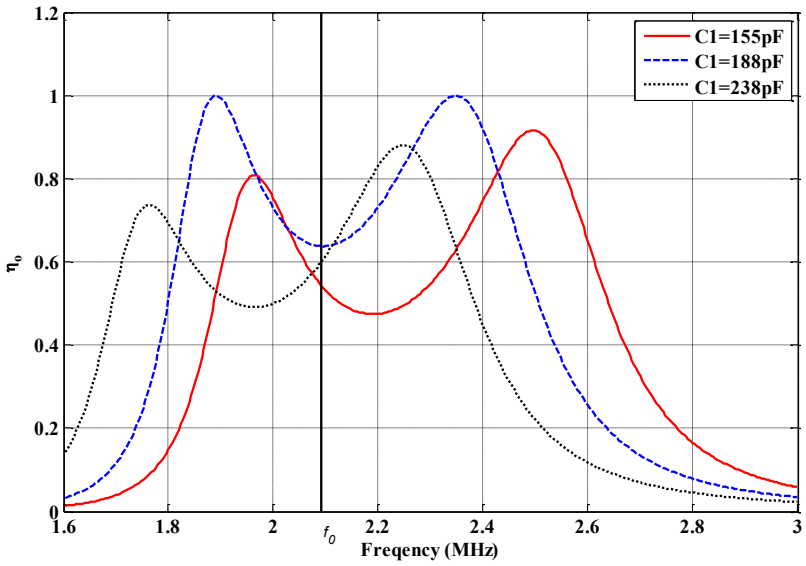

Figure 4.6 Figure of merit versus frequency at 5cm distance (a) Tuning C_1 when C_2 = 188pF

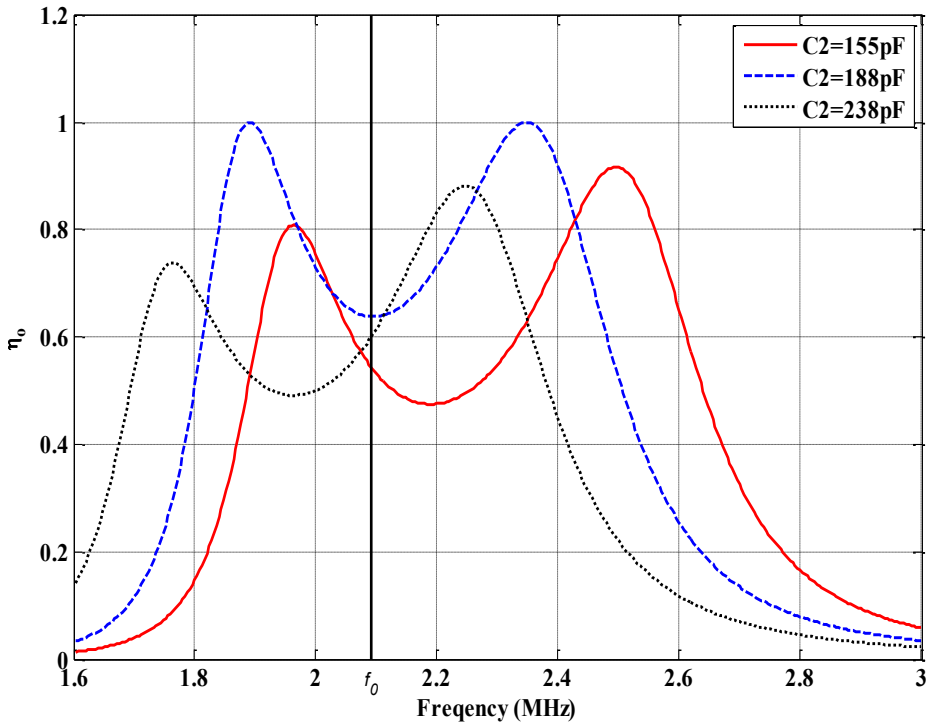

Figure 4.7 Figure of merit versus frequency at 5cm distance (a) Tuning C_2 when C_1 = 188pF

Showing that in a different way, Figure 4.8 shows the figure of merit as a function of one of the two capacitors (C_1 in this curve), and C_2 = 188pF (the original value) at resonant frequency 2.1MHz. It is clear from the figure that the highest figure of merit occurs when the two capacitors are equal.

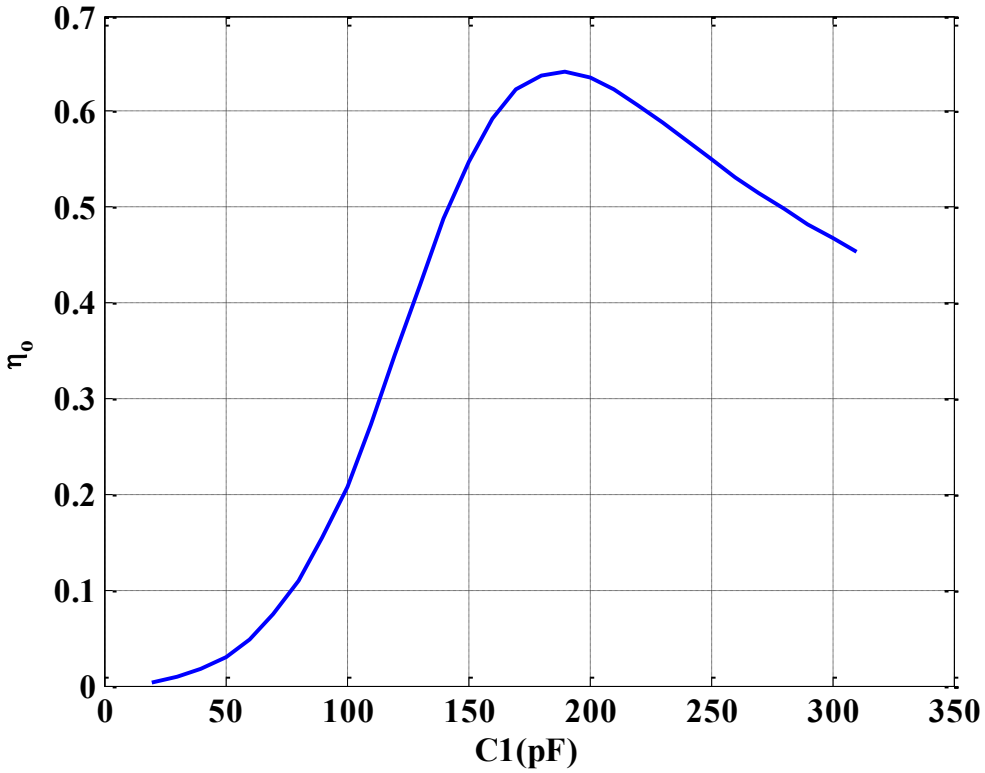

Figure 4.8 Figure of merit versus C_1 at gap=5cm, C_2 = 188pF and f_o = 2.1MHz

From the last three figures, it is clear that tuning only one of the capacitors is ill advised in this case, and the symmetric performance is a feature of the system. Therefore, tuning the two capacitors together or Symmetric Capacitive Tuning (SCT) offers a solution.

4.3.2 Symmetric capacitance tuning

By tuning both receiver and transmitter capacitors together, it is possible to obtain maximum figure of merit at two values of them, as seen in Figure 4.9. The figure shows the figure of merit as a function of C_1 and C_2 together at gap = 5cm and resonant frequency = 2.1MHz.

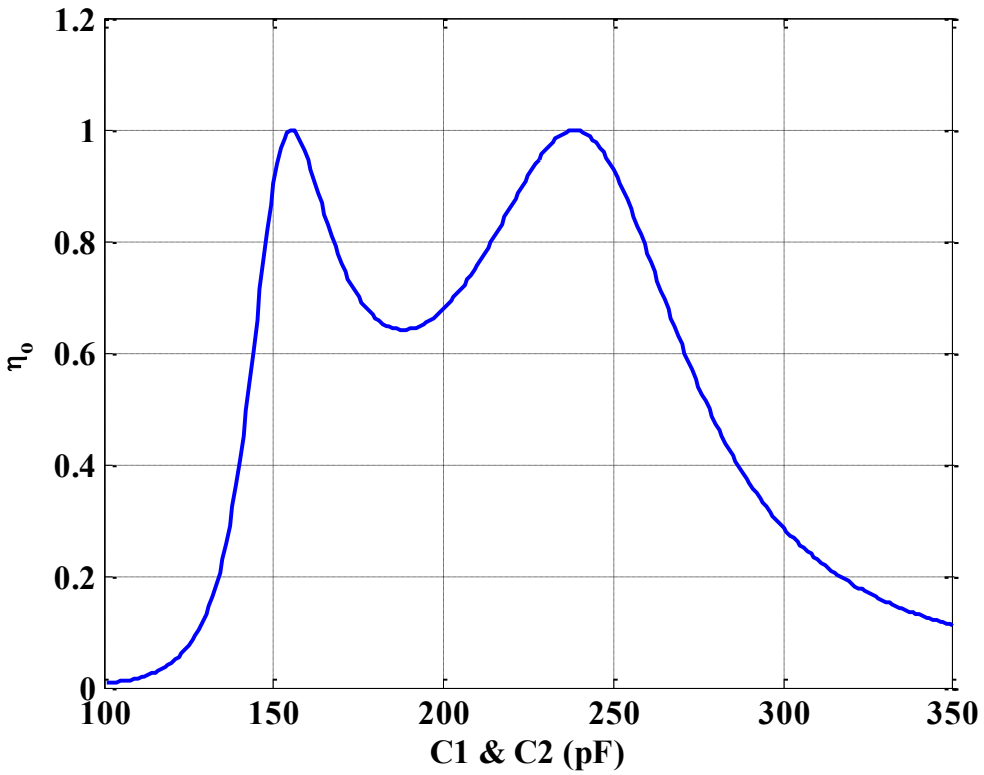

Figure 4.9 Figure of merit versus C_1 & C_2 together at gap = 5cm, f_o = 2.1MHz

Figure 4.9 shows that there are two values of the capacitors together which leads to the maximum transference of power. At gap = 5cm, this occurs when $C_1 = C_2$ = 155pF = C_{n1} and when $C_1 = C_2$ = 238pF = C_{n2}. These two values do not achieve the original resonant frequency condition that is achieved by the original capacitors values, f_o = 2.1MHz with $C_1 = C_2$ = 188pF. Each one of these two capacitors values achieves the condition of one of the new frequencies (1.89MHz and 2.35MHz in case of gap=5cm). Therefore, these two capacitors values can be defined by:

$$C_{n1,n2} = \frac{1}{(2\pi f_{1,2})^2 L_1} \tag{4.14}$$

where C_{n1} and C_{n2} are the small and large new capacitors which are required for tuning to obtain maximum figure of merit.

To find the effect of symmetric capacitance tuning on the input impedance of the system, equation (4.12) was used to plot Figure 4.10, demonstrating the importance of the proposed method. The figure shows how the real and the imaginary parts of the input impedance change with tuning C_1 and C_2 together. It illustrates that the input impedance of the circuit is equal to 50Ω pure resistance and the imaginary part equals zero at two specific values of C_1 & C_2 (155pF and 238pF in the case of gap 5cm) i.e. impedance matching with the source internal resistance.

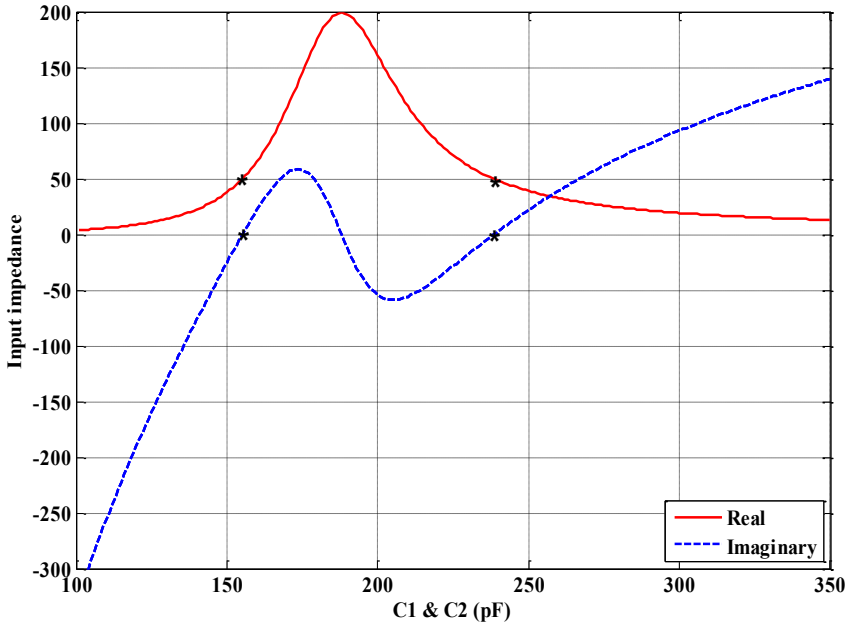

Figure 4.10 Input impedance figure by tuning C_1 & C_2 together at gap = 5cm, f_o = 2.1MHz

These two values, 155pF and 238pF, can move the original splitting curve to the right or left, respectively, at a 5cm gap between the resonators as shown in Figure 4.11 and Figure 4.12.

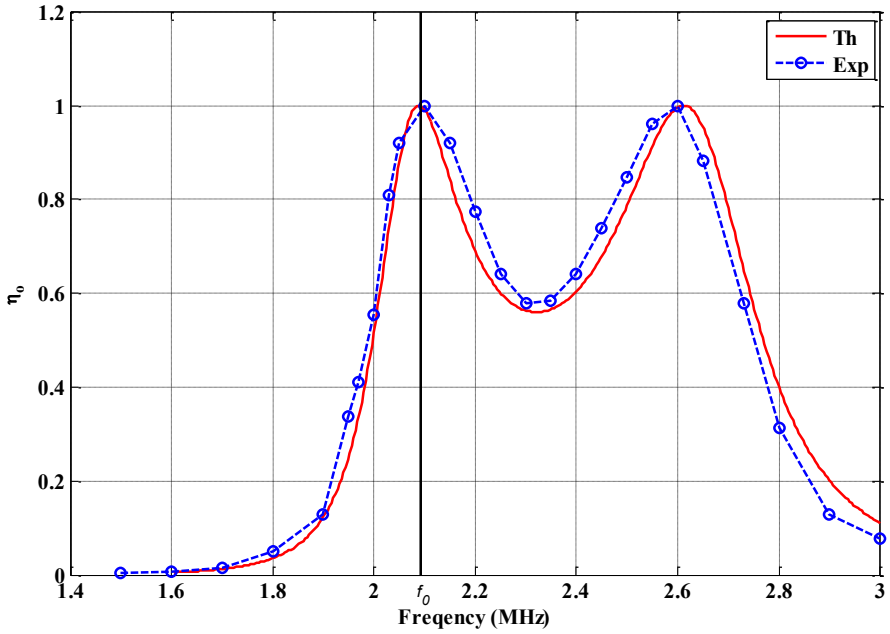

Figure 4.11 Figure of merit versus frequency at gap = 5cm with C_1 & C_2 = 155pF

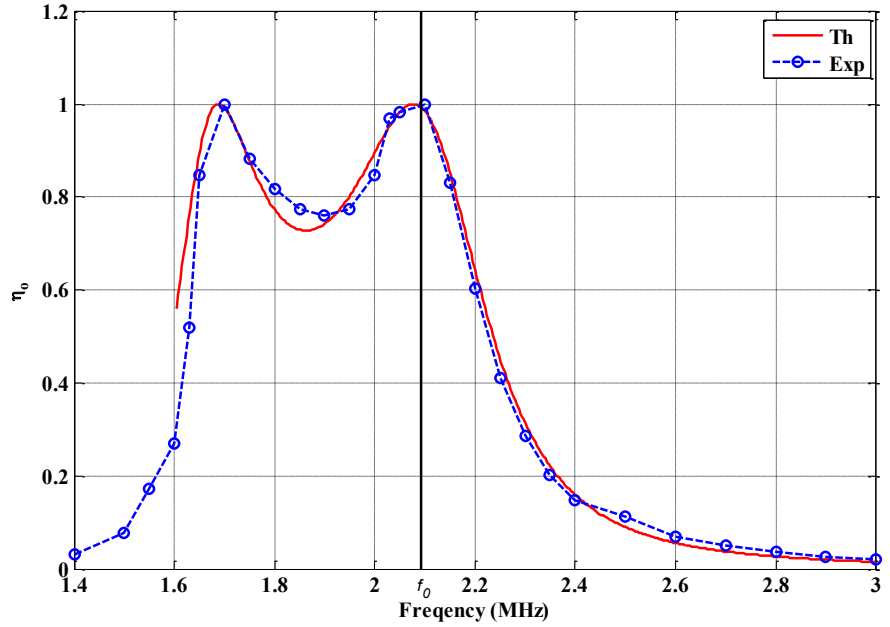

Figure 4.12 Figure of merit versus frequency at gap = 5cm with C_1 & C_2 = 238pF

These two figures demonstrate the idea of tuning both capacitors together at gap = 5cm. Figure 4.11 shows how a specific small value of C_1 & C_2 (155pF) can move the lower new resonant frequency (1.89MHz) to match the original one (2.1MHz), and Figure 4.12 shows how a specific larger value of C_1 & C_2 (238pF) can move the higher new resonant frequency (2.35MHz) to match the original. The two figures also show good matching between the theoretical and experimental results. The method is applicable to other resonant frequencies as shown in the next section.

4.4 Comparison and Evaluation

The Symmetric Capacitance Tuning (SCT) method is superior to other methods for solving the frequency spitting problem, such as impedance matching and frequency tracking. The proposed method is compared to other systems to evaluate figure of merit whilst remaining inside the ISM band.

A. Impedance Matching

This method works satisfactorily, but it is not efficient in all cases, as seen in [54]. There is 0.6 to 0.85 power transfer efficiency at a 9-20cm gap between the coils, and lower values at smaller gaps. When applying our proposed method to the same configuration we achieved higher power transfer efficiency or figure of merit at different gaps within the transfer distance, as described in detail shortly. The configuration consists of two similar resonators; each one has an inductor of 10.3μH and a capacitance of 13.26pF to work at a resonant frequency of 13.56MHz [54]. The performance of this configuration at gap = 9cm appears in the relationship between the figure of merit and the frequency as shown in Figure 4.13. The figure shows the splitting in the original resonant frequency to a new couple of frequencies, 12.84MHz

and 14.56MHz. From these two frequencies, the required capacitors values are calculated to tune both sides in order to move either of them to match the original resonant one; and they are 15.1pF and 11.78pF for this case. Tuning both C_1 and C_2 to 15.1pF moves the figure of merit curve to the left and the maximum figure of merit at 14.56MHz will fit the original frequency 13.56MHz as shown in Figure 4.14, while tuning them to 11.78pF moves the figure of merit curve to the right and the maximum figure of merit at 12.84MHz will fit the original frequency as shown in Figure 4.15.

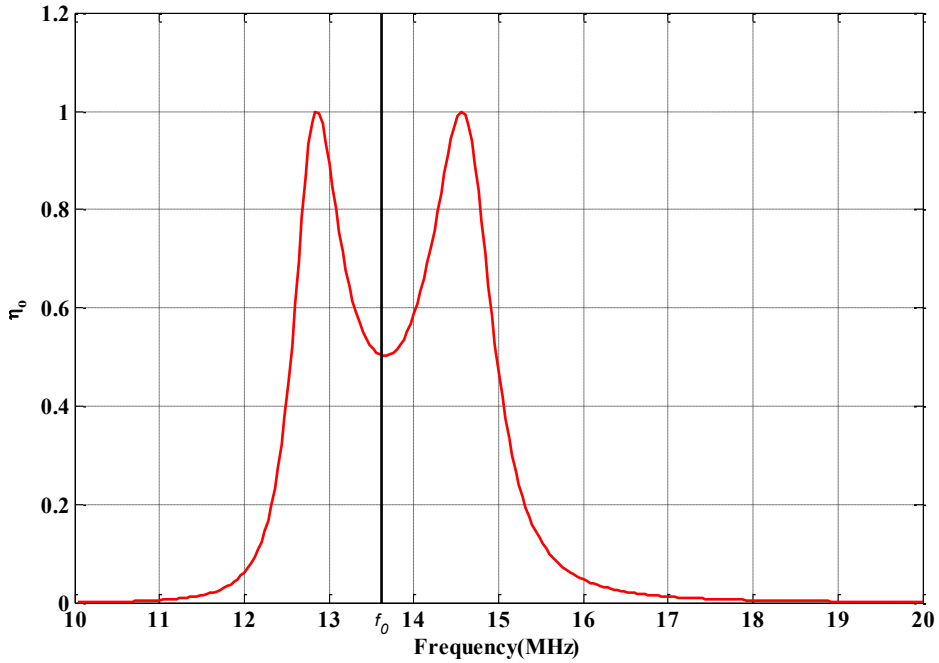

Figure 4.13 Figure of merit versus frequency at resonant frequency 13.56MHz with original values of C_1 & C_2 = 13.26pF at gap 9cm

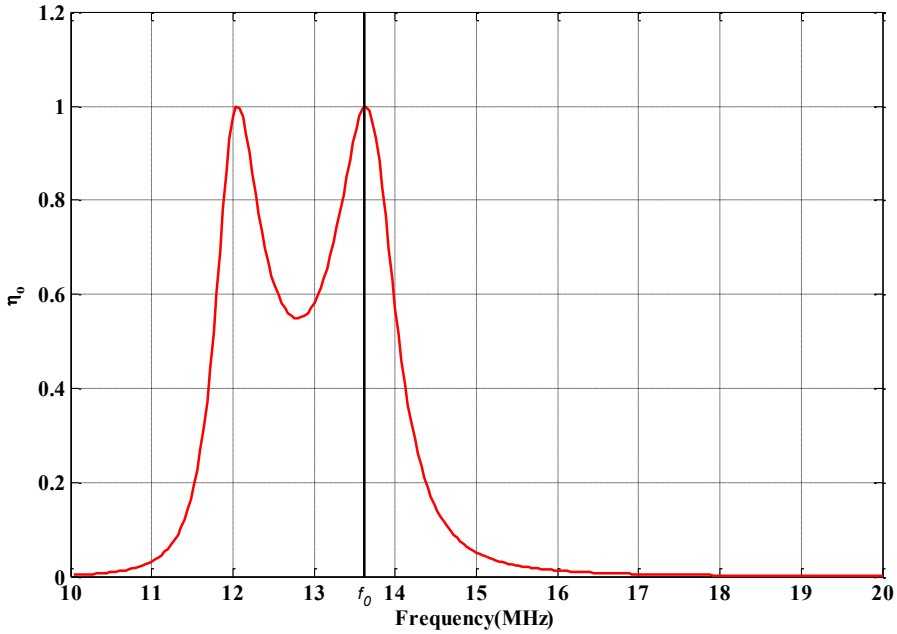

Figure 4.14 Figure of merit versus frequency at resonant frequency 13.56MHz by tuning C_1 & C_2 = 15.1pF at gap 9cm

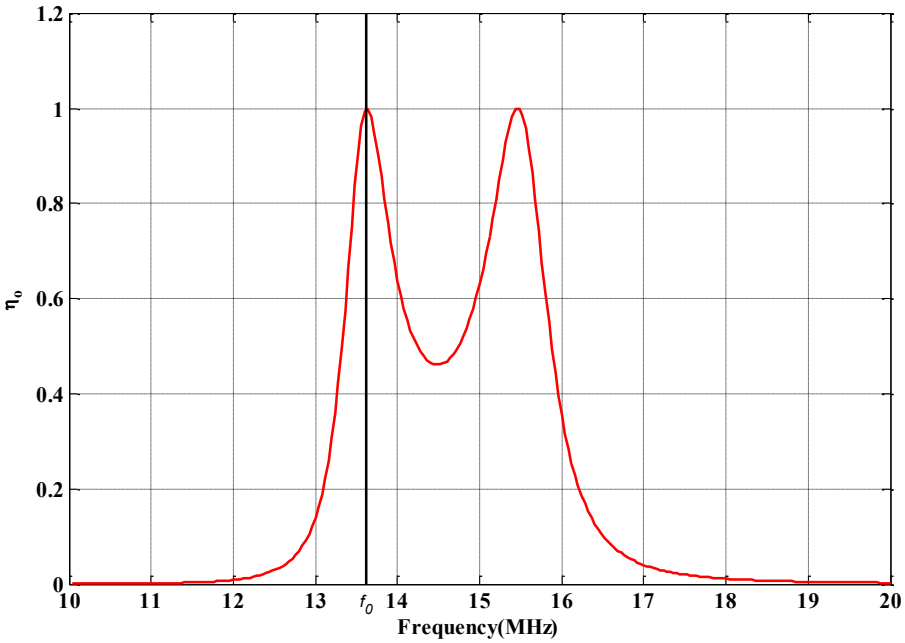

Figure 4.15 Figure of merit versus frequency at resonant frequency 13.56MHz by tuning C_1 & C_2 = 11.78pF at gap 9cm

At a smaller gap, the two splitting frequencies diverge. The two new frequencies of the maximum figure of merit at gap = 5cm are 12.4MHz and 15.36MHz as shown in Figure 4.16. The required capacitor's values for tuning in this case are 16.75pF and 10.95pF. Tuning both C_1 and C_2 to 16.75pF moves the figure of merit curve to the left and the maximum figure of merit at 15.36MHz will fit the original frequency 13.56MHz as shown in Figure 4.17. Tuning them to 10.95pF moves the figure of merit curve to the right and the maximum figure of merit at 12.4MHz will fit the original frequency as shown in Figure 4.18. Therefore, it is possible to achieve the maximum transfer of power at the same resonant frequency at different gaps within the transfer distance of the system by symmetric tuning of the capacitors in both the transmitter and receiver sides.

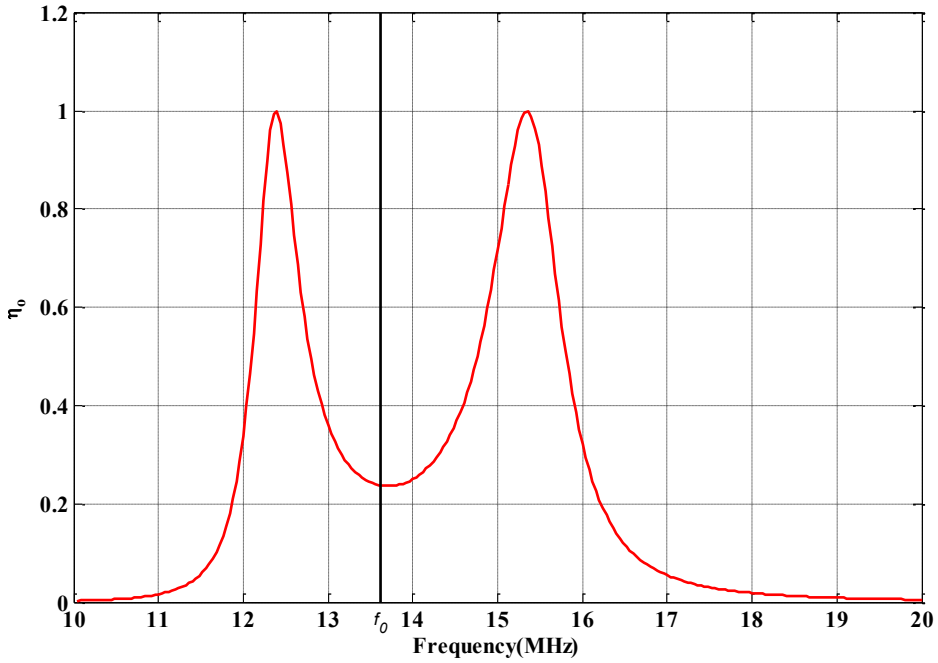

Figure 4.16 Figure of merit versus frequency at resonant frequency 13.56MHz with original values of C_1 & C_2 = 13.26pF at gap 5cm

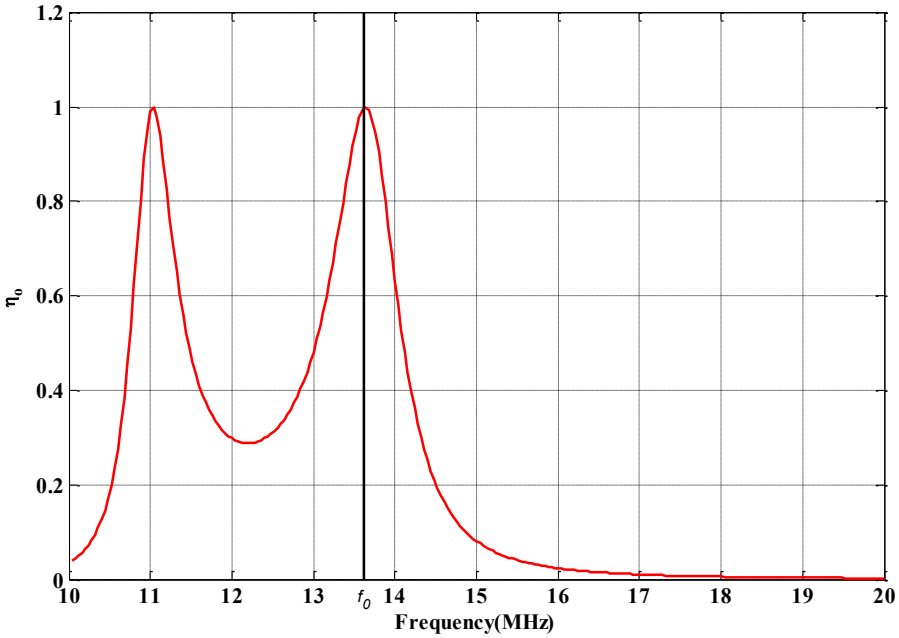

Figure 4.17 Figure of merit versus frequency at resonant frequency 13.56MHz by tuning C_1 & C_2 = 16.75pF at gap 5cm

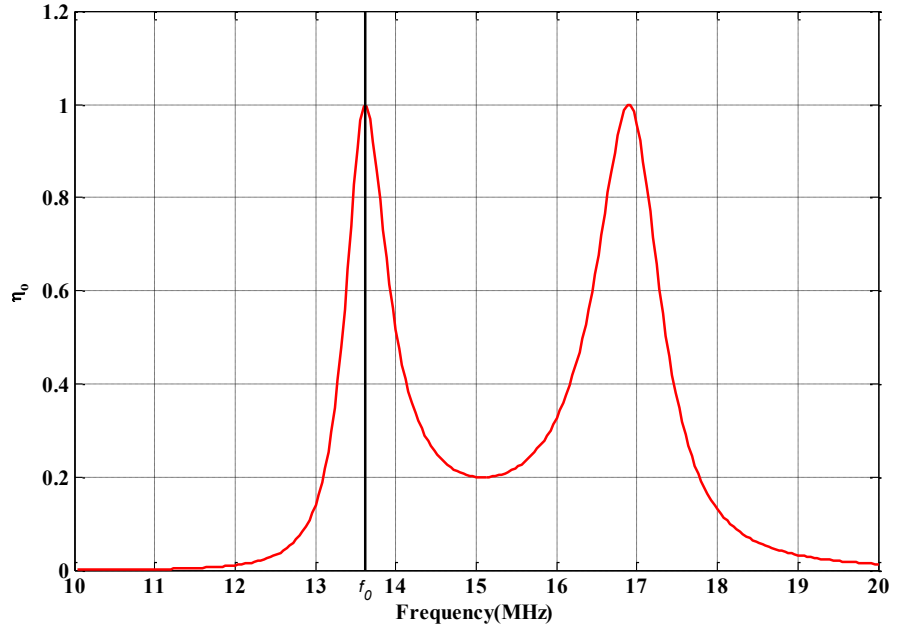

Figure 4.18 Figure of merit versus frequency at resonant frequency 13.56MHz by tuning C_1 & C_2 = 10.95pF at gap 5cm

B. Frequency Tracking

In this method, the frequency of the power source tracks one of the two maximum power transfer frequencies. However, it is more likely the system will wander out of the ISM band especially at small gaps where the two splitting frequencies diverge. For example, in Figure 4.13 the two splitting frequencies are 12.84MHz and 14.56MHz at gap = 9cm and in Figure 4.16 the two splitting frequencies are 12.4MHz and 15.36MHz at gap = 5cm. In both cases, the tracking frequencies will be out of the ISM band, where the 13.56MHz band has a frequency range of 13.553MHz and 13.567MHz [91].

In [69], the researchers worked on a 1MHz prototype system to explain the idea of frequency tracking without regard to the ISM band, while in [70] they achieved around 0.7 figure of merit within power transfer distances of 0.5m and their system dropped to less than the minimum edge of the ISM band to reach 12.8MHz.

4.5 Implementation Proposal

In this section, a practical design is suggested to implement the symmetric capacitance tuning automatically. This is an efficient solution for the frequency splitting issue encountered in some applications such as wireless charging of electric vehicles. The block diagram of the suggested design is presented in Figure 4.19. It shows that the transmitter consists of the power source, a directional coupler, a capacitor tuner, and a transmitting resonator. The receiver consists of a receiving resonator, a rectifier to provide the load with dc voltage, as well as the microcontroller with capacitor tuner. The system includes a microcontroller in both sides of the wireless power system

because the assumption is that the microcontrollers can communicate with each other by wireless link in order to achieve the symmetric tuning.

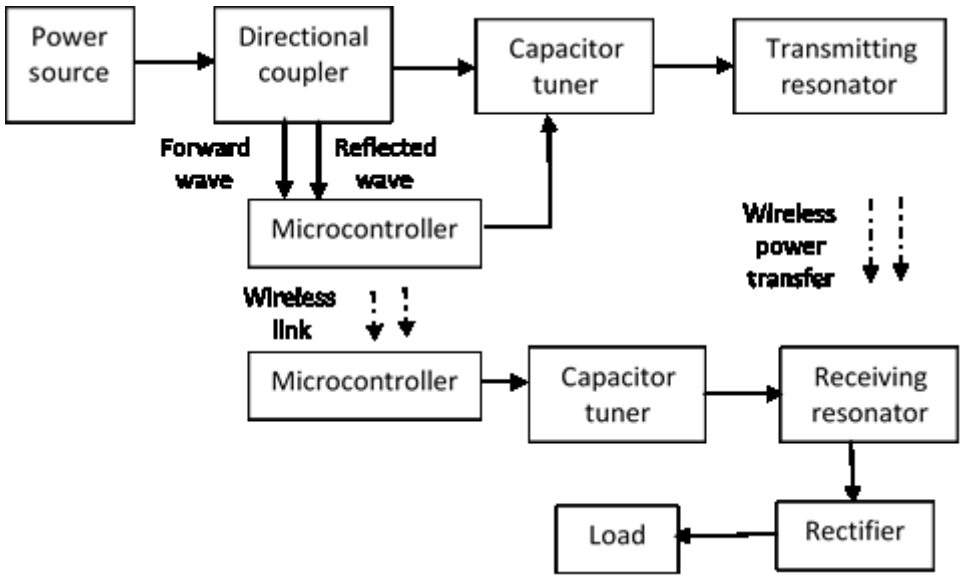

Figure 4.19 Block diagram of the suggested symmetric capacitors tuning design

A directional coupler is an electronic device that categorized as passive reciprocal network. It has four-port circuits [92]. Two of them are the main input and output. The third one is being isolated from the input port, while the last port is considered as a through port. The instrument is normally used to split the input signal and distributed power. The instrument couples part of the transmission power by a particular factor through one port. There is a wide range of applications that use directional couplers such as power monitoring and measurement. In this proposed design, the directional coupler is used to sample a small amount of wave power for measurement purposes. The power measurements include forward power and reflected power. Connecting a directional coupler in the transmitter side enables the microcontroller to measure the percentage of the reflected wave to the forward wave. That percentage should be as

small as possible in order to obtain higher wireless power transfer efficiency [54], [57], [58].

In the transmitter side, the microcontroller decides to increase or decrease the capacitance in order to reduce the percentage of the reflected wave. The decision is sent through the wireless link to the microcontroller of the receiver. Then the two microcontrollers start to communicate while adjusting the value of the capacitors to keep symmetric tuning of both sides.

Adjusting the capacitor value is achieved electronically by using a type of programmable array of capacitors that are included inside one chip such as the RFAC3612. This is a 6-bit, 64-state PAC (Programmable Array of Capacitors) for tuneable applications. It normally consists of a set of binary-weighted capacitors connected in parallel [93].

The wireless communication link between the two microcontrollers may or may not be a part of the magnetic resonance coupling itself. The process of including the link in the magnetic resonance coupling is achieved by modulation, such as amplitude modulation (AM), where tuning decisions are the information and the resonance frequency is the carrier frequency.

The dc supply of the receiver microcontroller also may or may not be a part of the magnetic resonance coupling itself. However, using the coupling for the wireless link and the supply to the receiver microcontroller needs a complicated design. To overcome the complexity, it is possible to:

- Attach a small battery in the receiver as a dc supply for the microcontroller.

- Use a separate wireless link for the microcontrollers' communication. This is achieved by different methods such as visible light communication (Li-Fi) and

infrared communication (IR) [94], [95]. Both are simple, efficient and fast methods to transmit information between the two microcontrollers [96], [97], [98]. Two ATtiny85s are used to test this type of communication. The used circuit contains an infrared emitting diode (TSAL6200) [99] in the transmitting side and a phototransistor (PT333-3C) [100] in the receiving side as shown in Figure 4.20; the test environment is shown in Figure 4.21.

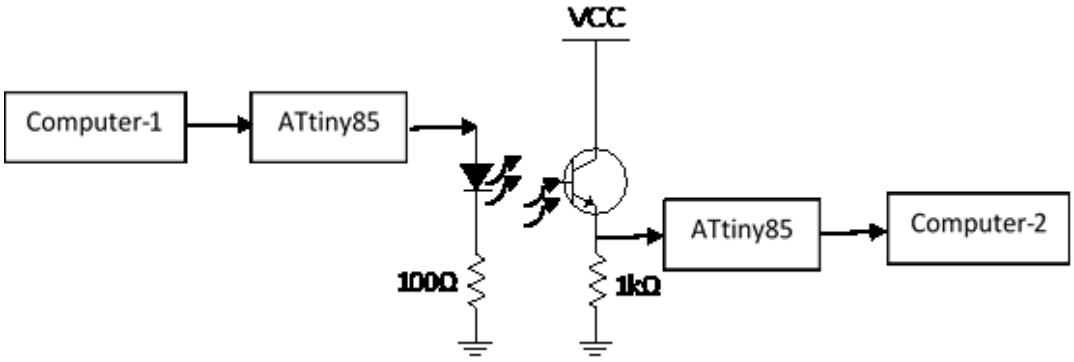

Figure 4.20 Wireless communication circuit between two microcontrollers using infrared

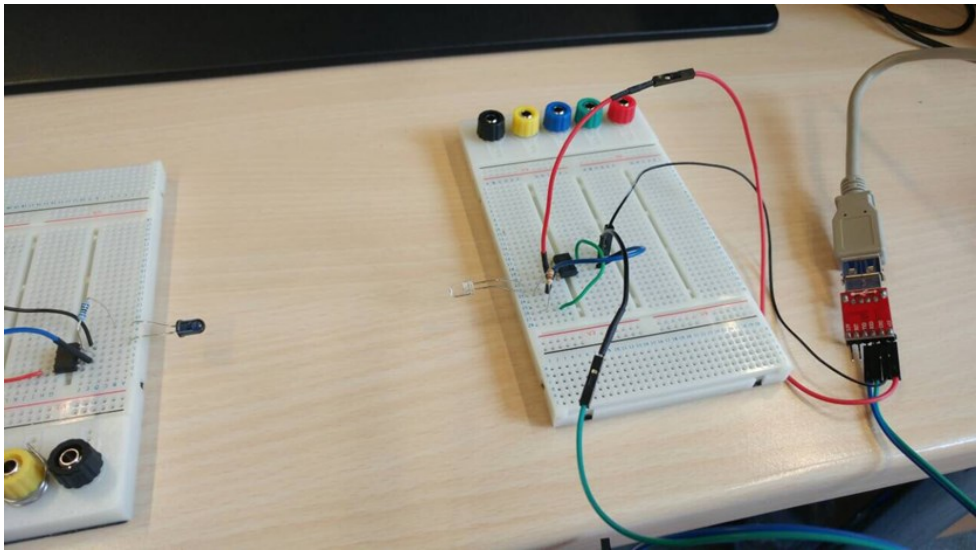

Figure 4.21 Environment of the wireless communication circuit between two microcontrollers using infrared

The information was transmitted from the first computer through the infrared devices and presented in the second computer. The used technique is software-serial which allows the serial communication between the two microcontrollers.

4.6 Conclusion

Changing the gap between the two coupled resonators in magnetic resonant wireless power transfer systems affects the maximum figure of merit. To solve the problem of splitting the original resonant frequency into two new resonance frequencies, the tuning of both capacitors simultaneously has been studied. The proposed method has more than one advantage when compared with other methods described in the literature:

- Compared to the existing frequency tracking methods, there is no moving out of the ISM band and the system keeps working at the same resonant frequency.
- Compared to the existing impedance matching methods, maximum figure of merit can be implemented easily for different gaps between the two resonators.

The Symmetric Capacitance Tuning Method is a promising way to keep maximum figure of merit at a resonant frequency with different gaps between coupled resonators which is required for practical real-world systems. Assuming there is data communication between them, the two microcontrollers control the capacitor value in both sides symmetrically in order to move the maximum figure of merit to the original frequency of the system.

Chapter 5

Connection Type Impact on the Power Transfer Efficiency of Wireless Power Transfer Systems

Magnetic resonance wireless power transfer systems consist of two resonating coils at the same resonant frequency to transfer power between them. The first resonator is the primary coil which transmits the power to the second one (the secondary or the receiver). The mutual inductance represents the magnetic coupling between the two coils, and it is calculated according to [86].

The connection in each resonator can be series or parallel. Therefore, series - series (SS) is not the only mode to design a magnetic resonant wireless power transfer system. There are three more possible topologies. These topologies are series - parallel (SP), parallel - series (PS), and parallel - parallel (PP). The performance of the system is different due to its type of connection or topology. Most researchers have worked on series-series connection in their analysis to study the power transfer efficiency [35], [54], [57], [58], [5], [75], [34].

As a near field technology, magnetic resonant wireless power transfer systems can achieve high power transfer efficiency in specific conditions. The power transfer efficiency is affected by several factors [34]: these are the resonant frequency, the parameters of the coils (inductance, size, and shape), the distance between them and so the mutual inductance, the load resistor, and the connection type of the transmitter and the receiver [101],[34]. To improve the performance of the wireless system, it is important to calculate the power transfer efficiency and understand how it is affected by each factor.

It is possible to apply magnetic resonant coupling theory on the other topologies not just the SS one (as explained in chapter 3). Each can be represented by an equivalent circuit according to the connection type of the two resonators. Analysis of these circuits is used to study the performance of different systems.

In this chapter, the figure of merit or power transfer efficiency formulas have been derived from the equivalent circuits for three of the four topologies of the power transfer system: SP, PS and PP (SS is explained in chapter 3). This analysis is used to form the basis of any wireless power system to find the best combination of connection type and distance between coils regarding the load impedance and the frequency of the circuit. Experiments were conducted inside a Faraday cage at about 2.1MHz to compare the theoretical results to the practical results. Selecting an operating frequency was based on practical considerations such as the dimensions of the coils and the available ac signal sources.

This chapter also presents an alternative method to calculate the maximum power transfer efficiency and its associated frequency which can be different from the resonant frequency in some cases. The method includes the numerical solution of the

input impedance equation. Series-parallel type connection has been chosen to examine the method and calculate the required values.

5.1 Series-parallel connection - SP

Figure 5.1 shows the wireless power transfer system and the equivalent circuit with SP connection. Applying Kirchhoff's law of voltage to each loop in the circuit provides:

$$\begin{bmatrix} V_S \\ 0 \\ 0 \end{bmatrix} = \begin{bmatrix} R_S + jX_{L1} - jX_{C1} & -jX_M & 0 \\ -jX_M & jX_{L2} - jX_{C2} & -jX_{C2} \\ 0 & -jX_{C2} & R_L - jX_{C2} \end{bmatrix} \begin{bmatrix} I_1 \\ I_2 \\ I_3 \end{bmatrix} \tag{5.1}$$

As:

$$P_{out} = \frac{1}{2}\left|I_3\right|^2 R_L \tag{5.2}$$

And under the condition of the maximum transfer of power, which is ($R_S = Z_{in}$), the source delivers maximum power to the system as:

$$P_{in,\max} = \frac{V_S^2}{8R_S} \tag{5.3}$$

The figure of merit η_0, which represents the ratio between the P_{out} and $P_{in,max}$, can be calculated as:

$$\eta_0 = 4R_S R_L \left|Z_{3,1}^{-1}\right|^2 \tag{5.4}$$

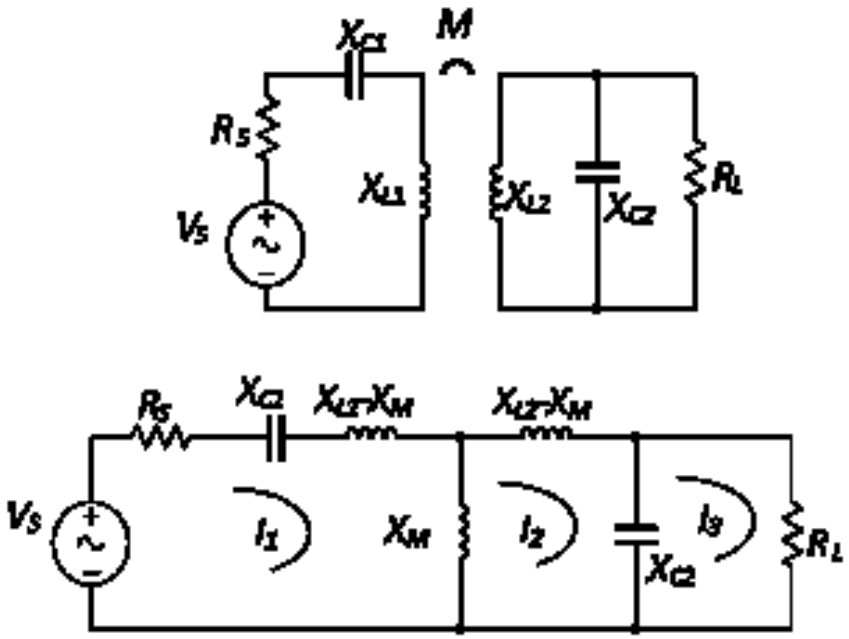

Figure 5.1 Magnetic resonant coupling circuit with series - parallel connection and the equivalent circuit

5.2 Parallel-series connection - PS

Figure 5.2 shows the wireless power transfer system and the equivalent circuit of PS connection. Applying Kirchhoff's law of voltage to each loop in the circuit provides:

$$\begin{bmatrix} V_S \\ 0 \\ 0 \end{bmatrix} = \begin{bmatrix} R_S - jX_{C1} & -jX_{C1} & 0 \\ -jX_{C1} & jX_{L1} - jX_{C1} & -jX_M \\ 0 & -jX_M & R_L + jX_{L2} - jX_{C2} \end{bmatrix} \begin{bmatrix} I_1 \\ I_2 \\ I_3 \end{bmatrix} \tag{5.5}$$

$$P_{out} = \frac{1}{2}|I_3|^2 R_L \tag{5.6}$$

$$\eta_0 = 4R_S R_L \left|Z_{3,1}^{-1}\right|^2 \tag{5.7}$$

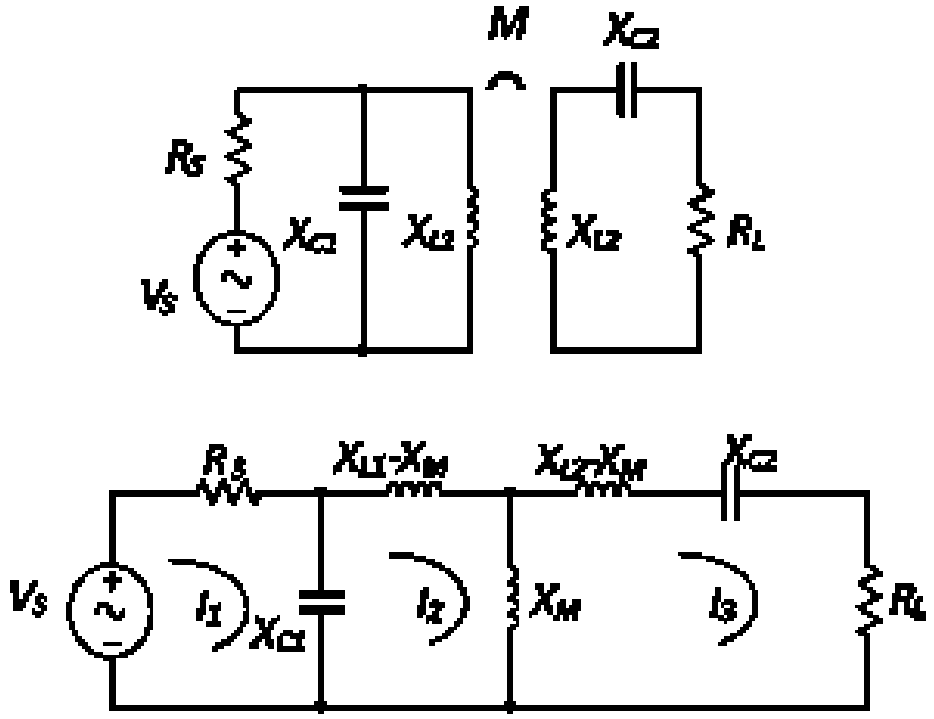

Figure 5.2 Magnetic resonant coupling circuit with parallel - series connection and the equivalent circuit

5.3 Parallel-parallel connection - PP

Figure 5.3 shows the wireless power transfer system and the equivalent circuit of PP connection. Applying Kirchhoff's law of voltage to each loop in the circuit provides:

$$\begin{bmatrix} V_S \\ 0 \\ 0 \\ 0 \end{bmatrix} = \begin{bmatrix} R_S - jX_{C1} & -jX_{C1} & 0 & 0 \\ -jX_{C1} & jX_{L1} - jX_{C1} & -jX_M & 0 \\ 0 & -jX_M & jX_{L2} - jX_{C2} & -jX_{C2} \\ 0 & 0 & -jX_{C2} & R_L - jX_{C2} \end{bmatrix} \begin{bmatrix} I_1 \\ I_2 \\ I_3 \\ I_4 \end{bmatrix} \tag{5.8}$$

$$P_{out} = \frac{1}{2}|I_4|^2 R_L \tag{5.9}$$

$$\eta_0 = 4R_S R_L \left| Z_{4,1}^{-1} \right|^2 \tag{5.10}$$

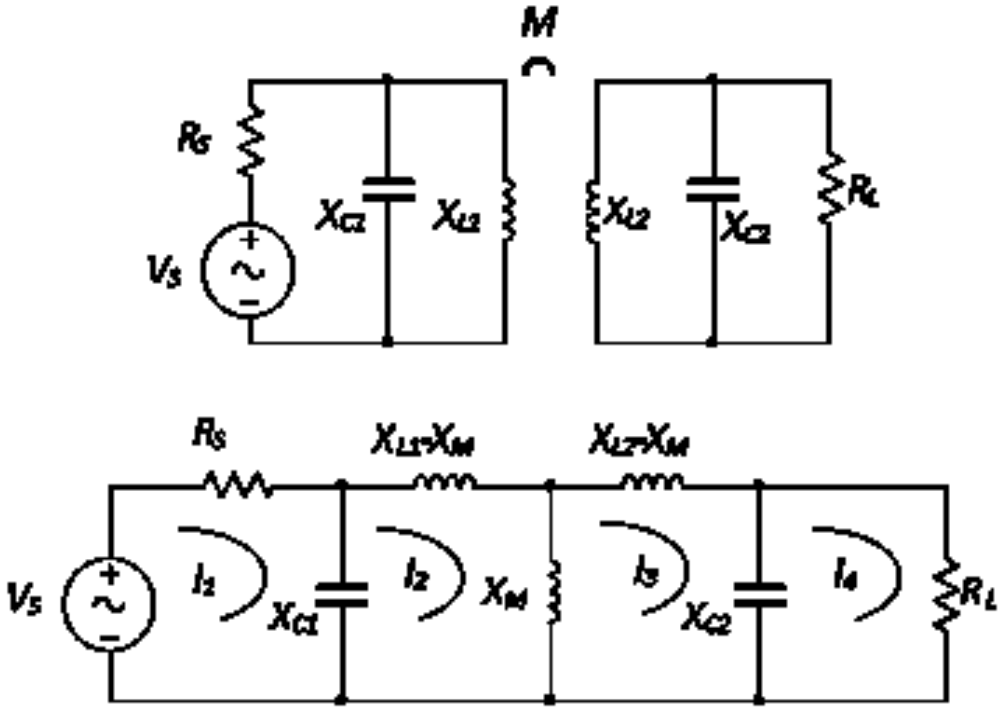

Figure 5.3 Magnetic resonant coupling circuit with parallel - parallel connection and the equivalent circuit

5.4 Mutual Inductance between Circular Pancake Coils

Another set of coils have been used to widen our study. It consists of two circular pancake coils. Figure 5.4 shows a sample of this type of coil.

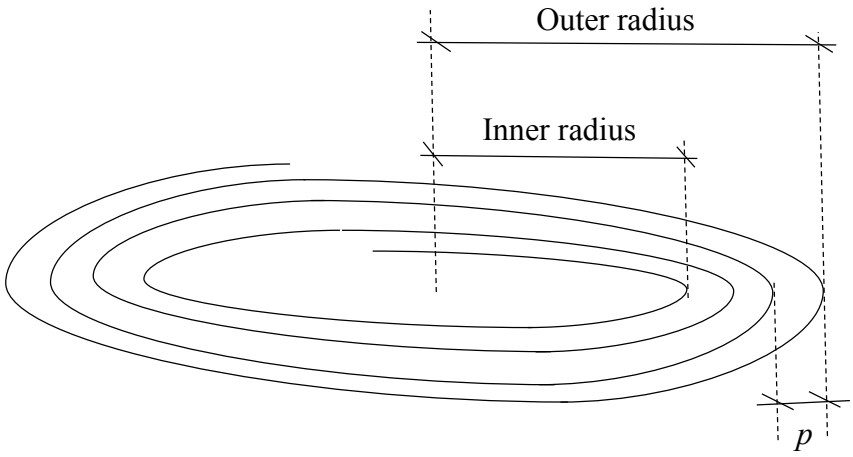

Figure 5.4 Circular pancake coil

The calculation of the mutual inductance between two circular pancake coils uses the same principle as the solenoid couple (The Neumann formula/ section 3.1). The result is the summation of the mutual inductance between each two turns. In the case of solenoid coils the radius is constant for all turns in each coil and the distance is changeable between them, while in the case of circular pancake coils, the distance between any two turns is constant at the same level and the radius of the turns is variable, as shown in Figure 5.5. Therefore, to calculate the mutual inductance between any two pancake coils by equations (3.3)-(3.6), the required modification is compensating the radius of each coil in the equations by the following formulas:

$$A(j_1) \rightarrow A + (j_1 - 1)p \tag{5.11a}$$

$$a(j_2) \rightarrow a + (j_2 - 1)p \tag{5.11b}$$

where $j_1 = 1 \rightarrow N_1$, $j_2 = 1 \rightarrow N_2$, N_1 and N_2 are the number of turns for each coil, and p is the pitch between turns (from centre to centre).

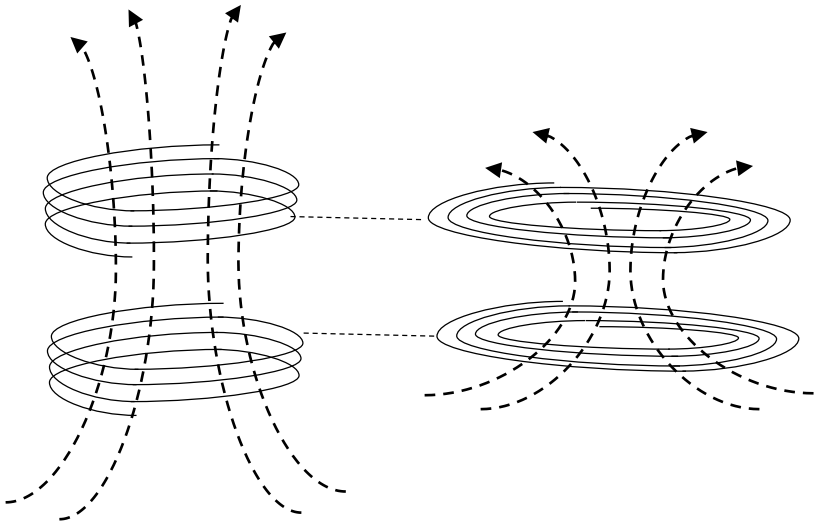

Figure 5.5 Mutual inductance between two coupled coils (a) Solenoid (b) Circular pancake

5.5 Results and Discussion

Theoretically, the four topologies are programmed in Matlab to calculate the mutual inductance and the figure of merit of each. Practically, several experiments have been conducted to support the theoretical results. In this work a set of two circular pancake coils (2.9cm inner radius and 8cm outer), with 17 turns, 3mm pitch, and an inductance equal to 31.4μH, are used in all experiments as a primary and secondary; these are shown in Figure 5.6. Additionally, a set of capacitors equal to 185pF, to resonate at 2.1MHz, were connected to the coils in series or in parallel to achieve the four topologies.

Figure 5.6 The set of the two circular pancake coils

5.5.1 SS connection

Experiment 1

Starting with a purely resistive load equal to 50Ω, the calculated figure of merit of the SS connection versus frequency is shown in Figure 5.7 at 10cm gap between the two coils. The theoretical results (Th) are compared with the experimental results (Exp) in the figure.

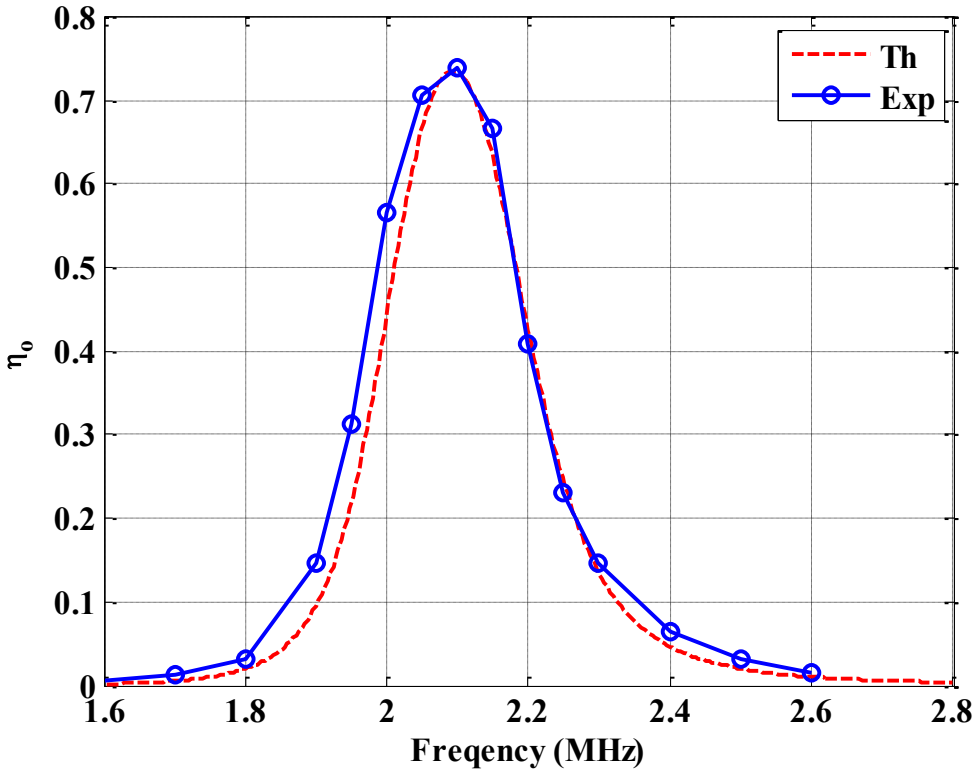

Figure 5.7 Figure of merit versus frequency for SS connection at 10cm gap, R_L = 50Ω

A. Effect of distance

Experiment 2

At the same resonant frequency, the effect of the distance between the same coils on the figure of merit is shown in Figure 5.8. The figure shows that the SS connection gives maximum figure of merit at a specific distance (7.5cm in this model) when the input impedance of our circuit matches the output impedance of the signal generator (50Ω) [34]. Comparing this result with that in Figure 3.12 (Experiment 6 / chapter 3), where the coils have the same inductance values, resonate at the same frequency, and the only difference between the two experiments is the shape of the coils, the finding

is that solenoid coils transfer power through a larger distance than pancake coils in the same circumstances.

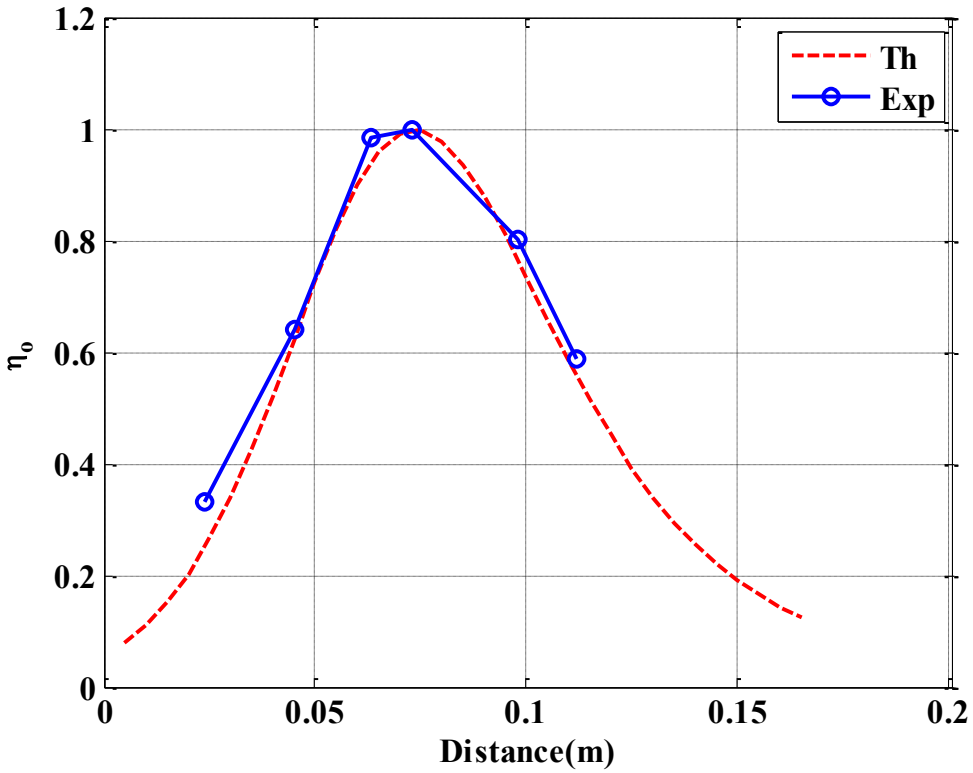

Figure 5.8 Figure of merit versus distance for SS connection at 2.1MHz, R_L = 50Ω

In summary of the performance of the SS connection system, Figure 5.9 shows a 3-D plot of the figure of merit versus frequency at different distances between the coils. The best performance of this system is at 7.5cm. At a greater distance the figure of merit decreases gradually, and at a smaller distance a splitting appears in the figure of merit pattern [34, 60].

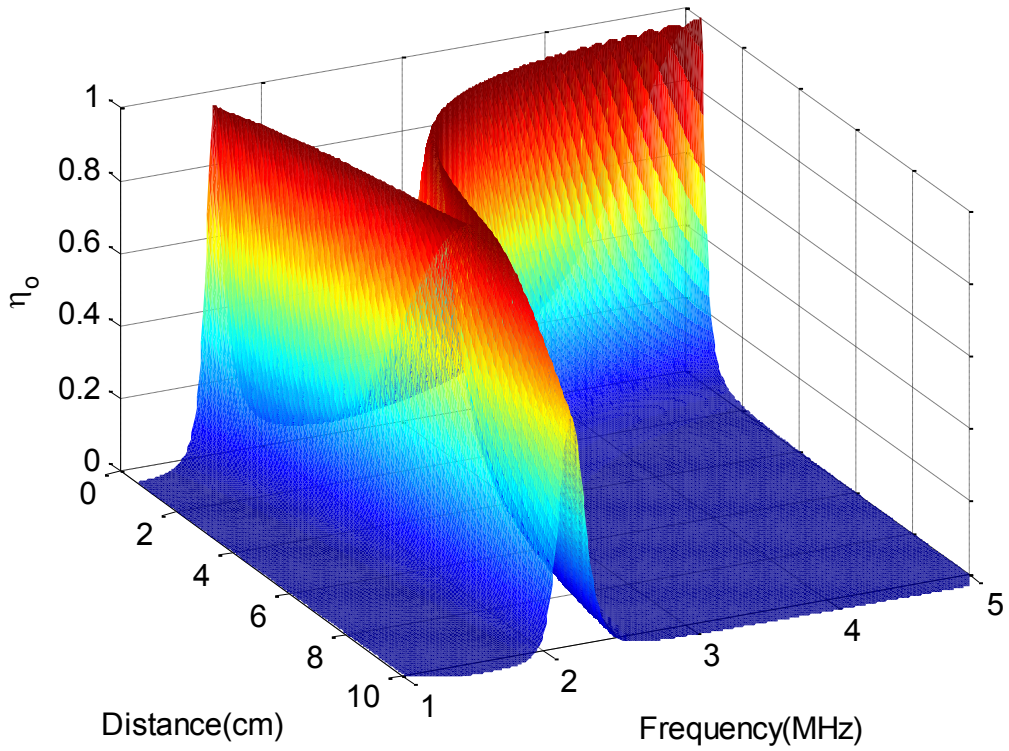

Figure 5.9 3-D plot of figure of merit versus frequency at different distances for SS connection, 50Ω

5.5.2 SP & PS connections

The next two types of connection, SP and PS, have been analysed to study the performance of the system for the same set of the pancake coils.

Experiments 3 & 4

Firstly, SP connection is used to find the relationship between the figure of merit and the frequency, with a 50Ω load at different distances (7.5cm and 3.5cm) between the coils as shown in Figure 5.10.

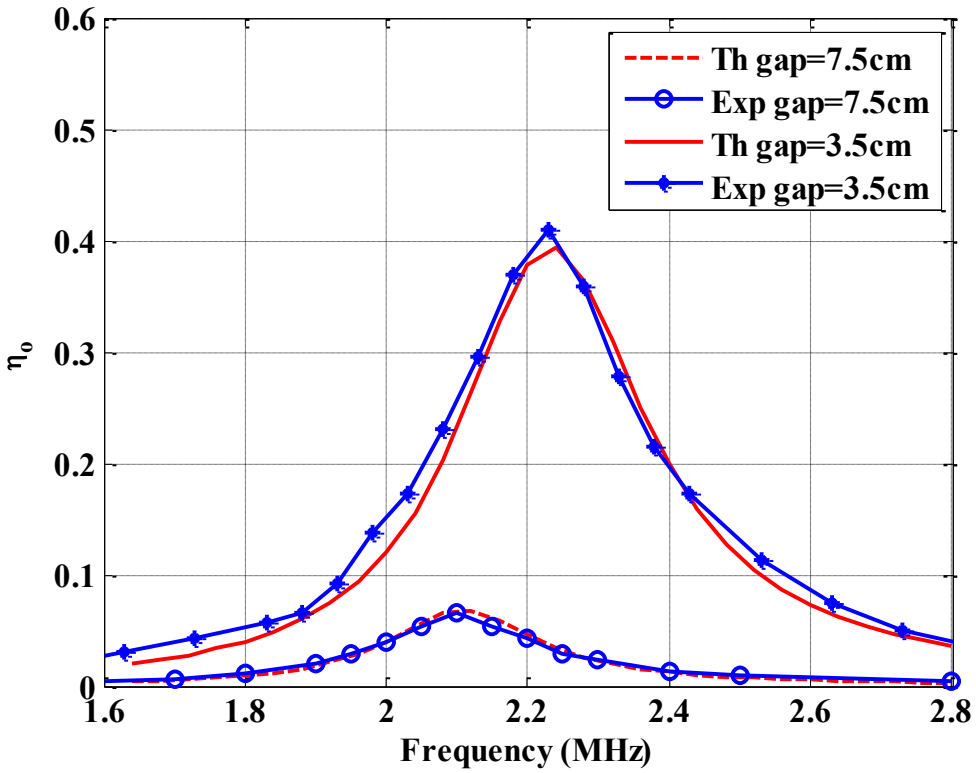

Figure 5.10 Figure of merit versus frequency for SP connection at 7.5, and 3.5cm gap, R_L = 50Ω

Experiments 5 & 6

Secondly, PS connection is used to find the relationship between the figure of merit and the frequency, with a 50Ω load at different distances (7.5cm and 3.5cm) between the coils as shown in Figure 5.11.

The Figures 5.10 and 5.11 show that the responses appear similar for SP and PS but have smaller efficiencies than the SS type at the same distance 7.5cm (Figure 5.8).

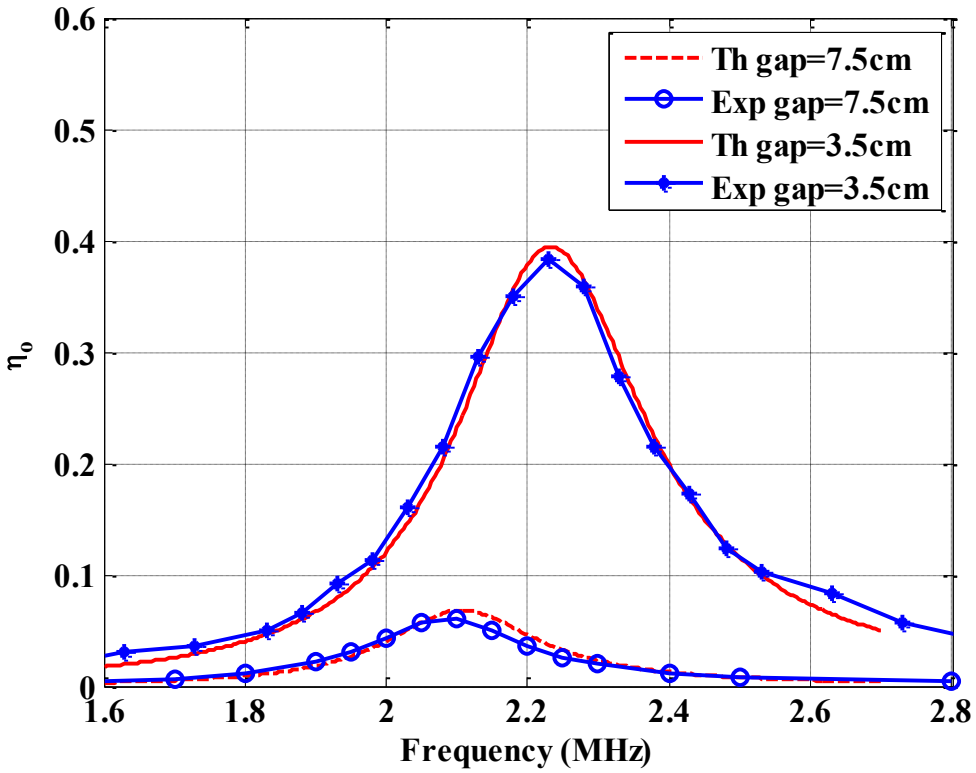

Figure 5.11 Figure of merit versus frequency for PS connection at 7.5cm and 3.5cm gap, R_L = 50Ω

B. Effect of load resistor

Experiments 7 & 8

Changing the value of the load affects the range of the power transfer. This is shown in Figure 5.12 by using 30Ω, and 1kΩ load resistors to find the figure of merit versus frequency for SP connection.

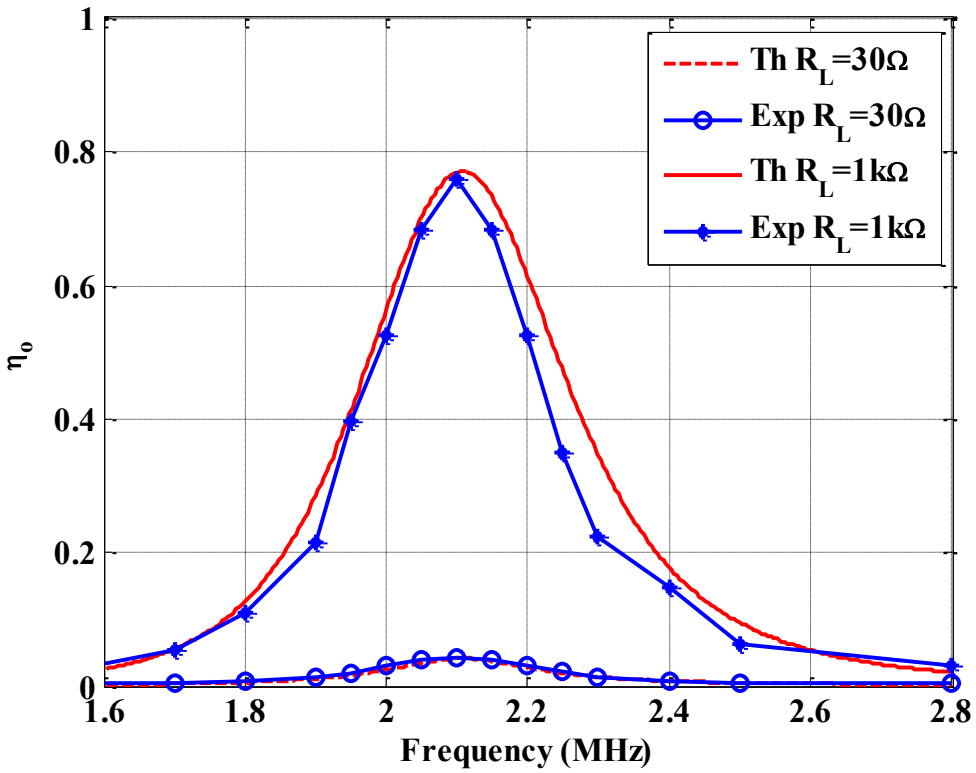

Figure 5.12 Figure of merit versus frequency for SP connection, R_L = 30Ω, 1kΩ, distance = 7.5cm

Experiments 9 & 10

Figure 5.13 shows the load effect on the range of the power transfer for PS connection by using 30Ω, and 1kΩ load resistors.

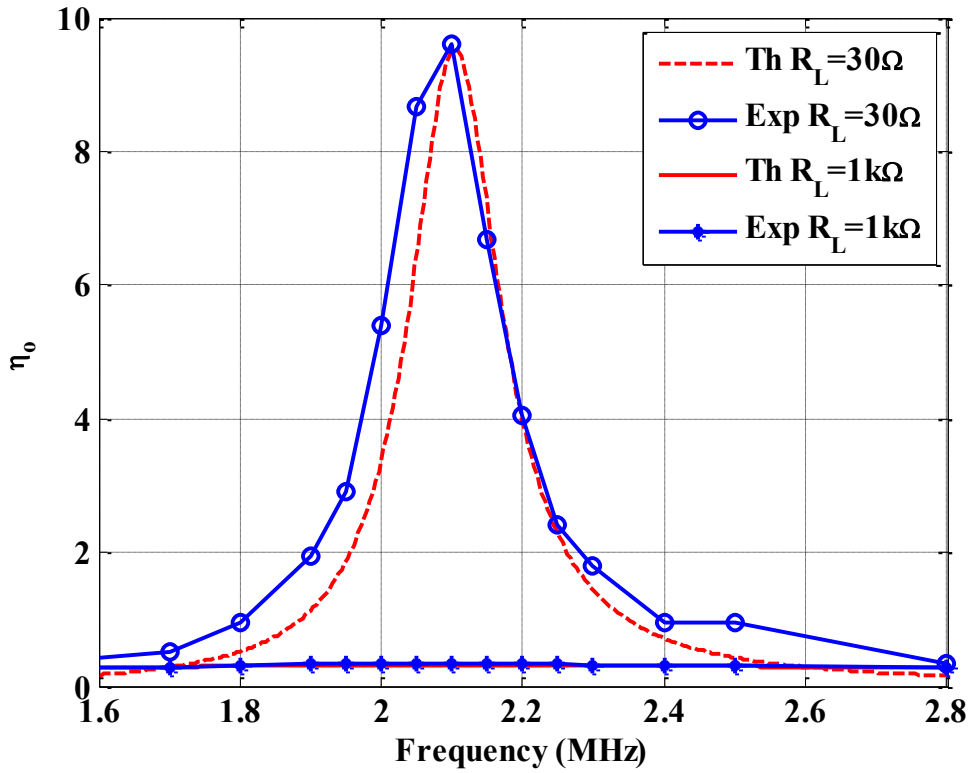

Figure 5.13 Figure of merit versus frequency for PS connection, R_L = 30Ω, 1kΩ, distance 7.5cm

The difference between the elements of the impedance matrix of SP and PS connections (see (5.1) and (5.5)), leads to different effect of the load resistor on the performance of each one. Therefore, with different values of R_L, the figure of merit of SP differs from PS as shown in Figure 5.12 and 5.13. The figure of merit of the SP connection improves with smaller values of load and the opposite occurs relative to the PS connection type.

5.5.3 PP connections

Experiments 11 & 12

Working on the PP connection with a 50Ω load provides a frequency response different to the previous types. As well as a low figure of merit, the PP connection has

a large shift in response away from the resonant frequency. Figure 5.14 shows this at two distances, 3.5cm and 7.5cm, between the two coils.

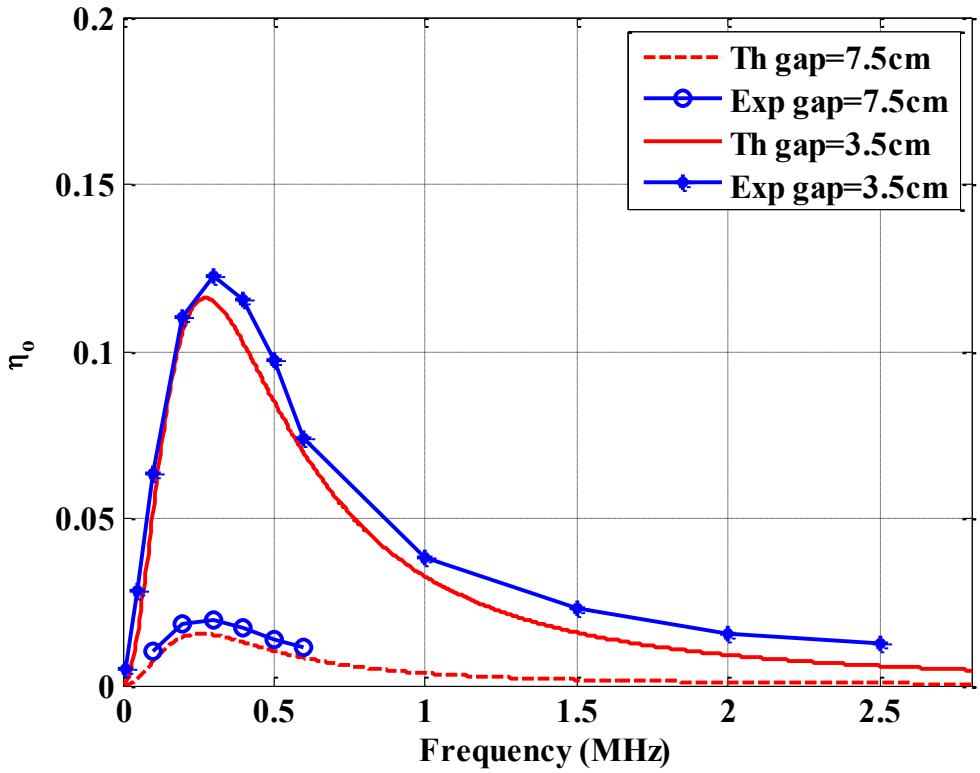

Figure 5.14 Figure of merit versus frequency for PP connection and $R_L = 50\Omega$, at gap distance = 3.5cm, 7.5cm

Experiments 13, 14 & 15

Because of the low figure of merit of the PP connection with a 50Ω load as shown in the last figure, it seems infeasible to employ it with this load. Therefore, other values of load have been used to test the performance of this type of connection, 100Ω, 1kΩ and 10kΩ as shown in Figure 5.15. It is clear from the figure that the PP connection has better performance with a smaller load.

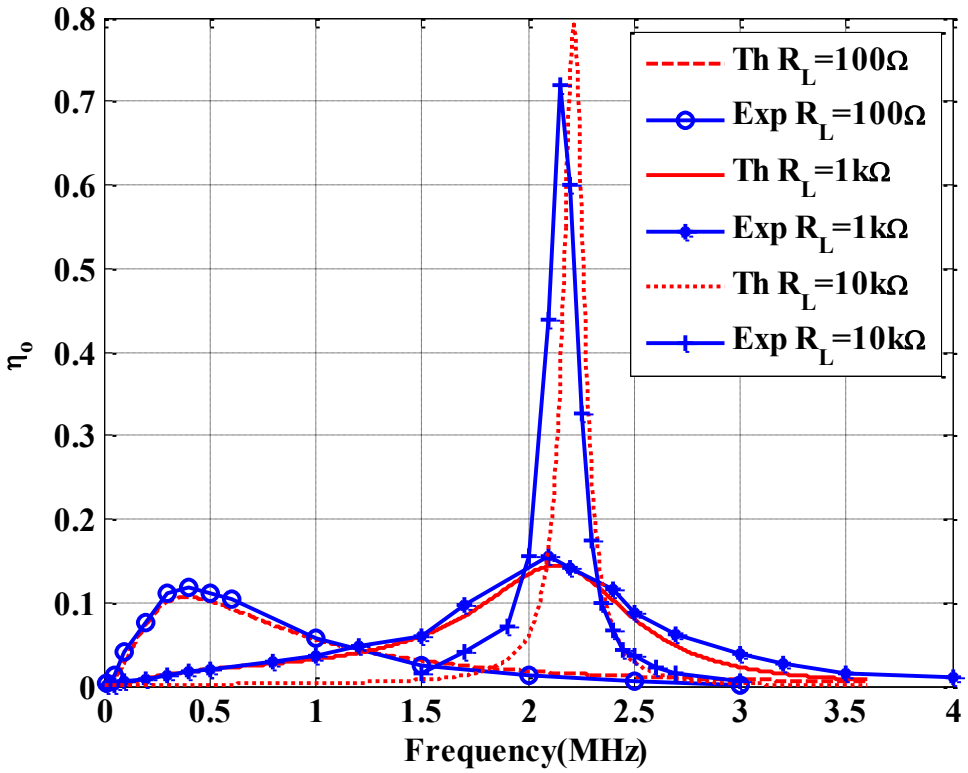

Figure 5.15 Figure of merit versus frequency for PP connection at distance = 3.5cm, using R_L = 100Ω, 1kΩ, 10kΩ

5.6 Maximum Figure of Merit Calculation by Numerical Solution of Input Impedance Equation

Analysis of magnetic resonant wireless power transfer systems aims to achieve maximum power transfer efficiency [102]. From the analysis we wish to derive the maximum power and the frequency at which this occurs. This section presents a second method to estimate these two required values and to achieve this requires the solution of the input impedance equation numerically. The frequency of the maximum figure of merit is found when the imaginary part of the input impedance is close to zero, and this could be different from the natural resonance frequency. We estimate the figure of merit value which depends on the real value part of the input impedance. The

proposed method has been applied to one of the four types of possible connections, a series-parallel (SP) connection, although similar approaches could be applied to the other types. The results of the two modes (the method presented in section 5.1 and the numerical calculation of the input impedance) are compared to evaluate the new mode and show the differences in the calculation methods. In some cases the maximum figure of merit shifts away from the resonant frequency. Therefore, this section shows how to use the same equations to achieve maximum figure of merit at resonance and suggests a design method to achieve this practically.

5.6.1 Theoretical analysis of new mode of figure of merit calculation

As previously mentioned, the equivalent circuit of a wireless power system can be expressed by applying Kirchhoff's law of voltage on each loop in the circuit producing a set of equations [101]. Starting with the impedance matrix representation, the second way to calculate the figure of merit is as follows:

$$V_S = I_1(R_S + Z_{in}) \tag{5.12}$$

where Z_{in} is the input impedance for the complete circuit as shown in Figure 5.16. From (5.1) and (5.12), it can be found that:

$$Z_{in} = \frac{1}{Z_{1,1}^{-1}} - R_S \tag{5.13}$$

and

$$Z_{in} = R_{in} + jX_{in} \tag{5.14}$$

where R_{in} and X_{in} are the real and the imaginary parts of the input impedance, respectively. Both of them are function of frequency because their calculations depend on the matrix form (5.1). From (5.1) and (5.14), X_{in} can be expressed as:

$$X_{in}(f) = A_1 f + \frac{A_2}{f} + A_3 f^3 + \frac{A_4}{f^3} \tag{5.15}$$

The values of A_1, A_2, A_3, and A_4 depend on the parameters of the circuit.

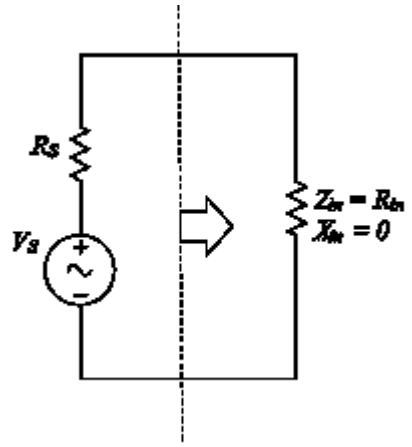

Figure 5.16 Equivalent circuit at the maximum transfer of power

According to the power transfer theorem for complex impedances, the maximum power will be transferred when $Z_S = Z_{in}^*$. As we have $Z_S = R_S$, the maximum figure of merit occurs when the imaginary part of the input impedance is equal to zero. Therefore, the frequency providing maximum figure of merit (even if it is different from the original resonant frequency) can be found from:

$$X_{in}(f) = 0 \tag{5.16}$$

It is apparent that solving (5.15) and (5.16) is complicated and does not have an analytical solution, therefore it must be solved numerically in order to calculate the required frequency. The second step is to find the value of the maximum figure of merit which is achieved by finding the real part R_{in} at that calculated frequency. The equivalent circuit in this stage is shown in Figure 5.16. Assuming maximum transfer of power the figure of merit is derived by:

$$\eta_0 = \frac{4R_S R_{in}}{(R_S + R_{in})^2} \tag{5.17}$$

5.6.2 Results and discussion of input impedance mode

The representation of the series-parallel circuit is modelled in Matlab to calculate the maximum figure of merit and the associated frequency using the input impedance mode. In this part the same set of the two circular pancake coils are used as the primary and secondary in order to compare the results to the previous method. Each coil has 2.9cm inner radius and 8cm outer, with 17 turns, 3mm pitch, and an inductance equal to 31.4μH. Additionally, a set of capacitors equal to 185pF, tuned to work at 2.1MHz was connected to the coils in series in the transmitter and in parallel in the receiver.

In this part of the study 30Ω, 50Ω, 100Ω, and 1kΩ impedances have been used to calculate the maximum figure of merit and the associated frequency at different gaps between the two coils. Table 5.1 contains the parameters and the results for each case. Using various values shows the effect of the load resistor as well as the effect of distance. Some of these cases were used in the experiments of the previous method (figure of merit versus frequency and figure of merit versus distance curves in section 5.5.2), and that is so we can compare the results of the two modes.

Table 5.1 Maximum figure of merit and associated frequency calculated by the input impedance for the different cases

Case	**1**	**2**	**3**	**4**	**5**	**6**	**7**
Gap (cm)	3.5	3.5	3.5	5	5	7.5	7.5
R_L (Ω)	30	50	100	50	100	100	1k
$f(X_{in}\approx 0)$(MHz)	2.23	2.23	2.23	2.15	2.15	2.11	2.11
R_{in} ($X_{in}\approx 0$) (Ω)	3.75	6.25	12.5	2.86	5.7	1.77	17.61
$\eta_{0\max}$	25.9	39.5	63.94	20.47	36.84	13.17	77.01

The maximum figure of merit and the associated frequency (calculated by the input impedance and included in Table 5.1 cases 2 & 7) are well matched; the curves are shown in Figures 5.10 & 5.12. It is clear from them that the maximum figure of merit increases and shifts away from the original resonant frequency for small gaps. Working with different load resistor values affects the figure of merit of the wireless system. The table shows the system has high figure of merit with small load at the same distance. In all cases there is a small shift in the maximum figure of merit point compared to the resonant frequency.

To show the shift in maximum figure of merit, the figure of merit and input impedance curves, including the real and the imaginary parts for case 3 in Table 5.1, are all shown in Figure 5.17. The figure also defines the exact original resonant frequency at 2.088MHz.

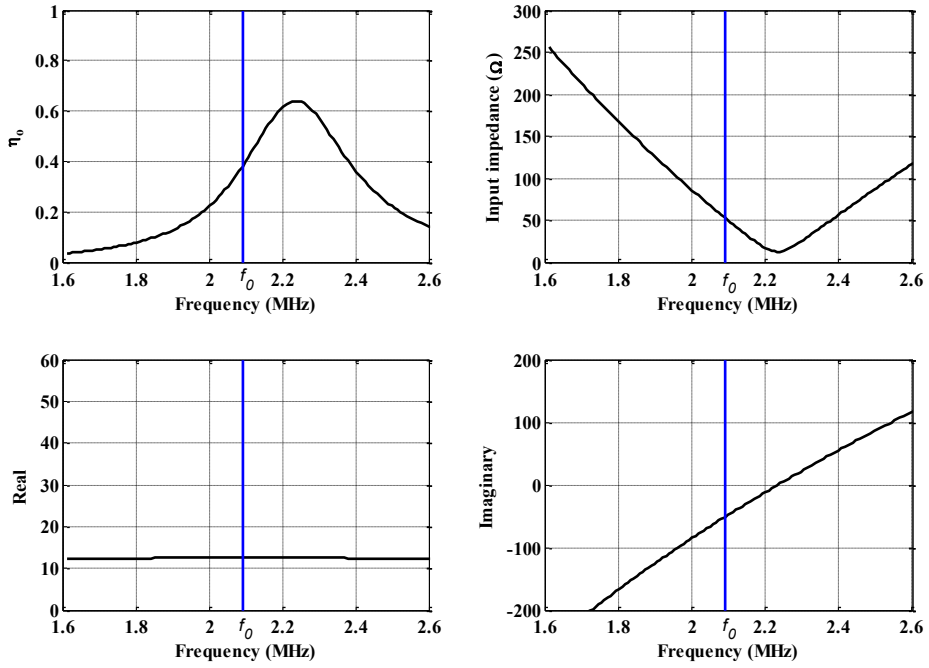

Figure 5.17 Figure of merit, input impedance, real, and imaginary versus frequency, R_L = 100Ω, gap = 3.5cm

5.6.3 Moving the maximum figure of merit to the resonance frequency

For practical and efficient systems, it is important to obtain maximum figure of merit at the resonant frequency, otherwise the system might lose a significant part of the transferred power. It is obvious from the previous figures that there is no symmetry in the curves, and the maximum figure of merit shifts to one side of the resonant frequency. It can be concluded that tuning one of the capacitors is sufficient to re-merge the maximum figure of merit with the original resonant frequency. This is possible by using the input impedance equation (the imaginary part) in a different way:

$$X_{in}(C_1) = 0 \tag{5.18}$$

Using the resonance frequency to solve the last equation provides the capacitor value C_1 that achieves the maximum figure of merit at that frequency, as shown in Figure 5.18. The figure shows that C_1 = 212pF is the required value; it can be calculated numerically from equation (5.18). Using the calculated value of C_1 equates the imaginary part of the input impedance to zero and then matches the highest figure of merit with the resonance frequency, as shown in Figure 5.19. The figure shows that the figure of merit at the original frequency is 0.64 instead of 0.38 (Figure 5.17), which provides about 26% improvement in this case.

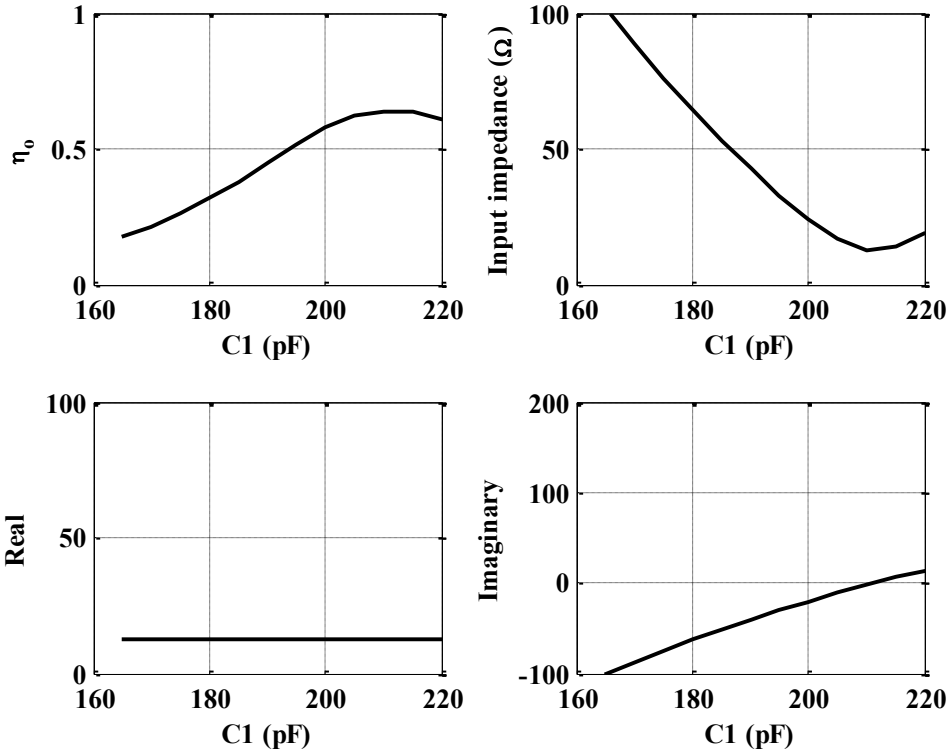

Figure 5.18 Figure of merit, input impedance, real, and imaginary versus C_1, at f_0 = 2.088MHz, R_L = 100Ω, gap=3.5cm

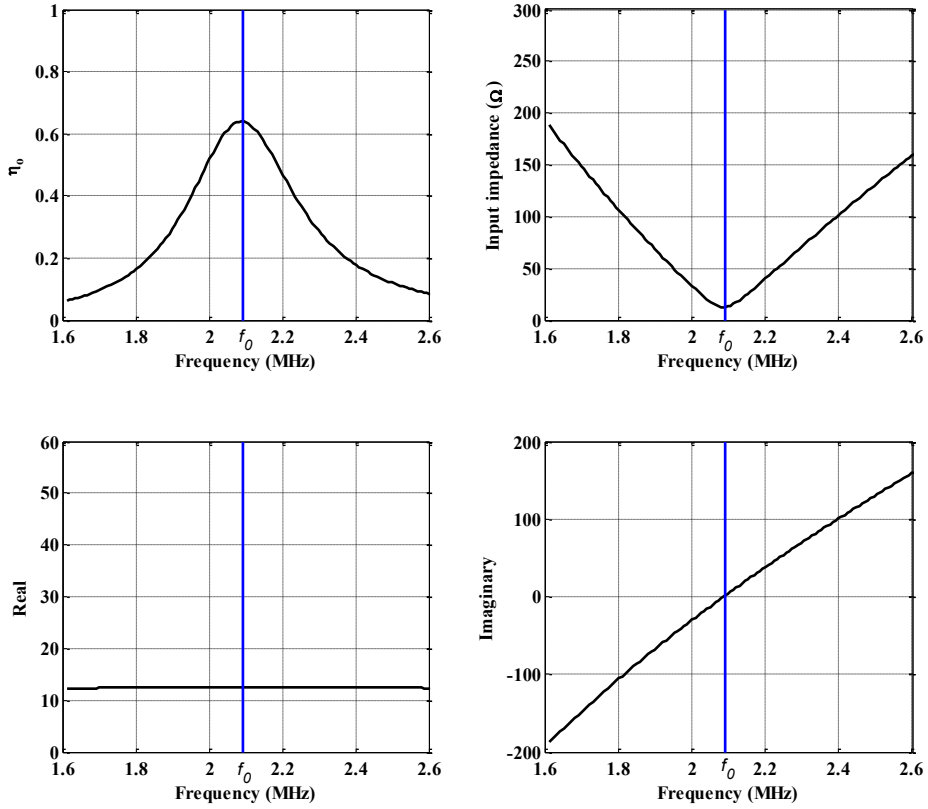

Figure 5.19 Figure of merit, input impedance, real, and imaginary versus frequency, R_L = 100Ω, gap = 3.5cm, C_1 = 212pF

Applying the proposed method empirically to improve the performance of the system by moving the maximum figure of merit to the original resonant frequency is achieved by measuring the phase shift between the real and the imaginary parts of the input impedance. The phase shift indicates the imaginary part; its zero value means that the imaginary part of the input impedance is zero and this is the required value from the design, according to the following formula:

$$phaseshift = \tan^{-1}\frac{X_C}{R} \tag{5.19}$$

The suggested design is shown in Figure 5.20. It is suitable for specific ranges in the series-parallel parameters, where a capacitive effect is observed in the input impedance of the wireless system. To reduce this effect, increasing the capacitance of the transmitter side is needed. The figure shows that the microcontroller controls the capacitor value in the transmitter side according to the calculation of the phase shift of the input impedance in order to reduce it to zero. The phase shift can be calculated by continuously comparing the signals during a complete period of time.

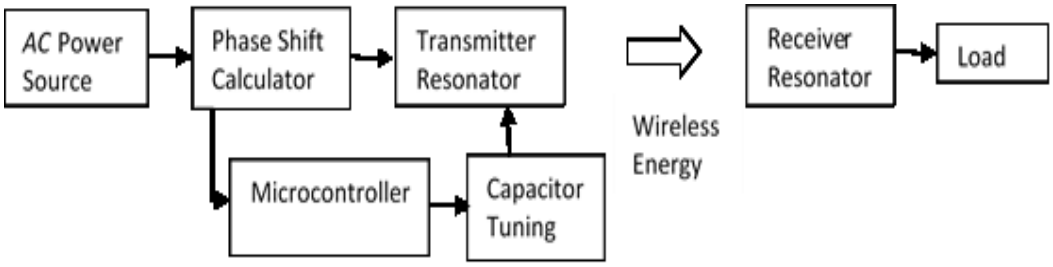

Figure 5.20 Block diagram of the suggested design

To design a system theoretically the steps are: specify the parameters of the circuit; choose the resonant frequency; calculate the required value of the tuning capacitor to achieve maximum figure of merit at resonance. To apply the system practically requires the following steps: calculate the phase shift of the input impedance; automatically tune the transmitter capacitor to reduce the phase shift; reduce the imaginary part of the input impedance.

5.7 Conclusion

The performance of a wireless power transfer system depends on the configuration of both the transmitter and receiver as well as other factors such as: the characteristics of

the coils; the distance; the mutual inductance between them, and the resonance frequency. This chapter presents two modes to analyse magnetic resonant wireless systems.

1. The first mode includes analysis of four types of connection SS, SP, PS and PP in order to understand the figure of merit of wireless power systems.

The theoretical analysis provides results which are well matched to the empirical results and can form the basis for any required design.

The following observations can be made:

- An SS connection is more suitable for systems with larger loads. The maximum transfer of power occurs at a specific distance between the two coils when the input impedance of the system is equal to the internal impedance of the source. This distance can change according to the load.
- SP and PS connections have similar performance for similar coils when the load impedance matches the internal resistance of the source. The performance of SP and PS will differ considerably with other values of the load. The performance of an SP connection improves with small load and the opposite is true for the PS type.
- A PP connection is more appropriate for systems with a small load. Maximum transfer increases at small distances between the coils with a frequency shift compared to the original resonance frequency.

However, having more than one mode to calculate the figure of merit is more convenient and allows results to be compared with one another.

2. The second proposed method is a quick and simple mode to identify i) the maximum figure of merit in a series-parallel wireless power transfer system

and ii) the associated frequency. The idea is to equate the imaginary part of the input impedance with zero to find the frequency, and then calculate the maximum figure of merit at that frequency from the real part.

- Initially, the proposed method was applied to the series-parallel case. In our future work, this method can be applied on the other topologies of resonant wireless power systems.
- This work markedly improves the figure of merit of a series-parallel wireless system. The limitations of achieving this practically are limited to specific ranges of parameters where a capacitive effect is observed in the input impedance.

Chapter 6

Intelligent Management and Control of Received Wireless Power

6.1 Introduction

The performance of the traditional wireless transformer (without iron core), which is based on inductive magnetic coupling between primary and secondary coils, improves when the two coils resonate at the same frequency [12, 72]. This forms the basis of most wireless charging systems, allowing transfer of energy across free space at distance. The amount of power transfer is dependent on the mutual inductance between the two coils, which is inversely proportional to the distance between them [38], [34]. The secondary coil needs to receive enough power to do useful work, otherwise work becomes impossible. Considering this the following questions come to mind [103]:

a. Can tiny amounts of power really do useful work?

Traditionally, very low resonant power systems have no major function. However, new systems are appearing [104] which store energy in capacitors and discharge larger currents for short periods of time thus doing useful work through large loads.

b. Can a device do useful work without access to a supply such as a battery?

Using wireless power transfer, it is possible to receive power wirelessly and do work without any storage medium at all [72], [105]. A low power example is the battery free receiver designed by the Power-Cast Group [84]. This product is the P2110B 915 MHz RF Power Harvester far field Receiver [106] and is designed for sensor networks and active Radio Frequency Identification RFID.

Question (a) illustrates the importance of including intelligent control in the secondary, and distinguishes our system from that of the Power-Cast group. With intelligent control, it is possible to run a load from a source which has less instantaneous energy than the requirements of the load; a bit like saving up to buy something one cannot immediately afford. This is achieved by accumulating power for a specific length of time, then feeding the load for the rest of the cycle. To accumulate a desired quantity of energy, it is necessary to observe/measure a resource. The act of performing a measurement is, in itself, parasitic to the secondary and the more frequently one measures a resource the more energy is consumed without doing useful work. An obvious approach is to perform measurements at regular intervals, but if the system is understood, observations need only be sparse achieving greater efficiency for a given setup.

This chapter introduces an intelligent algorithm for power accumulation which optimally adapts to variations in primary sources and secondary loads, subject to losses from the microcontroller and capacitance leakage.

6.2 Intelligent Control

Wireless transfer of power by magnetic resonance is important for charging devices such as mobile phones and vehicles [107-110]. This has motivated researchers to study how to improve the performance of wireless power transfer systems by increasing the efficiency with different techniques [36], [58], [111]. As well as improving efficiency, managing the power consumption of the control system itself can also improve performance. To illustrate intelligent control of wireless power transfer an algorithm was created and examined in a test bed. The idea was to periodically run a load from a source which has less power than the continuous requirements of the load. This was achieved by scheduling the work time for the load into short bursts or shifts in the duty cycle according to the voltage accumulated on a capacitor. The steps to achieve this were: turn the load off; wait for energy accumulation on the capacitor; turn the load on for a specific time; deplete the capacitor to a known level; turn off and repeat from the beginning. The block diagram of the system is shown in Figure 6.1(a). Power is transferred through the wireless system. The received voltage is rectified and stored in the reservoir capacitor. The capacitor represents the dc source of the receiver. The microcontroller makes a decision to turn the load on or off according to the charge state of the capacitor.

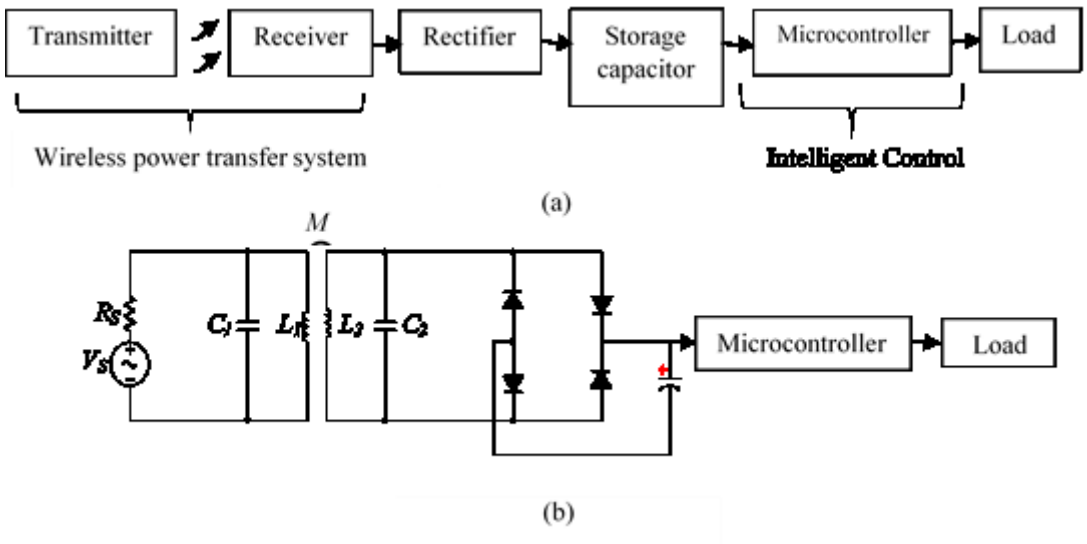

Figure 6.1 Wireless power transfer system with intelligent control: (a) block diagram (b) schematic diagram

Figure 6.1(b) shows the simplified schematic diagram of the system. The voltage source V_s has an internal resistor of R_S. The wireless power transfer system consists of the primary resonator (L_1 in parallel with C_1) and the secondary resonator (L_2 in parallel with C_2). The mutual inductance between the two resonators is represented by M in the figure.

The testbed uses a loop antenna similar to those used for far field transceivers. It is used for convenience due to its impedance characteristics. Loop antennas are common for applications in the HF band (3-30 MHz) [112], [113]. The loop antenna is a radio device which consists of one or more loops [114]. In our design, two loops have been used as shown in Figure 6.2. The first one is the coaxial oscillating loop or coupling loop which has a 50Ω impedance to match the source which is a signal generator. The second one is the main loop or the free running loop (in resonance), which represents the transmitter for the overall design; its circumference generally is less than 1/10 wavelength [114], [115]. A tuning capacitor is also used for fine adjustments.

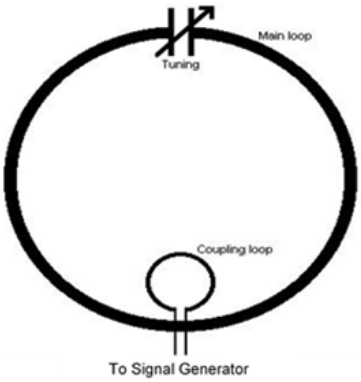

Figure 6.2 Loop antenna

6.3 The Algorithm

To manage energy over time, it is necessary to read the capacitor voltage regularly until a target voltage is attained. Then a decision can be made to run the load. This could be done using discrete electronics or a low power microcontroller. The new generation of ultra-low power controllers such as the Atmel ATtiny85 and the TI MSP430 [116], [117] have comparable or better power consumption than bespoke electronics with the added advantage of onboard computation.

A microcontroller in the awake state can consume 2-3 orders of magnitude more power than when asleep [118]. Our system moves beyond simply 'sitting' and waiting for the capacitor to charge before doing anything; the capacitor voltage will be the V_{CC} of the microcontroller. Two readings are taken of the capacitor voltage at separate times and used to calculate the time constant of the system. From this the required sleep time can be calculated, so the microcontroller awakes at the point where the capacitor has reached the desired charge (recall sleep is much more energy efficient than awake). Two readings are used in the first cycle followed by a single reading in subsequent

cycles to update the estimated time constant. The outline of the algorithm is described as follows:

1) Read V_{CC}
2) Sleep for a short time
3) Read V_{CC}
4) Calculate τ_{ch} (time constant for charging)
5) Find (t_{sleep}) the required time for sleeping until target
6) Sleep for t_{sleep}
7) Wake up, read V_{CC} and turn the load on
8) Delay for short time
9) Read V_{CC}
10) Calculate τ_d (time constant for discharging)
11) Find (t_{on}) the required time for turning the load on
12) Delay for t_{on}
13) Repeat from step 5

6.3.1 Charging time constant (τ_{ch}) calculation

Step 4 in the algorithm needs some clarification, where τ_{ch} is the time constant of charging the capacitor in the system. It is known as:

$$\tau_{ch} = R_{ch}C \tag{6.1}$$

where R_{ch} is the equivalent impedance in series with capacitor C [119]. Figure 6.3 shows the mechanism of charging and discharging the capacitor. The dc source V_{dc} in our system is the output of the full-wave rectifier.

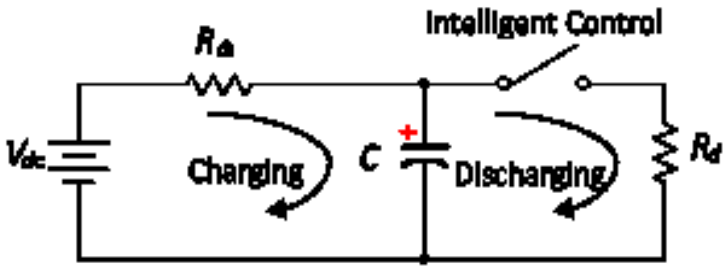

Figure 6.3 Circuit of charging and discharging a capacitor

In this system R_{ch} is not a constant impedance. It is the equivalent impedance of the combined circuit before the capacitor and is difficult to calculate as it changes with coupling and load. Therefore, the time constant needs to be calculated regularly and updated.

It is possible to calculate the time constant from two readings of the capacitor's voltage at any given time while it is charging. The time constant for charging can be calculated in this way starting with the basic capacitor charging formula, as shown below:

$$V_0 = V_{in}\left(1 - e^{-t_0/\tau_{ch}}\right) \tag{6.2a}$$

$$V_1 = V_{in}\left(1 - e^{-t_1/\tau_{ch}}\right) \tag{6.2b}$$

where V_1 and V_0 are the voltage readings at t_1 and t_0, respectively, and V_{in} is the maximum voltage as shown in Figure 6.4. The figure shows the capacitor charging curve (V_C versus time), including $V_{target1}$ (the target voltage during charging) and t_{sleep} (the required time to reach the target voltage). These two equations can be re written:

$$t_0 = -\tau_{ch} \ln\left(1 - \frac{V_0}{V_{in}}\right) \tag{6.3a}$$

$$t_1 = -\tau_{ch} \ln\left(1 - \frac{V_1}{V_{in}}\right) \tag{6.3b}$$

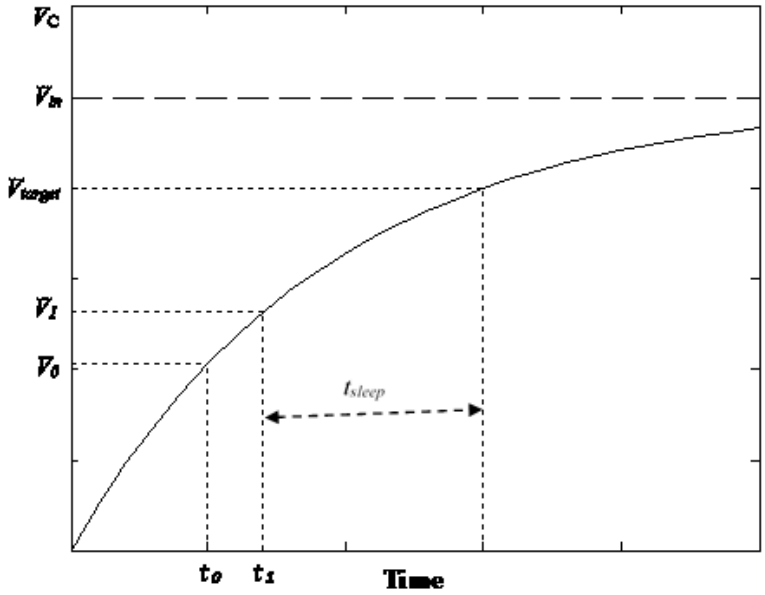

Figure 6.4 Capacitor charging

Taking the difference between the two times leads to:

$$t_1 - t_0 = -\tau_{ch} \ln\left(1 - \frac{V_1}{V_{in}}\right) + \tau_{ch} \ln\left(1 - \frac{V_0}{V_{in}}\right) \tag{6.4}$$

$$\tau_{ch} = \frac{t_1 - t_0}{\ln\left(1 - \frac{V_0}{V_{in}}\right) - \ln\left(1 - \frac{V_1}{V_{in}}\right)} \tag{6.5}$$

$$\tau_{ch} = \frac{t_1 - t_0}{\ln\left(\frac{V_{in} - V_0}{V_{in} - V_1}\right)} \tag{6.6}$$

giving an estimate for the time constant regardless of where we are on the charging curve. From the calculated charging time constant the microcontroller can find the required sleep time as in step 5 of the algorithm by:

$$t_{sleep} = \tau_{ch} \ln\left(\frac{V_{in} - V_1}{V_{in} - V_{target1}}\right) \tag{6.7}$$

6.3.2 Discharging time constant (τ_d) calculation

Similar to the above, the time constant for discharging can be calculated as required in step 10. The time constant in the discharging process, τ_d, depends on the parallel load resistance R_d [119]. In this system R_d represents the equivalent resistance of the circuit beyond the capacitor, and it is defined as:

$$\tau_d = R_d C \tag{6.8}$$

As before, taking two voltage readings (V_2 and V_3 from Figure 6.5) is sufficient to find the discharging time constant. The figure shows the capacitor discharging curve, including $V_{target2}$ (the target voltage during discharging) and t_{on} (the required time to reach the target voltage). The first reading is taken at the highest charged point t_2. The second reading should be taken a short while afterwards, t_3, as shown in Figure 6.5.

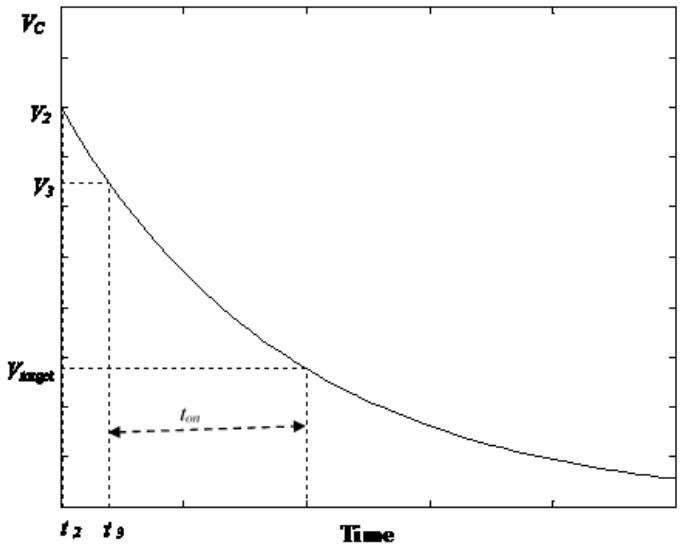

Figure 6.5 Capacitor discharging

Starting with the capacitor discharging formula, τ_d is derived as shown below:

$$V_2 = V_{start} e^{-t_2/\tau_d} \tag{6.9a}$$

$$V_3 = V_{start} e^{-t_3/\tau_d} \tag{6.9b}$$

where V_{start} is the initial voltage of discharging.

These two equations can be re-written:

$$t_2 = -\tau_d \ln\left(\frac{V_2}{V_{start}}\right) \tag{6.10a}$$

$$t_3 = -\tau_d \ln\left(\frac{V_3}{V_{start}}\right) \tag{6.10b}$$

Taking the difference between the two times leads to:

$$t_3 - t_2 = -\tau_d \ln\left(\frac{V_3}{V_{start}}\right) + \tau_d \ln\left(\frac{V_2}{V_{start}}\right) \tag{6.11}$$

$$\tau_d = \frac{t_3 - t_2}{\ln\left(\frac{V_2}{V_{start}}\right) - \ln\left(\frac{V_3}{V_{start}}\right)} \tag{6.12}$$

$$\tau_d = \frac{t_3 - t_2}{\ln\left(\frac{V_2}{V_3}\right)} \tag{6.13}$$

With reference to step 11 in the algorithm, the calculated discharge time constant can be used to estimate the required time to spend the accumulated energy as useful work:

$$t_{on} = \tau_d \ln\left(\frac{V_3}{V_{target2}}\right) \tag{6.14}$$

The flowchart in Figure 6.6 provides specific details of the implementation tested here. The highlighted shapes represent the remaining parts in force in subsequent cycles. This shows that the time constants are calculated only in the first cycle and then updated as new conditions occur. After the first cycle, just one reading is required during charging and one reading during discharging.

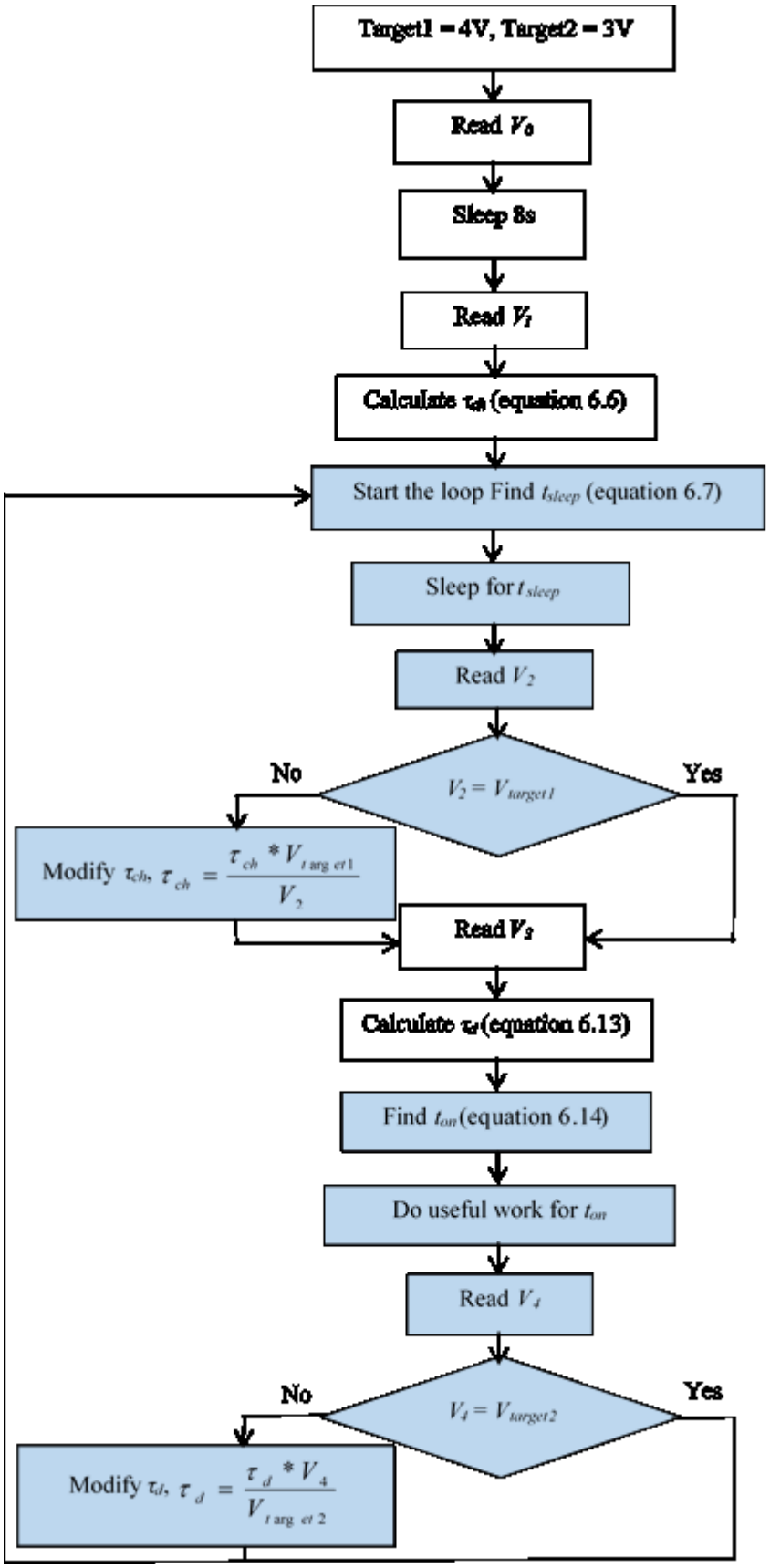

Figure 6.6 Flowchart of time constant calculation method

6.4 Comparison with Continuous Measurement

Continuously measuring the stored energy on the capacitor can be achieved by regularly reading (e.g. every few seconds) its voltage until it just exceeds the target. Reading voltages in this way is wasteful of power because of the awake state power requirements of the microcontroller. Logically, reducing the number of readings by increasing the sleep time between successive readings will improve the efficiency of the system. Nevertheless, there are limitations to maximum sleep times. Arbitrary values could exceed the target and even overvoltage the microcontroller. The action of reading the analogue voltage has the direct effect of also increasing the time to target, so regular reading also requires increased charging times to compensate for the cost of the awake states.

Figure 6.7 shows the periodic sampling approach for charging and discharging the capacitor. The samples generated during the charging cycle are every 8 seconds in this example and require the microcontroller to be awake for 2.5ms. During the rest of the cycle the microcontroller is sleeping using 2 orders of magnitude less power. If the system has a time constant of 150 seconds, it requires 15 readings to reach $target_2$ (if sampled every 8 seconds) as well as the samples required during discharging to reach $target_1$. It seems that there are two disadvantages to the regular sampling approach: as well as decreasing the efficiency, the system requires more time to reach the target because of the increased additional consumption.

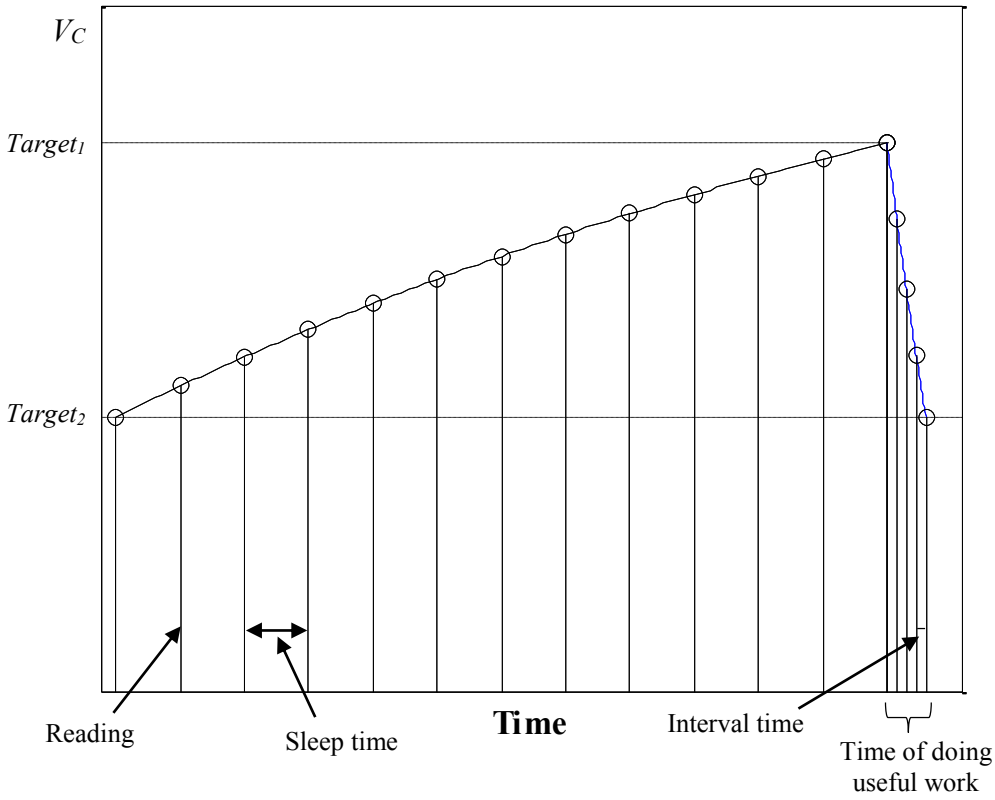

Figure 6.7 Continuous reading during charging and discharging

With an accurate estimate of the time constant for charging, an appropriate sleep time can be found for the microcontroller allowing efficient accumulation of energy, waking only once at the point where $Target_1$ has been exceeded. With the associated knowledge of the discharging time constant, $Target_2$ can be reached without depleting the capacitor below the microcontroller's minimum operational voltage.

In terms of energy, it is possible to calculate the efficiency η of the charging process of the capacitor as follows:

$$\eta = \frac{Output.Energy}{Input.Energy} \times 100\% \tag{6.15}$$

$$\eta = \frac{P_a T_d - P_r T_r N_d}{P_a T_d + P_s T_s N + P_r T_r N} \times 100\% \quad (6.16)$$

where P_a is the accumulated power, T_d is the discharging time, P_s is the power consumption of the microcontroller during sleep time, T_s is the sleep time, P_r is the power consumption of the microcontroller for each voltage reading, T_r is the time it takes for each reading, N_d is the number of readings during discharging, and N is the number of readings during charging time.

6.5 Results and Discussion

The system shown in Figure 6.3 has been simulated in Matlab to evaluate the charging process of the capacitor controlled by an ATtiny85. The variables in the simulation are shown in Table 6.1. The two factors of interest are the efficiency of the charging process and the extra time required to compensate for the losses incurred from the regular reading during the charging process. Different sleep times are used to show the impact on efficiency of the system.

Looking now at the discharging, without any interval time between two subsequent readings, the efficiency will be zero for the given setup shown in the table because all the stored energy will be spent driving the microcontroller and performing continuous readings. Figure 6.8 shows the effect of interval time between readings during discharging on the efficiency. The figure illustrates that the longer the interval time, the higher the efficiency for a specific sleep time (4 seconds). Moreover, increasing the sleep time improves the efficiency for a specific interval time (5ms) as shown in Figure 6.9. The figure also shows that the higher efficiency is obtained by using τ calculation method.

Table 6.1: Variable values

Objectives	Definition
C = 4700 μF	The used capacitor
R_{ch} = 33 kΩ	The equivalent serial resistance
R_d = 700 Ω	The equivalent parallel resistance
I_s = 5 μA	The microcontroller current during sleep mode
I_r = 5 mA	The average current when the microcontroller is on
T_{on} = 2.5 ms	The wake up time for each reading
$V_{target1}$ = 4 V	The upper level of voltage
$V_{target2}$ = 3 V	The lower level of voltage

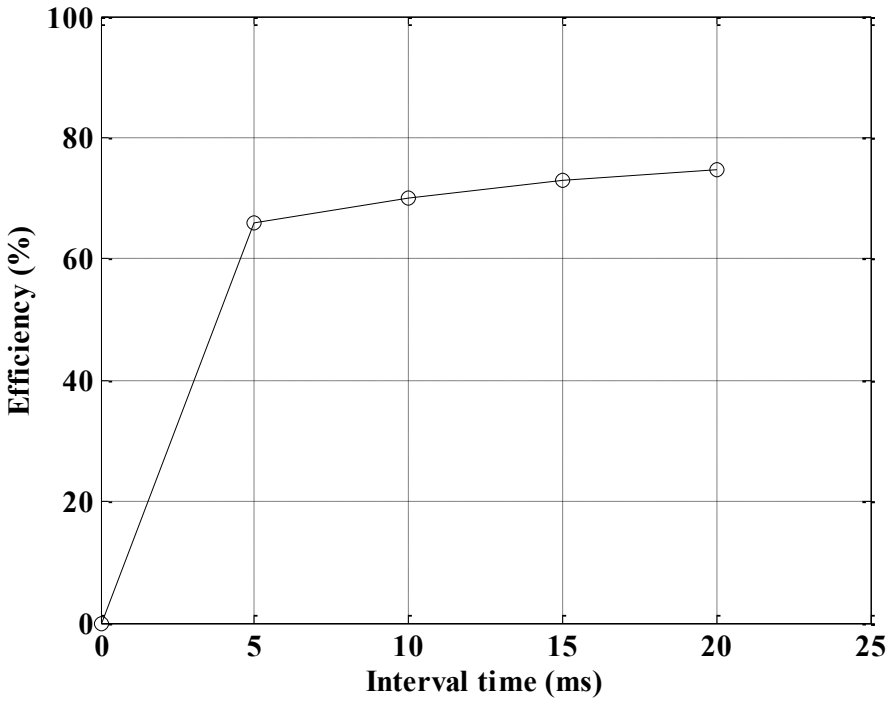

Figure 6.8 Efficiency versus interval time for 4 second sleep time

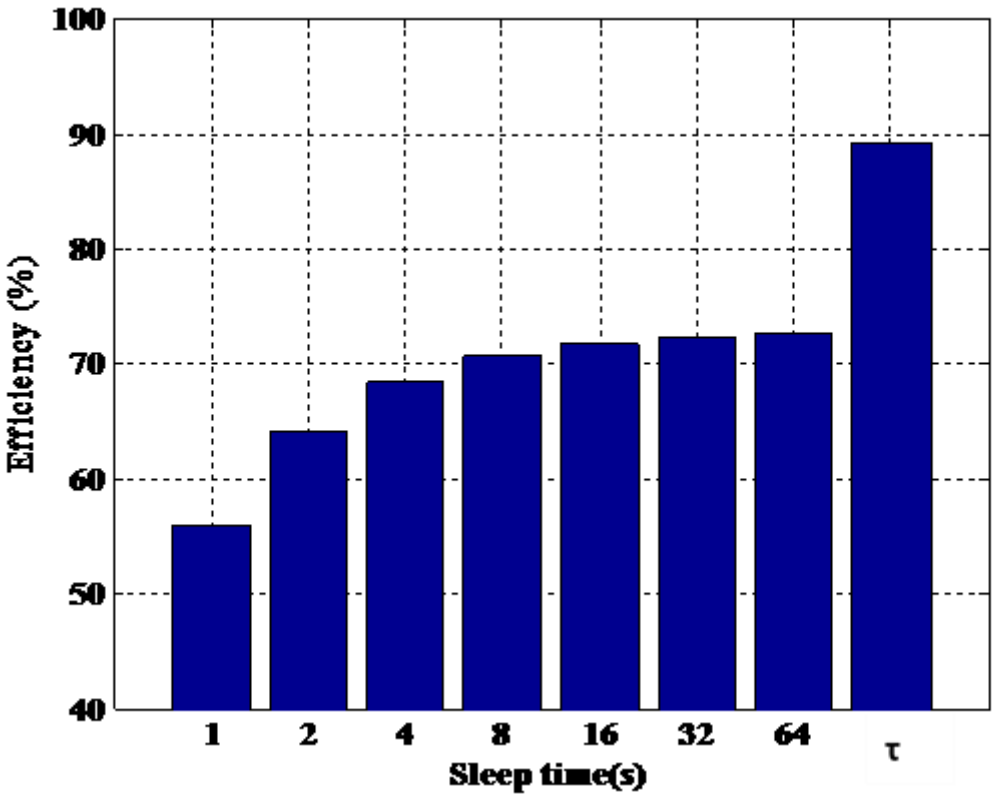

Figure 6.9 Efficiency of regular reading method with different sleep times compared to the τ calculation method

The comparison between continuous reading and our selective time constant based method is shown in Figure 6.9. It is clear from the figure that the efficiency of the time constant calculation method is almost 18% higher than the regular reading with 64 second sleep time and 5ms discharge interval time for the given 150 second Tau setup (τ).

Figure 6.10 presents the additional charging time (extra time) as a result of multiple readings compared to the required time of our proposed method, calculated as following:

$$Extra.Time = t_r - t_p \tag{6.17}$$

where t_r is the charging time of regular reading method and t_p is the charging time of proposed method.

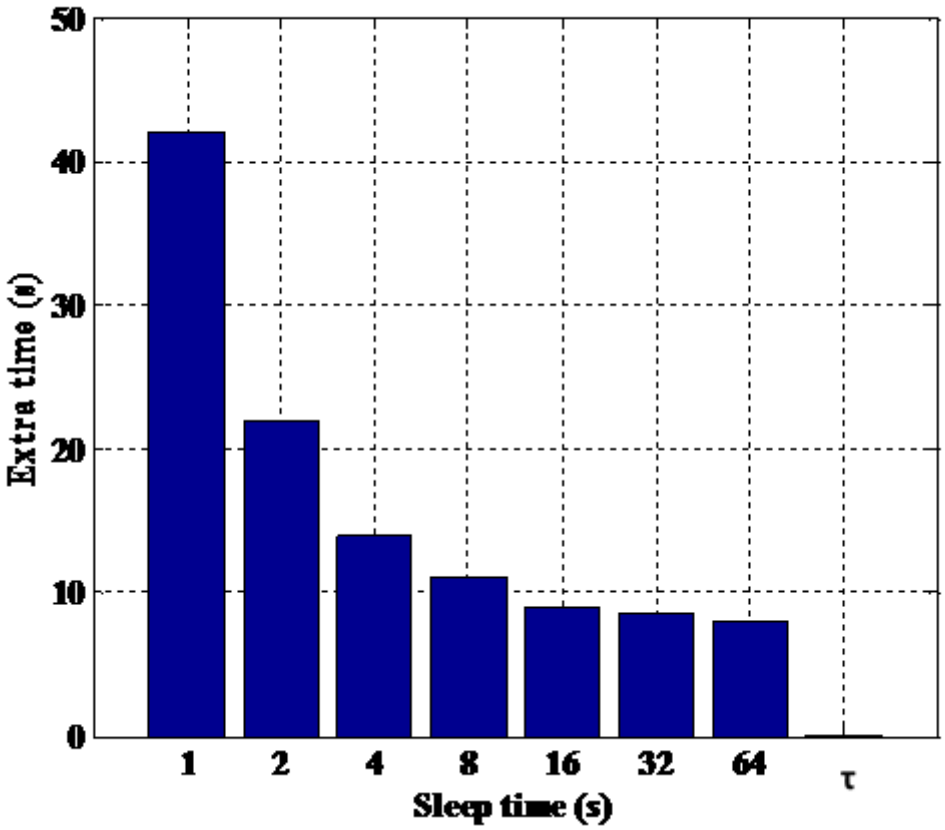

Figure 6.10 Extra charging time for regular reading compared to the zero extra time required by the proposed τ method

From Figures 6.9 and 6.10, using small sleep times is infeasible due to poor efficiency and increased charging times.

6.6 Implementation of the Circuit

To implement the circuit practically, the following system was built: a loop antenna was prepared, due to the chosen resonant frequency which was 4MHz. We chose 1/20

wavelength that has two turns coil with a diameter of 60cm. The tuning capacitor was attached for adjustments.

On the receiver side, the coil was a printed circuit board connected in parallel with another tuning capacitor, followed by a full wave rectifier consisting of four germanium diodes to obtain the dc voltage. A super capacitor of 4700µF was used to be the storage part of the energy; this represented the dc source of the microcontroller.

The used microcontroller was an ATtiny85. Practically it was necessary to wait to charge the storage capacitor to enter the safe operating range of the ATtiny85, which is 1.8V- 5.5V, before turning it on [118]. In order to achieve that a battery protection circuit was used as a driver to the microcontroller [120].

When the voltage of the storage capacitor reaches the required voltage, the ATtiny85 starts the task of controlling the received power as the algorithm's steps show in the flowchart (Figure 6.6). The implementation of the algorithm was written in Arduino and was tested in the environment discussed previously in this section to observe how it works practically. Figure 6.11 shows the system. (Note: the transmit coil is 100 times the area of the receive coil which is integrated onto the printed circuit board.)

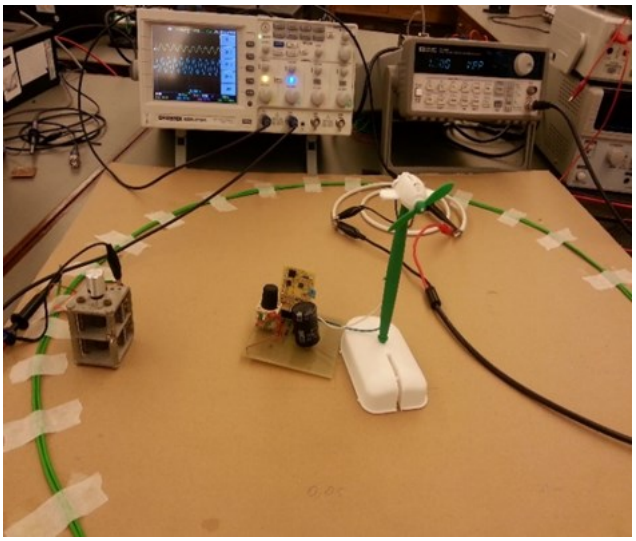

Figure 6.11 Practical wireless power transfer system with intelligent control

6.7 Conclusion

Power management can be achieved by implementing intelligent control in the design of a wireless power transfer system, and has far reaching implications for other low power applications. This study presented an algorithm to run a load with a source which has less power than the load's continuous requirements. Utilization has been achieved by using an ultra-low power microcontroller that makes sleep and awake decisions in order to accumulate the maximum amount of usable energy. At the appropriate time the micro wakes up and briefly runs the load, keeping sufficient power to allow it (the micro) to stay alive.

The presented algorithm is easily realized in code and achieves best case utilization from just two readings. This contribution represents a significant improvement in efficiency over the periodic analysis method. It keeps charging times fixed without marked expansion of these times and allows increased discharging time to do more useful work.

Chapter 7

Conclusions and Future Works

The main goal of this research was to investigate magnetic resonant wireless power transfer systems. The research focused on studying the performance of the system with different types of connection and the existence of multiple receivers, and in addition, to presenting a solution to some observed problems in the performance in some cases. The study was supported by theoretical derivation, and simulation results. The results were simulated in Matlab and about 70% of them were tested practically to verify the simulation results.

In this chapter, contributions and results of this research are concluded. A future work plan is presented in this chapter as well.

7.1 Research Summary

Magnetic resonant coupling is a near field wireless power transfer method. The principle of this technique is the transfer of power wirelessly between two coils in the same field by resonating both of them at the same frequency. This method has some advantages over the wired transfer of power and other wireless technologies. In this

thesis systems using this method were studied, and solutions were presented for some observed problems in order to improve the performance and the figure of merit of the system.

- The performance of magnetic resonant wireless power transfer systems was studied in detail including the effects of the parameters of the system. The figure of merit of the maximum transfer of power is affected by several factors such as the resonance frequency, the quality factor of the resonators, the value and the shape of the coils, the mutual inductance including the distance between the coils, and the load resistor. The study of the existence of **multiple receivers** in the field of the transmitter is the main contribution of this part. In addition, high figure of merit was achieved for relatively **small coil area ratios** (CAR) by adjustment of the turns ratio.
- **Symmetric Capacitive Tuning** (SCT) was presented as a solution for the splitting problem which is normally observed in the serial to serial connection system at small gaps between the coils. This method includes tuning both capacitors symmetrically in order to move one of the two peaks of the splitting curve to match the original resonance frequency of the system. SCT has advantages over the other known methods, impedance matching and frequency tracking. Applying symmetric capacitive tuning achieves higher figure of merit than the impedance matching method and does not need an extra impedance matching circuit; it obtains maximum figure of merit in all cases without moving out of the used ISM band, as happens in some frequency tracking systems. The implementation proposal was presented to achieve the method practically.

- Different applications or different loads need different **types of connection**. Therefore, the four potential types of connection were studied as well as the effect of the load on the figure of merit of each one. Serial to serial connection is more suitable for large loads while parallel to parallel connection is more appropriate for small loads. Serial to parallel and parallel to serial connections have equal performance in some cases and differ in others, and SP is more efficient with large loads than PS.

  Also in the same chapter, another method was presented to calculate the maximum figure of merit of wireless power transmission by the numerical solution of the input impedance equation. This method was applied to the serial to parallel connection type (SP).

- **Power management** was applied to prove the idea that tiny amounts of power can really do useful work in a magnetic resonance wireless power transfer system. This was achieved through intelligent control to run the load by using the microcontroller in the receiver side. The microcontroller switches between the asleep and awake modes to save some energy. We presented the algorithm to manage the required time for sleeping and waking. The algorithm was evaluated to show how efficient it is and the performance of the programmed microcontroller was tested in the real environment.

7.2 Future Work

Recognising our promising results, represented by the detailed study of the performance of magnetic resonant wireless power transfer systems with the four potential connection types and presenting solutions for some problems such as the frequency splitting problem in the serial to serial connection, and management of a

small amount of received wireless power presented in this thesis, there are still many possibilities of how to extend the demonstrated work.

Asymmetric multiple receivers

In the area of multiple receivers, we worked on identical devices that led to dividing the power equally among them and each one had a similar figure of merit or power transfer efficiency. For future work, we aim to work on asymmetric receivers (different size or shape) to observe their performance, for example working on a solenoid coil receiver with a pancake one. Different receivers have different efficiencies: which one of the parameters of the receiver is the dominant one to obtain higher figure of merit?

Multiple receivers in other types of connection

The performance of the multiple receiver systems was demonstrated in a serial to serial connection wireless system in the thesis. The performance of multiple receivers in other types of connection is future work in this field.

Sequential charging for multiple receivers

Study of the design of a multiple receiver wireless power system with charging time division. The idea in this design is that the transmitter charges the receivers sequentially. This technique can have more than one application: for example, charging the receivers according to their level of charge, starting with the low one. Charging the device which has the lowest level alone offers faster charging than feeding all the receivers together.

Bibliography

[1] T. W. Versloot, D. J. Barker, and X. O. One, “Optimization of Near-Field Wireless Power Transfer Using Evolutionary Strategies,” *The 8th European Conference on Antennas and Propagation, Netherlands*, 2014.

[2] J. Wang, S. Ho, W. Fu, and M. Sun, “Analytical design study of a novel WiTricity charger with lateral and angular misalignments for efficient wireless energy transmission,” *Magnetics, IEEE Transactions on,* vol. 47, no. 10, pp. 2616-2619, 2011.

[3] H. Dai, Y. Liu, G. Chen, X. Wu, T. He, A. X. Liu, and H. Ma, “Safe charging for wireless power transfer,” *IEEE/ACM Transactions on Networking,* vol. 25, no. 6, pp. 3531-3544, 2017.

[4] A. Mahmood, A. Ismail, Z. Zaman, H. Fakhar, Z. Najam, M. Hasan, and S. Ahmed, “A Comparative Study of Wireless Power Transmission Techniques,” *Journal of Basic and Applied Scientific Research,* vol. 4, no. 1, pp. 321-326, 2014.

[5] Y. Zhang, Z. Zhao, and K. Chen, “Frequency-Splitting Analysis of Four-Coil Resonant Wireless Power Transfer,” *Industry Applications, IEEE Transactions on,* vol. 50, no. 4, pp. 2436-2445, 2014.

[6] J. Gozalvez, “WiTricity-the wireless power transfer [Mobile radio],” *Vehicular Technology Magazine, IEEE,* vol. 2, no. 2, pp. 38-44, 2007.

[7] X. Wang, Y. Wang, G. Fan, Y. Hu, X. Nie, and Z. Yan, “Experimental and Numerical Study of a Magnetic Resonance Wireless Power Transfer System Using Superconductor and Ferromagnetic Metamaterials,” *IEEE Transactions on Applied Superconductivity,* vol. 28, no. 5, pp. 1-6, 2018.

[8] F. Hadley. "Goodbye wires!," 2018, [Online]. Available: http://news.mit.edu/2007/wireless-0607, 2007.

[9] O. Rönnbäck, “Optimization of Wireless Power,” M.S. thesis, Dept. of Computer Science, Electrical and Space Engineering, Luleå University of Technology, 2013.

[10] H. Widmer, N. P. Cook, and L. Sieber, "Wireless power transmission in electric vehicles," Google Patents, US9561730B2, 2017.

[11] M. Perry, P. Reynolds, S. Taffler, and A. Joyce, "Motion prediction for wireless power transfer," Google Patents, US20180097546A1, 2017.

[12] S. Ho, J. Wang, W. Fu, and M. Sun, “A comparative study between novel witricity and traditional inductive magnetic coupling in wireless charging,” *Magnetics, IEEE Transactions on,* vol. 47, no. 5, pp. 1522-1525, 2011.

[13] M. J. Chabalko, J. Besnoff, and D. S. Ricketts, “Magnetic field enhancement in wireless power with metamaterials and magnetic resonant couplers,” *IEEE Antennas and Wireless Propagation Letters,* vol. 15, pp. 452-455, 2016.

[14] J. Dai, and D. C. Ludois, “A survey of wireless power transfer and a critical comparison of inductive and capacitive coupling for small gap applications,” *IEEE Transactions on Power Electronics,* vol. 30, no. 11, pp. 6017-6029, 2015.

[15] F. Musavi, M. Edington, and W. Eberle, "Wireless power transfer: A survey of EV battery charging technologies." *IEEE*, pp. 1804-1810, 2012.

[16] J. Garnica, R. A. Chinga, and J. Lin, “Wireless power transmission: from far field to near field,” *Proceedings of the IEEE,* vol. 101, no. 6, pp. 1321-1331, 2013.

[17] N. P. Cook, P. Meier, L. Sieber, M. Secall, and H. Widmer, "Wireless energy transfer using coupled antennas," Google Patents, US9634730B2, 2017.

[18] F. M. Dickey, and T. E. Lizotte, *Laser beam shaping applications*: CRC Press, 2005.

[19] M. S. John, "Wireless power harvesting and transmission with heterogeneous signals," Google Patents, US20180115185A1, 2018.

[20] L. Frenzel, "What's the Difference Between EM Near Field and Far Field?," *Electronic Design*, 2018, [Online]. Available: http://www.electronicdesign.com/energy/what-s-difference-between-em-near-field-and-far-field, 2012.

[21] M. N. O. Sadiku, *Elements of Electromagnetics*, New York: Oxford University Press, 2010.

[22] P. Vorenkamp, R. Van Der Lee, I. Van Loo, and A. C. Spice, "Wireless power transfer system," Google Patents, US20100201310A1, 2010.

[23] N. A. Keeling, and M. Kissin, "Wireless power transfer system coil arrangements and method of operation," Google Patents, US9672975B2, 2017.

[24] A. Karalis, J. D. Joannopoulos, and M. Soljačić, "Efficient wireless non-radiative mid-range energy transfer," *Annals of Physics,* vol. 323, no. 1, pp. 34-48, 2008.

[25] I. Poole. "Electromagnetic waves and radio propagation," 2018, [Online]. Available: http://www.radio-electronics.com/info/propagation/em_waves/electromagnetic_waves.php.

[26] B.-J. Jang, S. Lee, and H. Yoon, "HF-band wireless power transfer system: Concept, issues, and design," *Progress in electromagnetics research,* vol. 124, pp. 211-231, 2012.

[27] Ofcom. "Frequency bands designated for Industrial, Scientific and Medical use (ISM)," 2018, [Online]. Available: https://www.ofcom.org.uk/__data/assets/pdf_file/0022/103297/fat-ism-frequencies.pdf.

[28] M. Kiani, U.-M. Jow, and M. Ghovanloo, "Design and optimization of a 3-coil inductive link for efficient wireless power transmission," *IEEE transactions on biomedical circuits and systems,* vol. 5, no. 6, pp. 579-591, 2011.

[29] J. D. Joannopoulos, A. Karalis, and M. Soljacic, "Wireless non-radiative energy transfer," Google Patents, US7741734B2, 2010.

[30] C. Balanis, *ANTENNA THEORY Analysis and Design*, 2nd ed., Canada: Wiley, 1997.

[31] N. P. Cook, L. Sieber, and H. Widmer, "Wireless power transmission for electronic devices," Google Patents, US8487481B2, 2013.

[32] V. Jiwariyavej, T. Imura, and Y. Hori, "Coupling Coefficients Estimation of Wireless Power Transfer System via Magnetic Resonance Coupling using Information from Either Side of the System." *IEEE Journal of Emerging and Selected Topics in Power Electronics*, vol. 3, no. 1, pp.191-200, 2015.

[33] D. Chaurasia, and S. Ahirwar, "An Optimal Parameter Estimation Technique for Wireless Electricity Transmission." Research India Publications, vol. 3, no. 1, pp. 1-9, 2013.

[34] T. Thabet, and J. Woods, "An Approach to Calculate the Efficiency for an N-Receiver Wireless Power Transfer System," *IJACSA,* vol. 6, no. 9, pp. 91-98, 2015.

[35] T. Imura, and Y. Hori, "Maximizing air gap and efficiency of magnetic resonant coupling for wireless power transfer using equivalent circuit and neumann formula," *Industrial Electronics, IEEE Transactions on,* vol. 58, no. 10, pp. 4746-4752, 2011.

[36] B. H. Waters, A. P. Sample, and J. R. Smith, "Adaptive impedance matching for magnetically coupled resonators." *PIERS Proceedings*, Moscow, pp. 694-701, 2012.

[37] J. Lee, Y. Lim, H. Ahn, J.-D. Yu, and S.-O. Lim, "Impedance-matched wireless power transfer systems using an arbitrary number of coils with flexible coil positioning," *IEEE Antennas and Wireless Propagation Letters,* vol. 13, pp. 1207-1210, 2014.

[38] J. Kim, H.-C. Son, K.-H. Kim, and Y.-J. Park, "Efficiency analysis of magnetic resonance wireless power transfer with intermediate resonant coil," *Antennas and Wireless Propagation Letters, IEEE,* vol. 10, pp. 389-392, 2011.

[39] J. Kim, D.-H. Kim, and Y.-J. Park, “Free-Positioning Wireless Power Transfer to Multiple Devices Using a Planar Transmitting Coil and Switchable Impedance Matching Networks,” *IEEE Transactions on Microwave Theory and Techniques,* vol. 64, no. 11, 2016.

[40] M. J. Sibakoti, and J. Hambleton, “Wireless Power Transmission Using Magnetic Resonance,” *Cornell College PHY312*, 2011.

[41] W. C. Brown, “The history of power transmission by radio waves,” *IEEE Transactions on Microwave Theory and Techniques,* vol. 32, no. 9, pp. 1230-1242, 1984.

[42] N. Tesla, "Apparatus for transmitting electrical energy," Google Patents, US1119732A, 1914.

[43] A. P. Smakhtin, and V. V. Rybakov, "Comparative analysis of wireless systems as alternative to high-voltage power lines for global terrestrial power transmission." *IEEE*, Proceedings of the 31st Intersociety Energy Conversion Engineering Conference pp. 485-488, 1996.

[44] J. M. Williams, “Biological effects of microwaves: Thermal and nonthermal mechanisms,” arXiv preprint physics/0102007, 2001.

[45] H. Matsumoto, “Research on solar power satellites and microwave power transmission in Japan,” *Microwave Magazine, IEEE,* vol. 3, no. 4, pp. 36-45, 2002.

[46] J. O. McSpadden, and J. C. Mankins, “Space solar power programs and microwave wireless power transmission technology,” *Microwave Magazine, IEEE,* vol. 3, no. 4, pp. 46-57, 2002.

[47] J. C. Lin, “Space solar-power stations, wireless power transmissions, and biological implications,” *Microwave Magazine, IEEE,* vol. 3, no. 1, pp. 36-42, 2002.

[48] S. Saunders, and A. Aragon-Zavala, *"Antennas and Propagation for Wireless Communication Systems"*, 2nd ed., England: Wiley, 2007.

[49] R. Pudur, V. Hanumante, S. Shukla, and K. Kumar, "Wireless Power Transmission: A survey." *IEEE International Conference on Recent Advances and Innovations in Engineering*, pp. 1-6, 2014.

[50] Z. Xian, L. Yang, C. Haiyan, and Y. Zhuo, "The application of non-contact power transmission technology (NPT) in the modern transport system." *IEEE, Proceedings of the International Conference on Mechatronics and Automation* pp. 345-349, 2010.

[51] X. Wei, Z. Wang, and H. Dai, "A critical review of wireless power transfer via strongly coupled magnetic resonances," *Energies,* vol. 7, no. 7, pp. 4316-4341, 2014.

[52] A. Bodrov, and S.-K. Sul, "Analysis of wireless power transfer by coupled mode theory (CMT) and practical considerations to increase power transfer efficiency," *Wireless Power Transfer-Principles and Engineering Explorations*: InTech, 2012.

[53] H. Shim, J. Park, S. Nam, and B. Lee, "A criterion Proposed for Inductive Coupling and Magnetic Resonance Coupling in Wireless Power Transfer System." *Proceeding of Asia-Pacific Microwaves*, pp. 1104-1106, 2014.

[54] T. Beh, M. Kato, T. Imura, and Y. Hori, "Wireless Power Transfer System via Magnetic Resonant Coupling at Fixed Resonance Frequency—Power Transfer System Based on Impedance Matching—," *EVS-25 Shenzhen, China*, 2010.

[55] M. Kiani, and M. Ghovanloo, "The circuit theory behind coupled-mode magnetic resonance-based wireless power transmission," *Circuits and Systems I: Regular Papers, IEEE Transactions on,* vol. 59, no. 9, pp. 2065-2074, 2012.

[56] K. S. Kiran, S. Brahma, S. Parida, and R. Behera, "Analysis of inductive resonant coupled WPT system using Reflected Load Theory." *IEEE International Conference on Power Electronics, Drives and Energy Systems*, pp. 1-6, 2014.

[57] T. Imura, H. Okabe, and Y. Hori, "Basic experimental study on helical antennas of wireless power transfer for electric vehicles by using magnetic resonant couplings." in *Proc. IEEE VPPC*, Sep. 7–10, pp. 936-940, 2009.

[58] T. C. Beh, M. Kato, T. Imura, S. Oh, and Y. Hori, "Automated impedance matching system for robust wireless power transfer via magnetic resonance coupling," *Industrial Electronics, IEEE Transactions on,* vol. 60, no. 9, pp. 3689-3698, 2013.

[59] B. L. Cannon, J. F. Hoburg, D. D. Stancil, and S. C. Goldstein, "Magnetic resonant coupling as a potential means for wireless power transfer to multiple small receivers," *Power Electronics, IEEE Transactions on,* vol. 24, no. 7, pp. 1819-1825, 2009.

[60] A. P. Sample, D. T. Meyer, and J. R. Smith, "Analysis, experimental results, and range adaptation of magnetically coupled resonators for wireless power transfer," *IEEE Transactions on Industrial Electronics,* vol. 58, no. 2, pp. 544-554, 2011.

[61] F. Zhang, S. A. Hackworth, W. Fu, and M. Sun, "The relay effect on wireless power transfer using witricity." *IEEE*, pp. 1-1, 2010.

[62] B. J. Lee, A. Hillenius, and D. S. Ricketts, "Magnetic resonant wireless power delivery for distributed sensor and wireless systems." *IEEE Topical Conference on Wireless Sensors and Sensor Networks (WiSNet)*, pp. 13-16, 2012.

[63] J. J. Casanova, Z. N. Low, and J. Lin, "A loosely coupled planar wireless power system for multiple receivers," *Industrial Electronics, IEEE Transactions on,* vol. 56, no. 8, pp. 3060-3068, 2009.

[64] Y. Wang, J. Song, L. Lin, X. Wu, and W. Zhang, "Research on magnetic coupling resonance wireless power transfer system with variable coil structure." IEEE PELS Workshop on Emerging Technologies: Wireless Power Transfer (WoW), pp. 1-6, 2017.

[65] R. Mobarhan, R. Burdo, and L. N. Bonacci, "Wireless power transfer in public places," Google Patents, US20100201201A1, 2010.

[66] S. Y. R. Hui, W. Zhong, and C. K. Lee, “A critical review of recent progress in mid-range wireless power transfer,” *IEEE Transactions on Power Electronics,* vol. 29, no. 9, pp. 4500-4511, 2014.

[67] H. Li, X. Yang, K. Wang, and X. Dong, "Study on efficiency maximization design principles for Wireless Power Transfer system using magnetic resonant coupling." *IEEE ECCE Asia Downunder (ECCE Asia)*, pp. 888-892, 2013.

[68] D. P. Kar, P. P. Nayak, S. Bhuyan, and S. Panda, “Automatic frequency tuning wireless charging system for enhancement of efficiency,” *Electronics Letters,* vol. 50, no. 24, pp. 1868-1870, 2014.

[69] W. Fu, B. Zhang, and D. Qiu, "Study on frequency-tracking wireless power transfer system by resonant coupling." *IEEE 6th International Conference of Power Electronics and Motion Control*, pp. 2658-2663, 2009.

[70] N. Y. Kim, K. Y. Kim, Y.-H. Ryu, J. Choi, D.-Z. Kim, C. Yoon, Y.-K. Park, and S. Kwon, "Automated adaptive frequency tracking system for efficient mid-range wireless power transfer via magnetic resonanc coupling." 42nd European Microwave Conference (EuMC), pp. 221-224, 2012.

[71] I. Awai, and T. Komori, "A simple and versatile design method of resonator-coupled wireless power transfer system." International Conference on Communications, Circuits and Systems (ICCCAS), pp. 616-620, 2010.

[72] A. Kurs, A. Karalis, R. Moffatt, J. D. Joannopoulos, P. Fisher, and M. Soljačić, “Wireless power transfer via strongly coupled magnetic resonances,” *science,* vol. 317, no. 5834, pp. 83-86, 2007.

[73] T. P. Duong, and J.-W. Lee, “Experimental results of high-efficiency resonant coupling wireless power transfer using a variable coupling method,” *IEEE Microwave and Wireless Components Letters,* vol. 21, no. 8, pp. 442-444, 2011.

[74] T. I. Anowar, S. D. Barman, A. Wasif Reza, and N. Kumar, “High-efficiency resonant coupled wireless power transfer via tunable impedance matching,” *International Journal of Electronics*, vol. 104, no. 10, pp. 1-19, 2017.

[75] M. Fu, T. Zhang, C. Ma, and X. Zhu, “Efficiency and Optimal Loads Analysis for Multiple-Receiver Wireless Power Transfer Systems,” *Microwave Theory and Techniques, IEEE Transactions on,* vol. 63, no. 3, pp. 801-812, 2015.

[76] P. Kamalinejad, C. Mahapatra, Z. Sheng, S. Mirabbasi, V. C. Leung, and Y. L. Guan, “Wireless energy harvesting for the internet of things,” *IEEE Communications Magazine,* vol. 53, no. 6, pp. 102-108, 2015.

[77] H. J. Visser, V. Pop, J. Op het Veld, and R. Vullers, "Remote RF Battery Charging." *IET 10th International Workshop Micro & Nanotechnology for Power Generation and Energy Conversion Applications*, Leuven, 2011.

[78] H. Ostaffe, “RF-based wireless charging and energy harvesting enables new applications and improves product design,” Mouser Electron., Mansfield, TX, USA, 2017. [Online]. Available: https://www.mouser.com/pdfdocs/rf-basedwireless-charging.pdf

[79] N. Shinohara, “Rectennas for Microwave Power Transmission,” *IEICE Electronics Express* vol. 10, no. 21, pp. 1-13, 2013.

[80] J. Zhang, and Y. Huang, “Rectennas for Wireless Energy Harvesting,” *University of Liverpool, Liverpool, L693GJ, UK, 1977.*

[81] S. Evanczuk. "capacitor characteristics impact energy harvesting efficiency," 2018, [Online]. Available: https://www.digikey.com/en/articles/techzone/2014/nov/capacitor-characteristics-impact-energy-harvesting-efficiency.

[82] J. Zhang, Y. Huang, and P. Cao, "Harvesting RF energy with rectenna arrays." *IEEE 6th European Conference on Antennas and Propagation (EUCAP)*, pp. 365-367, 2012.

[83] A. N. Parks, and J. R. Smith, "Sifting through the airwaves: Efficient and scalable multiband RF harvesting." *IEEE International Conference on RFID (IEEE RFID)*, pp. 74-81, 2014.

[84] Powercast Groap. "Powerharvester Receivers," 2018, [Online]. Available: http://www.powercastco.com/products/powerharvester-receivers/.

[85] Powercast Group. "Powercaster Transmitter," 2018, [Online]. Available: https://www.mouser.com/ds/2/329/TX91501-manual-3020.pdf

[86] A. C. M. de Queiroz, "Mutual inductance and inductance calculations by Maxwell's Method," *Home page of Dr. Antonio Carlos M. de Queiroz*, 2005.

[87] C. Akyel, S. I. Babic, and M.-M. Mahmoudi, "Mutual inductance calculation for non-coaxial circular air coils with parallel axes," *Progress In Electromagnetics Research,* vol. 91, pp. 287-301, 2009.

[88] C. K. Lee, W. Zhong, and S. R. Hui, "Recent progress in mid-range wireless power transfer." *IEEE Energy Conversion Congress and Exposition (ECCE)*, pp. 3819-3824, 2012.

[89] M. Yasir, and M. S. Haque, "The Witricity: Revolution in Power Transmission Technology," *International Journal of Scientific & Engineering Research,* vol. 4, no. 8, pp. 565-570, 2013.

[90] Department of Physics and Astronomy: Georgia State University; "Mutual Inductance," 2017, [Online]. Available: http://hyperphysics.phy-astr.gsu.edu/hbase/magnetic/indmut.html.

[91] Radio Regulations, "International Telecommunication Union," *Radiocommunication Sector. ITU-R. Geneva*, 2008.

[92] P. Bernard, "VHF/UHF filters and multicouplers : applications of air resonators ," John Wiley & Sons, 2013.

[93] RFMD. "RFAC3612 6-Bit, PAC Datasheet," 2017, [Online]. Available: file:///C:/Users/tfytha/Downloads/rfac3612_data_sheet.pdf.

[94] R. Karthika, and S. Balakrishnan, “Wireless communication using Li-Fi technology,” *SSRG International Journal of Electronics and Communication Engineering (SSRG-IJECE),* vol. 2, no. 3, pp. 32-40, 2015.

[95] F. Arvin, K. Samsudin, and A. R. Ramli, "A short-range infrared communication for swarm mobile robots." *IEEE International Conference on Signal Processing Systems*, pp. 454-458, 2009.

[96] P. Goswami, and M. K. Shukla, “Design of a Li-Fi Transceiver,” *Wireless Engineering and Technology,* vol. 8, no. 04, pp. 71, 2017.

[97] P. S. M. Shaik. Shakeera , M.Shahin Begum ,V.V.Bhargav , P.D.N.Malleswara Rao “PC to PC File Transfer using Li-Fi Technology,” *International Journal of Engineering Trends and Technology (IJETT)* vol. 46, no. 3, pp. 143-145, 2017.

[98] C. W. Fox, "System for communication between a central controller and items in a factory using infrared light," Google Patents, US5742238A , 1998.

[99] V. Semiconductors. "TSAL6200 Datasheet," 2017, [Online]. Available: https://www.vishay.com/docs/81010/tsal6200.pdf.

[100] Everlight Electronics. "5mm Phototransistor PT333-3C Datasheet," 2017, [Online]. Available: http://www.everlight.com/file/ProductFile/PT333-3C.pdf.

[101] T. Thabet, and J. Woods, "Impact of connection type on the efficiency of wireless power transfer systems." IEEE International Conference on Circuits, System and Simulation (ICCSS), pp. 146-150, 2017.

[102] T. Thabet, and J. Woods, “Using Input Impedance to Calculate the Efficiency Numerically of Series-Parallel Magnetic Resonant Wireless Power Transfer Systems,” *Special Issue on Multidisciplinary Sciences and Engineering, Advances in Science, Technology and Engineering Systems Journal* vol. 3, no. 3, pp. 38-42, 2018.

[103] T. Thabet, and J. Woods, "Intelligent management and control of received wireless power." IEEE International Conference on Circuits, System and Simulation (ICCSS), pp. 76-81, 2017.

[104] P. Nintanavongsa, U. Muncuk, D. R. Lewis, and K. R. Chowdhury, "Design optimization and implementation for RF energy harvesting circuits," *Emerging and Selected Topics in Circuits and Systems, IEEE Journal on,* vol. 2, no. 1, pp. 24-33, 2012.

[105] N. P. Cook, L. Sieber, and H. Widmer, "Passive receivers for wireless power transmission," Google Patents, US8432070B2, 2013.

[106] Powercast Group. "P2110B Datasheet "; 2017, [Online]. Available: http://www.powercastco.com/test566alpha/wp-content/uploads/2009/03/p2110b-datasheet-v12.pdf.

[107] L. Olvitz, D. Vinko, and T. Švedek, "Wireless power transfer for mobile phone charging device." *IEEE Proceedings of the 35th International Convention MIPRO*, pp. 141-145, 2012.

[108] S. Y. Choi, B. W. Gu, S. Y. Jeong, and C. T. Rim, "Advances in wireless power transfer systems for roadway-powered electric vehicles," *IEEE Journal of Emerging and Selected Topics in Power Electronics,* vol. 3, no. 1, pp. 18-36, 2015.

[109] S. Li, and C. C. Mi, "Wireless power transfer for electric vehicle applications," *IEEE journal of emerging and selected topics in power electronics,* vol. 3, no. 1, pp. 4-17, 2015.

[110] C. C. Mi, G. Buja, S. Y. Choi, and C. T. Rim, "Modern Advances in Wireless Power Transfer Systems for Roadway Powered Electric Vehicles," *IEEE Transactions on Industrial Electronics,* vol. 63, no. 10, pp. 6533-6545, 2016.

[111] F. L. Cabrera, and F. R. de Sousa, "Achieving Optimal Efficiency in Energy Transfer to a CMOS Fully Integrated Wireless Power Receiver," *IEEE Transactions on Microwave Theory and Techniques,* vol. 64, no. 11, pp. 3703, 2016.

[112] A. Boswell, A. J. Tyler, and A. White, “Performance of a small loop antenna in the 3-10 MHz band,” *IEEE Antennas and Propagation Magazine,* vol. 47, no. 2, pp. 51-56, 2005.

[113] A. Boswell, “Loop antennas in the 3-30 MHz band,” *IET 8th International Conference on High-Frequency Radio Systems and Techniques*, pp. 33-36, 2000.

[114] S. Yates-AA5TB, “Small Transmitting Loop Antennas.” 2017, [Online]. Available: http://www.aa5tb.com/loop.html

[115] B. A. Austin, A. Boswell, and M. A. Perks, “Loss Mechanisms in the Electrically Small Loop Antenna [Antenna Designer's Notebook],” *IEEE Antennas and Propagation Magazine,* vol. 56, no. 4, pp. 142-147, 2014.

[116] A. B. Dolgov, and R. Zane, "Low-power wireless medical sensor platform." IEEE 28th Annual International Conference of Engineering in Medicine and Biology Society, pp. 2067-2070, 2006.

[117] T. Paing, E. Falkenstein, R. Zane, and Z. Popovic, "Custom IC for ultra-low power RF energy harvesting." IEEE 24th Annual Conference of Applied Power Electronics Conference and Exposition, pp. 1239-1245, 2009.

[118] Atmel Corp. "ATtiny25-ATtiny45-ATtiny85 datasheet," 2017, [Online]. Available: http://www.atmel.com/Images/Atmel-2586-AVR-8-bit-Microcontroller-ATtiny25-ATtiny45-ATtiny85_Datasheet-Summary.pdf.

[119] A. Hambley, "*Electrical Engineering Principles and Applications*," New Jersey: Prentice-Hall, 1997.

[120] A. LEE, “Li-Ion Battery Protection Circuit Draws Only 4.5 µA,” *ELECTRONIC DESIGN*, 1999.